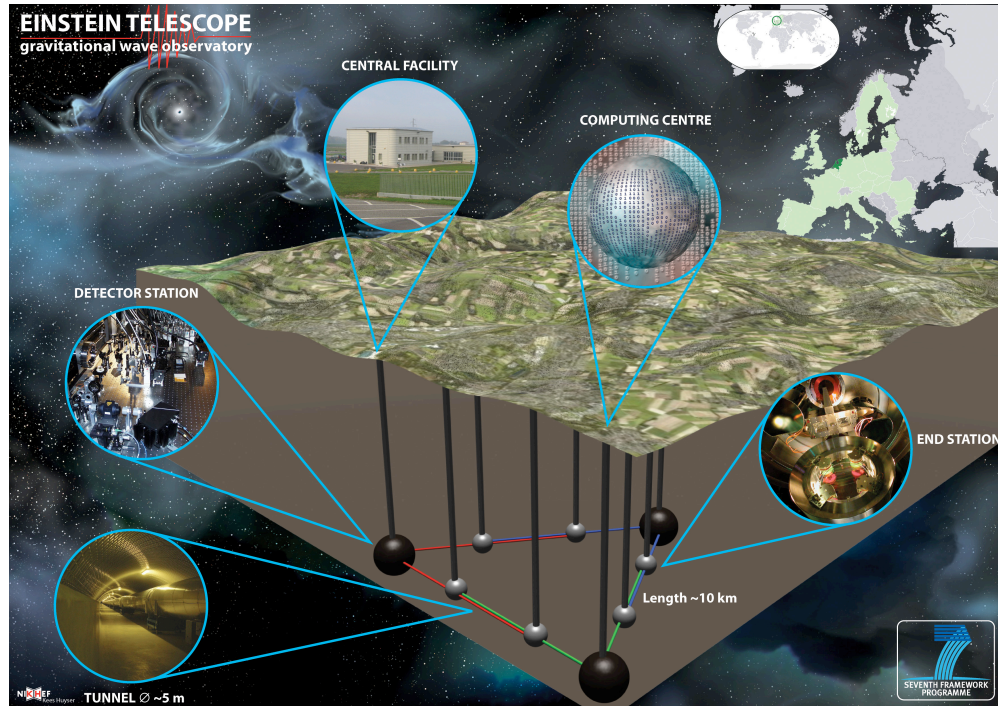# Einstein Telescope Design Study: Vision Document

FIG. 1: Artist's conception of an underground, cryogenic, third-generation gravitational-wave detector.

Pau Amaro-Seoane, Nils Andersson, K.G. Arun, Sukanta Bose, Leone Bosi, James Clark, Thomas Dent, Jonathan Gair, Kostas Glampedakis, Mark Hannam, Siong Heng, Sascha Husa, Gareth Jones, Badri Krishnan, Richard O'Shaughnessy, Christian Ott, Jocelyn Read, Tania Regimbau, Luciano Rezzolla, B.S. Sathyaprakash, Chris Van Den Broeck, Alberto Vecchio, John Veith

Executive Summary

Einstein Telescope (ET) is a third generation gravitational wave antenna which is hoped to be a factor 10 better in sensitivity than advanced detectors with a wide band sensitivity from 1 Hz, all the way up to 10 kHz. A possible sensitivity curve is shown in Fig. 25 but several variants are being considered.

The goal of the Design Study is to identify potentially interesting problems and address them in greater depth in the context of instrument design. This *Vision Document* will serve as a reference for an in-depth exploration of what science goals should be met by ET.

Working Group-4 will address not only the ET science goals but also the associated data analysis and computational challenges. In the frequency window of ET we can expect a wide variety of sources. The sensitivity will be deep enough to address a range of problems in fundamental physics, cosmology and astrophysics. The ET frequency range and sensitivity pose serious and unprecedented technological challenges. The goal is to get the best possible sensitivity in the range $[1, 10^4]$ Hz but compromises might have to be made based on the level of technical challenge, the cost to meet those challenges, site selection, etc. The ultimate design should be based on the scientific merit of the different trade-offs.

This Vision Document will set forth key *science requirements* to be met by a third generation detector. Examples include,

1. Studying cores of compact objects and General Relativistic instabilities,

2. Solving the enigma of gamma-ray bursts and resolving their different classes,

3. Understanding the mass-spectrum of compact stars and their populations,

4. Measuring the cosmological parameters with GW standard sirens, etc.

We aim to evaluate the science potential of ET for different geometrical and optical configurations, choice of materials and site, corresponding to different sensitivity curves.

A detector with such a sensitivity window and span will pose new data analysis challenges. There will be many classes of sources all visible at the same time, requiring a paradigm shift in the way data is currently analyzed. Moreover, some of the souces that are considered to be transient in current detectors will not be so in ET, requiring greater computational costs as well as the development of new search algorithms. A careful and comprehensive study of the data analysis challenges and solutions will be carried out along side the science goals. In the light of this the research groups will have three primary responsibilities:

1. Address the science that ET can do which a second generation detector can't. Group the science into one of fundamental physics, cosmology and astrophysics and prioritize the science potentials.

2. Develop tools that can be used to evaluate the performance of different detector configurations in the context of science goals and develop a metric based figure-of-merit to pick an optimal choice for the design of ET.

3. Evaluate the data analysis requirements and study if computational cost is a limiting factor in meeting the science goals.

I. EINSTEIN TELESCOPE SCIENCE GOALS/REQUIREMENTS

Some three hundred years after Galileo observed the Jovian satellites, the twentieth century heralded a new era in observational astronomy with radio and microwave antennas, gamma- and x-ray detectors, which revolutionized astronomy and opened the entire electromagnetic window for observing and understanding the Universe. A remarkable revelation coming from these observations is that about 96 percent of our Universe is invisible and that gravitational interaction powers the most luminous and spectacular objects and phenomena such as quasars, gamma-ray bursts, ultra luminous X-ray sources, pulsars, the big bang, etc.

Einstein's theory of gravity predicted that dynamical systems in strong gravitational fields will release vast amounts of energy in the form of gravitational radiation. This radiation has the potential to open a new window on the Universe, complementing the electromagnetic window. Russell Hulse and Joe Taylor were awarded the 1993 Nobel Prize in Physics for the discovery of a binary consisting of two neutron stars in close orbit in which indirect evidence for the emission gravitational waves was found.

Interferometric gravitational wave (GW) detectors that are currently taking data and advanced detectors that will be built over the next ten years will be the first steps in establishing the field of gravitational astronomy through their detection of the most luminous sources such as the merger of binary neutron stars and black holes. Einstein Telescope will make it possible to observe a greater variety of phenomena, and provide a new tool for expanding our knowledge of fundamental physics, cosmology and relativistic astrophysics. Is the nature of gravitational radiation as predicted by Einstein's theory? Are black hole spacetimes uniquely given by the Kerr geometry? Are naked singularities the final state of gravitational collapse? How did the black holes at galactic nuclei form? What were the physical conditions at the time of the big bang? What is the nature of quantum gravity and what is the origin of space and time? Are there really ten spatial dimensions? These are some of the key questions at the forefront of physics that future GW observations might shed some light on.

A. Fundamental physics

Astronomical sources of gravitational waves are essentially systems where gravity is extremely strong and often characterized by relativistic bulk motion of massive objects. The emitted radiation carries uncorrupted signature of the nature of the space-time geometry and therefore an invaluable tool to understand the behaviour of matter and geometry in extreme conditions of density, temperature, magnetic fields and relativistic motion. Here are some examples of how GW observations can impact fundamental physics.

In Einstein's theory, the radiation travels at the speed of light and has two polarization states. In alternative theories of gravity neither could be true due to massive gravitons or the presence of a scalar field (in addition to the tensor field) mediating gravity. Experimental tests of gravity, as well those afforded by the data from the Hulse-Taylor binary, are consistent with both Einstein's theory and one of its alternatives called the Brans-Dicke theory. Gravitational wave detectors will bring these theories vis-a-vis observations that could decisively rule out one or the other.

According to Einstein's gravity the space-time in the vicinity of black holes is described by a unique geometry called the Kerr solution. Observation of the radiation from the infall of stellar-mass black holes into intermediate-mass black holes will make it possible to

test such uniqueness theorems. X-ray astronomy has provided firm indirect evidence that intense sources of x-rays may well host a black hole. An unambiguous signature of black holes, however, could eventually be provided by the detection of black-hole quasi-normal modes – gravitational radiation that has characteristic frequency and decay time. Failure to detect such radiation from, for example, a newly formed black hole would mean that gravity is more exotic than what we currently believe (e.g., gravitational collapse might lead to entities called naked singularities) and reveal new phases of matter at extremely high densities.

The most attractive versions of string theory require an eleven dimensional space-time, far larger than what we perceive. Certain phenomenological models at the interface of string theory and cosmology suggest that what we perceive as a four-dimensional Universe (the brane) could indeed be part of a higher dimensional Universe (bulk) with large spatial dimensions. The key feature of this theory is that gravitational interaction, and in particular gravitational waves, propagate in the bulk, while other interactions are restricted to the brane, which partly explains why gravity is so weak. Brane world models predict a specific signature in the spectrum of gravitational waves. Future ground- and space-based gravitational wave detectors offer the exciting possibility of observing radiation from the bulk and thereby explore if the Universe has large extra dimensions.

B.   Relativistic Astrophysics

Astronomy has revealed a very diverse and exotic Universe which remain an enigma decades after their first discovery. Examples include supernovae – end-states of stellar evolution resulting in the gravitational collapse followed by a huge explosion of in-falling matter; gamma-ray bursts – intense sources of gamma radiation that last only a few seconds to minutes yet emit more energy than would a star in its entire life time; radio pulsars – compact objects as massive as the Sun but only about 10 km in size, the regularity of their radio pulses rivaling the best atomic clocks in the world; transient sources of intense radio waves thousands of light years away with associated magnetic fields so strong that the emitted radiation could breakdown terrestrial radio stations. In each of these cases the source is believed to be couched in dense environs and strong gravitational fields and, therefore, a potential source of gravitational radiation. For example, source of gamma-ray bursts could be colliding neutron stars which are electromagnetically invisible for most of their lives but are very powerful emitters of GW. Transient radio sources could be the result of quakes in neutron stars with concomitant emission of GW. Observing such 'multi-messengers' (sources that are strong emitters of both EM and GW radiation) will help understand phenomena that have remained puzzles for decades.

The nucleus of every galaxy is believed to host a compact object a million to a billion times as massive as our Sun and powerful emitters of optical, radio and other radiation. What is the nature of this object? How and when it form? Did it form from small 100 solar mass seeds and then grew by accreting gas and other compact objects? What is its relation to the size of the galaxy as a whole? These are but some of the questions which a model of the formation of structure in the Universe must answer. While electromagnetic observations have provided valuable data, GW observations can help address some of the key questions on the formation and nature of these objects.

Future gravitational wave detectors will be sensitive to a population of sources at very high red-shifts, helping us study cosmological evolution of sources, the history of star forma-

tion and its dependence on the matter content of the Universe, development of large-scale structure in the Universe, etc.

C. Cosmology

Twentieth century was the golden age of cosmology. With the advent of radio and microwave astronomy it was possible to finally address key questions about the origin of the Universe and if it really started in a big bang. The cosmic microwave background is a relic radiation from the big bang. Since the early Universe was very dense, this radiation was in thermal equilibrium with matter for about 380,000 years after the big bang and cannot directly reveal the conditions in the very early phase of the Universe's history. The most direct way of observing the primeval Universe is via the gravitational window with a network of two or more detectors. Theoretical predictions based on fairly general assumptions predict the production of stochastic GW in the early Universe, which have been traveling to us unscathed as a consequence of their weak coupling to matter.

The most amazing aspect of the Universe is that only about 4% of its content is in the form of visible matter, the rest being dark matter and dark energy. In order to understand the nature of these 'dark' contents it is necessary to have a standard candle – sources whose distance from Earth can be inferred from their luminosity. Compact binaries are an astronomer's ideal standard candle: By measuring the signature of the gravitational radiation they emit, it is possible to infer their intrinsic parameters (e.g., the masses and spins of the component objects) and accurately deduce their luminosity distance. In fact, compact binaries eliminate the need to build a cosmic distance ladder – the process by which standard candles at different distances are calibrated in astronomy since there is no source that is suitable at all distances.

The synergy of multi-messenger astronomy is no where more apparent than in the use of standard sirens of gravity to verify the concordance model of comsology. ET might detect several hundred compact binary coalescence events each year in coincidence with short-hard gamma-ray bursts, provided, of course, the two are related. While gravitational obsrevations would provide an unambiguous measure of the luminosity distance, the host galaxy of the GRB could be used to measure the red-shift. By fitting the observed population to a cosmological model, it will be possible to measure the Hubble parameter, dark matter and dark energy densities, as well as the dark energy equation-of-state parameter.

The early history of the Universe must have witnessed several phase transitions as the energy scale changed from that of Grand Unified Theory (GUT) to Electro-Weak interaction and finally to the current state in which we see four different fundamental interactions. Cosmic strings are one-dimensional topological defects that form at the boundaries of different phases of the Universe. Vibrations of these strings at the speed of light can sometime form a kink which can then break emitting a burst of gravitational radiation. The spectrum of the radiation has again a unique signature which can help us detect cosmic strings and thus provide a glimpse of the Universe as it underwent phase transitions.

Perhaps the most exciting discovery of the new window will be none of the above. If astronomical legacy is an example, then gravitational astronomy should unravel phenomena and sources never imagined in wildest possible theories – an eventuality of any new observational tool.

II. SOURCES OF GRAVITATIONAL WAVES IN ET

The goal of this Section is to give an overview of the sources expected to be observed by ET and problems to be addressed in the context of the Design Study. We will begin with a very brief introduction to gravitational waves and then go on to describe the sources, their properties and the problems that need to be addressed over the next two years.

Gravitational waves are described by a second rank tensor $h_{\alpha\beta}$, which, in a suitable coordinate system and gauge, has only two independent components h_+ and $h_\times$, $h_{xx} = -h_{yy} = h_+$, $h_{xy} = h_{yx} = h_\times$, all other components being zero. A detector measures only a certain linear combination of the two components, called the *response* $h(t)$, given by

$$h(t) = F_+(\theta,\, \varphi,\, \psi)h_+(t) + F_\times(\theta,\, \varphi,\, \psi)h_\times(t), \tag{2.1}$$

where F_+ and $F_\times$ are the detector antenna pattern functions, ψ is the polarization angle, and $(\theta,\, \varphi)$ are angles describing the location of the source on the sky. The angles are all assumed to be constant for a transient source but time-dependent for sources that last long enough so that the Doppler modulation of the signal due to the relative motion of the source and detector cannot be neglected.

A. Compact binary coalescences

Sathya, Vicere, Guidi

A compact binary, consisting of neturon stars (NS) and/or black holes (BH), evolves by emitting gravitational radiation which extracts the rotational energy and angular momentum from the system, thereby leading to an inspiral of the two bodies towards each other. The dynamics of a compact binary consists of three phases: (i) The *early inspiral phase* in which the system spends 100's of millions of years and the luminosity in GW is rather low and the dynamics can be solved using approximation methods - the most popular being the post-Newtonian (PN) approximation. The inspiral signal has a characteristic shape, with slowly increasing amplitude and frequency and is called a *chirp* waveform. A binary signal that chirps (i.e. its frequency changes perceptibly during the course of observation) is an astronomer's *standard candle* [1] (see below) and by observing the radiation from a *chirping* binary we can measure the luminosity distance to the source. (ii) The *plunge* phase when the two stars are moving at a third of the speed of light and experiencing strong gravitational fields with the gravitational potential being $\varphi = GM/Rc^2 \sim 0.1$. This phase requires the full non-linear structure of Einstein's equations as the problem involves strong relativistic gravity, tidal deformation (in the case of BH-BH or BH-NS) and disruption (in the case of BH-NS and NS-NS) and has only recently been solved by numerical relativists (see below). Analytical solutions based on resummation of the PN series have been very successful in describing the merger phase. (iii) The *merger,* or *ringdown,* phase when the two systems have merged to form either a NS or BH, settling down to a quiescent state by radiating the deformations inherited during the merger. The emitted radiation can be computed using perturbation theory and gives the quasi-normal modes (QNM) of BH and NS. The QNM carry a unique signature that depends only on the mass and spin angular momentum in the case of BH, but depends also on the equation-of-state (EOS) of the material in the case of NS.

1. Post-Newtonian description of the inspiral phase

The adiabatic evolution of a compact binary, during which the emission of gravitational waves causes the component stars of the system to *slowly* spiral-in towards each other, can be computed very accurately using the post-Newtonian (PN) expansion of the Einstein equations. Currently, the dissipative dynamics is known [2] to order $O(v^7/c^7)$, where v is the characteristic velocity in the system.

For a binary consisting of two stars of masses m_1 and m_2 (total mass $M \equiv m_1 + m_2$ and symmetric mass ratio $\nu \equiv m_1 m_2/M^2$) and located at a distance $D_{\rm L}$, the dominant gravitational wave amplitudes are

$$h_+(t) = \frac{2\nu M}{D_{\rm L}}(1 + \cos^2\iota)\left[M\omega(t; t_0, M, \nu)\right]^{\frac{2}{3}}\cos\left[2\Phi(t; t_0, M, \nu) + \Phi_0\right], \qquad (2.2)$$

$$h_\times(t) = \frac{2\nu M}{D_{\rm L}}2\cos\iota\,\left[M\omega(t; t_0, M, \nu)\right]^{\frac{2}{3}}\sin\left[2\Phi(t; t_0, M, \nu) + \Phi_0\right], \qquad (2.3)$$

where ι is the angle of inclination of the binary's orbital angular momentum with the line-of-sight, $\omega(t)$ is the angular velocity of the equivalent one-body system around the binary's centre-of-mass and $\Phi(t; t_0, M, \nu)$ is the corresponding orbital phase. Parameters t_0 and Φ_0 are constants giving the epoch of merger and the orbital phase of the binary at that epoch, respectively.

The above expressions for h_+ and $h_\times$ are the dominant terms in what is essentially a PN perturbative series, an approximation technique that is used in solving the Einstein equations as applied to a compact binary. This dominant amplitude consists of only twice the orbital frequency. Higher order amplitude corrections contain other harmonics (i.e., phase terms consisting of $k\,\Phi(t)$, $k = 1, 3, 4, \ldots$). Also, the above expressions are written down for a system consisting of non-spinning components on a quasi-circular orbit. In reality, we can assume neither to be true. Waveforms for binaries on an eccentric inspiral orbit are known as are those with spin effects but we shall not discuss them in this Vision Document.

2. Standard Sirens of Gravity

Cosmologists have long sought for standard candles that can work on large distance scales without being dependent on the lower rungs of cosmic distance ladder. In 1986, Schutz [3] pointed out that gravitational astronomy can provide such a candle, or, more appropriately, a *standard siren*, in the form of a chirping signal from the coalescence of compact stars in a binary. The basic reason for this is that the gravitational-wave amplitude depends only on the ratio of a certain combination of the binary masses and the luminosity distance. For chirping signals observations can measure both the amplitude of the signal and the masses very accurately and hence infer the luminosity distance.

The detector response depends only on a small number of signal parameters, which can all be measured either directly or indirectly. The signal is insensitive to the composition of the component stars and there is no complicated modelling that involves the structure of the stars or their environments. Consequently, the measurement of the luminosity distance is precise, except for statistical errors, whose magnitude depends on the signal-to-noise ratio (SNR), and systematic errors due to weak gravitational lensing. We will discuss the relative magnitude of these errors later in this Vision Document.

Substituting the expressions given in Eq. (2.3) for h_+ and $h_\times$ in Eq. (2.1), we get

$$h(t) = \frac{2\nu M}{D_{\text{eff}}} \, [M\omega(t)]^{\frac{2}{3}} \cos[2\Phi(t) + \Phi_0']. \qquad (2.4)$$

Here D_{eff} is the effective distance to the binary, which is a combination of the true luminosity distance and the antenna pattern functions, and Φ_0' is a constant phase involving the various angles,

$$D_{\text{eff}} \equiv \frac{D_{\text{L}}}{[F_+^2(1 + \cos^2 \iota)^2 + 4F_\times^2 \cos^2 \iota]^{1/2}}, \quad \Phi_0' \equiv \Phi_0 + \arctan\left[-\frac{2F_\times \cos \iota}{F_+(1 + \cos^2 \iota)}\right]. \qquad (2.5)$$

Note that $D_{\text{eff}} \geq D_{\text{L}}$. In the case of non-spinning binaries on a quasi-circular orbit, therefore, the signal is characterized by nine parameters in all, $(M, \nu, t_0, \Phi_0, \theta, \varphi, \psi, \iota, D_{\text{L}})$.

Since the phase $\Phi(t)$ of the signal is known to a high order in PN theory, one employs matched filtering to extract the signal and in the process measures the two mass parameters (M, ν) (parameters that completely determine the phase evolution) and the two fiducial parameters (t_0, Φ_0). In general, the response of a single interferometer will not be sufficient to disentangle the luminosity distance from the angular parameters. However, EM identification (i.e., electromagnetic, especially optical, identification) of the source will determine the direction to the source, still leaving three unknown parameters $(\psi, \iota, D_{\text{L}})$. If the signal is a transient, as would be the case in ground-based detectors, a network of three interferometers will be required to measure all the unknown parameters and extract the luminosity distance.

Although the inspiral signal from a compact binary is a standard siren, there is no way of inferring from it the red-shift to a source. The mappings $M \to (1+z)M$, $\omega \to \omega/(1+z)$, and $D_{\text{L}} \to (1+z)D_{\text{L}}$, in Eq. (2.3), leave the signal invariant. Note that a source with an intrinsic (i.e., physical) total mass $M_{\text{phys.}}$ at a red-shift z will appear to an observer to be a binary of total mass $M_{\text{obs.}} = (1+z)M_{\text{phys.}}$. One must optically identify the host galaxy to measure its red-shift. Thus, there is synergy in GW and EM observations which can make precision cosmography possible, without the need to build a cosmic distance ladder. Later in this Vision Document we will see how to exploit compact binaries for fundamental physics and cosmography.

3. Harmonics from higher order amplitude corrections

In the simplest case of an interferometer that is stationary with respect to the source, the observed signal including amplitude corrections is given by [4–7]

$$h(t) = \frac{2M\nu}{D_L} \sum_{k=1}^{7} \sum_{n=0}^{5} A_{(k,n/2)} \, [M\,\omega(t)]^{\frac{n+2}{3}} \cos[k\,\Phi(t) + \Phi_{(k,n/2)}], \qquad (2.6)$$

where the coefficients $A_{(k,n/2)}$ and $\Phi_{(k,n/2)}$ are functions of $(\nu, \theta, \varphi, \psi, \iota)$. The quantities $(2M\nu/D_L)[M\omega(t)]^{\frac{n+2}{3}} A_{(k,n/2)}$ and $\Phi_{(k,n/2)}$ are the 'polarization' amplitude and phase of the wave, respectively, corresponding to the kth harmonic at the $(n/2)^{\text{th}}$ PN order. The orbital phase $\Phi(t)$ is a PN series, which, in the case of non-spinning binaries, is known to 3.5 PN order. The restricted post-Newtonian waveform corresponds to an approximation in which only the $k = 2$ and $n = 0$ (i.e., the lowest-order) term is retained.

Clearly, the full waveform has a lot more structure than what is revealed by the restricted waveform. The importance of the additional terms for detection in the context of ground-based and space-based interferometers was explored by Van Den Broeck and Sengupta [8, 9] and Arun, Iyer, Sathyaprakash and Sinha [10], respectively, who found that higher harmonics can extend the mass reach of the detectors by factors of 2 to 4. In the case of LISA this helps to detect binaries comprised of black holes that are more commonly found in galactic nuclei.

Furthermore, Sintes and Vecchio [11, 12] and Moore and Hellings [13, 14] in the case of LISA and, more recently Van Den Broeck and Sengupta [15], showed that the estimation of parameters improves remarkably when using the above waveform, as compared to the restricted waveform. More precisely, we will be able to measure the arrival time and chirp mass of a source an order-of-magnitude or better than if we had only used the restricted waveform.

4. Numerical relativity simulations

Hannam and Husa

Following breakthroughs in 2005 [16–18], it is now possible to numerically solve the full Einstein equations for the last orbits, merger and ringdown of comparable mass black-hole-binary systems, and to calculate the emitted GW signal. Subsequent dramatic progress has lead both to simulations of rapidly increasing numerical accuracy and physical fidelity, and to the inclusion of larger numbers of GW cycles before merger, allowing full GR waveforms to be in principle useful for searches of black-hole binaries of ever lower mass; see Fig. 3 in [19]. In order to extend numerical relativity waveforms to lower frequencies, hybrid post-Newtonian–numerical waveforms have been constructed, and comparisons of numerical results with post-Newtonian predictions are being continuously refined [20–23].

Results from numerical simulations of BH coalescence aid gravitational-wave astronomy in a number of ways, the consequences of which are still being explored:

- Template banks with complete inspiral-merger-ringdown waveforms may be constructed from phenomenological representations that attempt to fit (at least a portion of) the BBH parameter space with a reasonably small number of simulations.

- The parameters of the end-states of a BBH coalescence (in particular final spin and mass and recoil velocity) can be computed, and fitting formulas constructed to interpolate in the parameter space.

- Numerical or hybrid post-Newtonian–numerical waveforms can be injected into detector noise in order to calibrate detection pipelines.

- Post-Newtonian results, on which current matched-filtering searches are typically based, can be verified in the frequency band where both methods give results.

Determining the end state of a BBH coalescence, which is of immediate astrophysical relevance, has been an obvious first application of black-hole-binary simulations, notably the first fully general relativistic predictions of the recoil of the final black hole due to asymetric GW emission [24–26], and the spin of the final black hole as a function of the parameters of the input binary [27–29]. These results have had a direct impact on models

of galaxy formation and galactic black-hole-binary populations, and observational evidence for the large recoils possible for spinning black holes has been reported in [30].

An immediate application of numerically generated waveforms to gravitational wave data analysis is to inject them into detector noise and then test potential GW search pipelines against "real" signals. A first study of this type (the NINJA project) has been performed with simulated LIGO and Virgo noise [31], and has demonstrated that while current search methods are adequate for detection, their parameter estimation accuracy is poor. This is perhaps not a surprising result, but highlights the potential of numerical injections for the development of improved search techniques. Numerical injection studies may prove ideal for addressing template generation and parameter estimation issues in ET. The NINJA study also demonstrated that Bayesian parameter estimation methods, which used a phenomenological template bank obtained from matching numerical and post-Newtonian waveforms, could indeed take more advantage of the information from numerical simulations than searches based on a coarse grid sufficient for detections. One of the most important applications of numerical relativity-based template banks may indeed be detection follow-up codes for accurate parameter estimation.

Searches in GW detector data require waveforms that include hundreds or thousands of cycles before merger. It is not yet feasible to numerically simulate more than tens of inspiral cycles, and may never be practically necessary, because approximate post-Newtonian (PN) waveforms should be accurate enough to model the inspiral phase. Detailed comparisons of the longest and most accurate numerical waveforms with their PN counterparts have established levels of phase and amplitude accuracy for the PN approximants in the cases of equal-mass nonspinning binaries [20–22], equal-mass binaries with non-precessing spins [32], equal-mass nonspinning eccentric binaries [33], and one configuration of an unequal-mass precessing-spin binary [23]. These studies suggest that PN waveforms are sufficiently accurate up to the point during the inspiral at which numerical simulations can take over, although a full study relevant to both GW detection and parameter estimation for ET is yet to be performed. Also, similar studies are yet to be performed for the full black-hole-binary parameter space, and it remains to be seen if in general PN-waveform accruacy continues to such close separations for precessing-spin binaries. The comparison of different PN approximants to numerical waveforms has shown some discrimination in terms of quality, e.g. while the TaylorT4 approximant has performed extraordinarily for the equal mass nonspinning case, equal-mass spinning [32] evolutions suggested the TaylorT1 approximant to be overall more robust.

Much work has been done in connecting PN and NR waveforms, and using these to construct analytic models of full inspiral-merger-ringdown waveforms for subsets of the parameter space. This work has followed two appraoches: (1) waveform mdels based on a phenomenological ansatz [34–36], which to date includes nonspinning binaries with mass ratios up to 1:4; (2) using NR waveforms to determine free paramteers in an effective-one-body (EOB) model, which has also been done for nonspinning binaries [37–42]. These models are now being extended to spinning binaries, but work is also required in quantifying further the robustness of these models with respect to different constructions, and the accuracy of waveform ingredients, both PN and numerical.

One might expect that full inspiral-merger-ringdown waveforms will aid both detection and parameter estimation, and indeed it has been shown that the horizon distance (the source distance at which the GW signal has some minimum signal-to-noise ratio) can increase by an order of magnitude over the use of only inspiral or ringdown templates [35]. Estimation

TABLE I: This Table gives the expected coalescence rates per Mpc^3 Myr in the local universe ($z \simeq 0$). Also shown are predicted event rates in Advanced LIGO (AL) and Einstein Telescope (ET)

Rate/Events	BNS	NS-BH	BBH
Rate (Mpc^{-1} Myr^{-1})	0.1-6	0.01-0.3	$2 \times 10^{-3} - 0.04$
Event Rate (yr^{-1} in AL)	1-30	1-300	3-300
Event Rate (yr^{-1} in ET)	$O(10^5 - 10^6)$	$O(10^4)$	30-?

of source parameters also improves, particularly for high-mass binaries (100-200 $M_\odot$), with the estimation of the mass, mass-ratio and sky location improving by an order of magnitude over inspiral templates [43]. For cases with extremely high signal-to-noise ratio, where only the last cycles and merger/ringdown are in the detector band, if the model waveform includes higher harmonics then estimates of the sky location can be accurate to within a few arcminutes [44, 45]; these studies were performed for the LISA detector, but the general result is likely to carry over to ET, How accurate do numerical waveforms need to be for ET, and how accurate *can* they be? It has been shown that the numerical accuracy of current waveforms is sufficient for both detection and parameter-estimation purposes with LIGO and Virgo [46], in that current equal-mass nonspinning waveforms will be indistinguishable as search templates in those detectors. For ET, where SNRs will often exceed 25, however, this is no longer the case, and more accurate waveforms will be required. Following the rapid progress in numerical simulations in the last four years, it seems quite reasonable to expect sufficient accuracy for ET requirements within the next 5-10 years. This includes greater accuracy in the calculation of subdominant harmonics, which is still a challenge in most codes.

Of more difficulty will be simulations of binaries with much larger mass ratios. To date long simulations (> 10 inspiral cycles) have been performed only for binaries with mass ratios up to 1:6. The computational requirements at present scale *at best* linearly with the mass ratio, and this makes long simulations of mass ratios above 1:10 difficult, and out of the question for 1:100. Simulating those cases in full general relativity will require real breakthroughs in either numerical techniques, the formulation of the problem, or both.

Intense efforts are underway within the numerical-relativity community to address all of these issues, and it is expected that accurate numerical-relativity-based template banks can be produced well within the time frame of the design and construction of ET.

5.   Cosmological evolution of compact object populations

Babak, Amaro-Seoane, Bulik

6.   Expected coalescence rates

Bulik and O'Shaughnessy

Coalescence rates: Black holes or neutron stars are expected to form after Type II supernovae, which occur roughly once a century in galaxies like our own. Most stars seem to form in binaries binaries; a fraction of compact binary progenitors will survive the kicks that
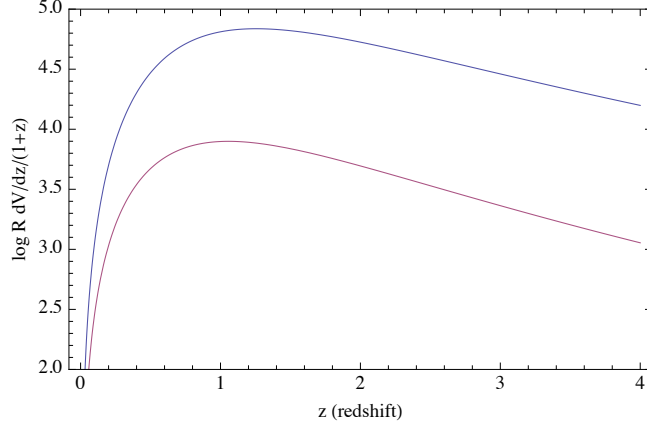
FIG. 2: (Log of the) rate of mergers on our past light cone per redshift, as expected for NS-NS (blue) and BH-NS (green) assuming (i) their merger rates trace the star formation history [47] and (ii) their present-day values agree with merger rate estimates.

supernovae impart; and roughly half of the remaining low-mass binaries (BH-NS; NS-NS) will inspiral and eventually merge through the gradual emission of radiation. With roughly 0.01 Milky Way-like galaxy per Mpc^3, we anticipate a rate per comoving volume ρ_c large enough to permit many detections even for advanced-LIGO scale detectors [Table I]. For example, the binary pulsar population in the Milky Way implies a local NS-NS merger rate $\rho_c^{(NS-NS)} \simeq 0.2 - 6$ Myr^{-1} Mpc^{-1} [48–50].

With its vastly greater sensitivity, the Einstein Telescope will reach deep back into the universe. Due to an enhanced the star formation rate between $z \simeq 1 - 3$ [47], ET will probe a regime of possibly significantly enhanced compact object merger rates [51? , 52]. By way of illustration, following Regimbau and Hughes [51], because double neutron stars have a relatively short delay time, their formation rate roughly traces the star formation rate of the universe. Scaling up from the Milky Way rate R_{MW} via an estimate for the star formation rate $\dot{\rho}_{SFR}$ [47], the rate at which mergers occur a redshift bin dz on our past light cone is approximately [Figure 2]

$$\frac{dR}{dz} = \frac{dV_c}{dz}\frac{\mathcal{R}(t)}{1+z} \simeq \frac{dV_c}{dz}R_{MW}\rho_{MW}\frac{\dot{\rho}_{SFR}/\dot{\rho}_{MW}}{1+z} \qquad (2.7)$$

Depending on the target sensitivity and beampattern of the ET network, the expected detection rate is roughly proportional to the integral of this rate up to some peak redshift. For most target ET sensitivities the angle-averaged redshift $z_{max} > 1$ for double neutron stars, suggesting $O(10^6)$ detections per year. The enormous collections of events that ET-scale instruments will provide permit high-precision modeling inaccessible with the sparse statistics available to smaller detectors.

Lacking direct observational input, predictions for BH-BH and BH-NS binaries rely entirely on theory. Studies of isolated binary evolution in the Milky Way [53–56] and local universe [52] produce event rates roughly in the ranges shown in Table [?], depending on the assumptions adopted in the model. As with the NS-NS rate, the BH-NS merger rate is roughly proprotional to the star formation rate [?] and therefore also increases substantially with redshift [Figure 2]; many detections are expected.

The BH-BH merger rate is much less certain. First, the long delays between BH-BH birth and merger imply black holes born in the early universe could merge now [52]. Second, BH
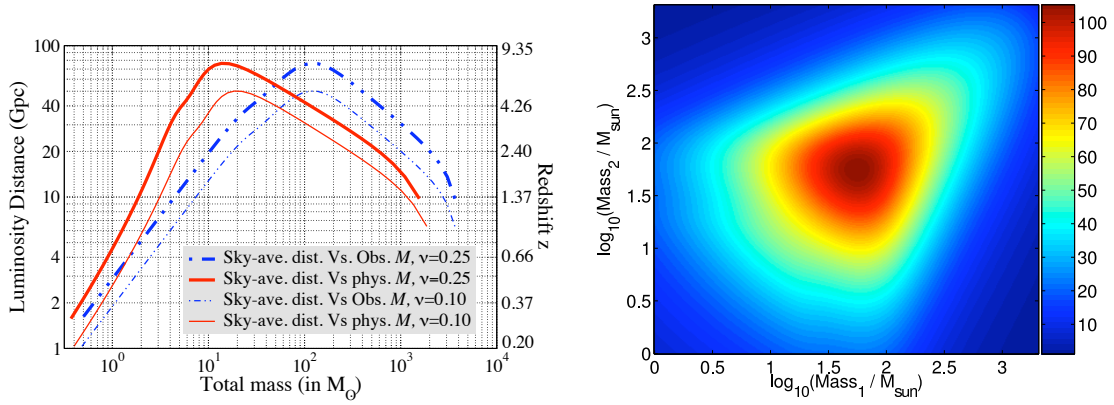
FIG. 3: The left panel shows the range of the Einstein Telescope for inspiral signals from binaries as a function of the *intrinsic* (red solid line) and *observed* (blue dashed line) total mass. We assume that a source is visible if it produces an SNR of at least 8 in ET. The right panel shows in the plane of component masses the SNR for binaries at a distance of 3 Gpc.

masses depend strongly on the metallicity of the gas from which the progenitor star forms, as stellar winds operate much less efficiently [57]; so does the BH-BH binary formation rate [58]. In other words, low metallicity environments form both more binaries and binaries that can be detected farther away. Even restricting attention to the local universe, low-metallicity environments should be significantly over-represented in the present-day detection rate [59]. For example, the nearby BH-BH progenitor binary IC 10 X-1 both lies in a low metallicity environment and suggests a high BH-BH detection rate for initial LIGO ($O(0.5)$yr, strongly dependent on survey selection effects; see [60]). Further, in the early universe, where fewer generations of stars have produced metals, very massive binaries could form very frequently [58]. Third, being the most massive compact objects, black holes can *mass segregate* in interacting protoclusters. If enough protoclusters persist long enough for this process to occur, the BH-BH binary merger rate could be vastly enhanced [61–63]. As a practical matter, theory provides no useful upper bound; for example, the local BH-BH rate per mass bin is constrained only by existing gravitational wave measurements CITE LIGO.

———-

TO SATHYA: Why no BH rate yet? ROS wants to think about the upper bound. The impact of low metallicity/Pop-III and clusters in particular; what the iLIGO upper limit would mean extrapolated to the early universe; and how the "exhaustion problem" comes in (e.g., if you assume the BH-BH rate traces the SFR, then increasing our range shouldn't increase the number of detections much; we've "exhausted" the supply on our light cone). I've included a safe lower bound.

More references will be needed to avoid offense – current selection is Belczynski/Bulik biased.

Check if rates.tex is available yet

If not, use Tania R's summary in [51] to cross-link against the table.

7. Expected distance reach and mass range

Sathya, Bose, Van Den Broeck

The sky-position averaged distance up to which ET might detect inspiral signals from coalescing binaries with an SNR of 8 is shown in Fig. 3. We plot the range both as a

TABLE II: Threshold between resolved and unresolved NS-NS binaries (left) and NS-BH binaries (right) for different estimates of the source rate $\dot{\rho}_c^o$ and detector lower frequency bound f_L. No value means that the number of sources at the detector is always < 1 or < 10.

f_L	$\dot{\rho}_c^o$	z_*	z_{**}	f_L	$\dot{\rho}_c^o$,	z_*	z_{**}
10	0.01	-	-	10	0.001	-	-
	0.4	0.8-0.9	-		0.04	-	-
	1	0.5-0.6	> 2		1	1.1-1.4	-
	10	0.2	0.5-0.6		10	-	-
5	0.01	-	-	5	0.001	-	-
	0.4	0.4	1-1.2		0.04	-	-
	1	0.25	0.6-0.7		1	0.5	> 1.6
	10	0.1	0.25		10	-	-
1	0.01	0.3	0.8	1	0.001	> 2.3	-
	0.4	0.08	0.2		0.04	0.3	0.8-0.9
	1	0.06	0.13		1	0.1	0.2
	10	0.03	0.06		10	-	-

function of the intrinsic (red solid lines) and observed (blue dashed lines) total mass. A binary comprising two $1.4\,M_\odot$-neutron stars (BNS) can be observed from a red-shift of $z \simeq 2$, and that comprising a $1.4\,M_\odot$-neutron star and a $10\,M_\odot$-black hole (NS-BH) from $z \simeq 4$.

8. Confusion background from compact binaries in ET

Regimbau With actual and advanced interferometers, whose horizon is only a tens or a hundreds of Mpc only, the detection of individual binaries is limited by the instrumental noise but with the third generation Einstein Telescope, which is expected to reach redshifts of $z \sim 1$ for NS-NS and $z \sim 2$ for NS-BH other problems may appear. For instance, after $z \sim 1$, gravitational lensing may become significant, altering distance measurements, and thus the quality of binaries as standard candles to proble cosmology and dark energy. Another problem at large distances is the formation of a confusion foreground, in which it may become difficult to resolve sources individually. Table II (Regimbau and Hughes 2009) [51] gives the redshifts z_* and z_{**} at which the number of NS-NSs and NS-BHs present at the detector becomes > 1 (column 2) and > 10 (column 3) for three values of the frequency lower bound (10, 5 and 1 Hz) and for optimistic, realistic and pessimistic estimates of the coalescence rate (see previous section).

For NS-NS, both z_* and z_{**} are well within the horizon of the planned Einstein Telescope, if its low frequency sensitivity is at $f_L = 1$ Hz (ET1). If $f_L = 5$ Hz (ET5), we expect the popcorn background to occur before the detection horizon, and more likely around $z_* \sim 0.25 - 0.4$, unless our most pessimistic coalescence rates are accurate ($\dot{\rho}_c^o < 0.015$ Myr^{-1} Mpc^{-3}). The transition to a Gaussian stochastic most likely occurs at $z_{**} \sim 0.6 - 1.2$, but can fall beyond the detection horizon if $\dot{\rho}_c^o < 0.15$ Myr^{-1} Mpc^{-3}. The conclusions for NS-BH binaries are similar to those for NS-NS for ET1, z_* and z_{**} are both more likely
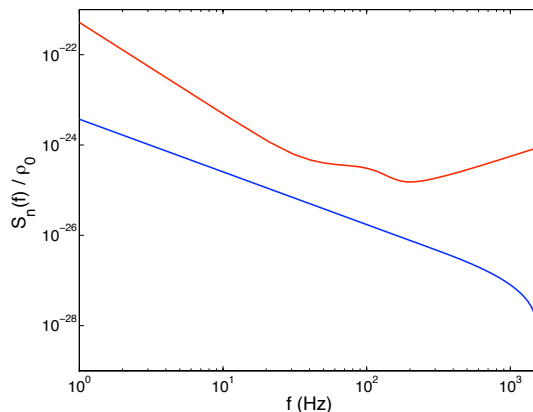
FIG. 4: Spectral energy density of the background produced by the coalescence of double neutron stars, compared to the planned sensitivity of Einstein Telescope.

to occur well below the horizon. For ET5 however there is not likely to be enough sources to create a Gaussian stochastic background (even a popcorn background), except for the most optimistic coalescence rates ($\dot{\rho}_c^o > 0.6$ Myr^{-1} Mpc^{-3}). As a consequence, NS-BHs may always be resolved provided that we can separate them with adequate data analysis strategies in the popcorn regime. This result motivates very careful analysis of how data would be analyzed. Experience from the Mock LISA Data Challenges (Babak et al. 2008) [64] and ideas developed for the Big Bang Observatory (Cutler et al. 2006) [65] prove that disentangling multiple signals in a gravitational-wave detector's datastream is certainly possible.

Figure 4 shows the foreground from the extragalactic population of double neutron stars, along with the planned ET sensitivity. Unless the coalescence rate is well above our current estimates, this foreground is well below the instrumental noise, and shouldn't affect the detection of other sources.

9. Measurement accuracies

Van Den Broeck

B. Continuous wave sources

Krishnan

The kinds of sources we consider in this section are ones which last for at least a few weeks or years, whose amplitude is constant (or at least roughly constant), and whose frequency varies relatively slowly over the observation time. These signals are expected to be produced by rapidly rotating non-axisymmetric neutron stars which are either isolated or in binary systems.

The waveforms for the two polarizations are taken to be

$$h_+(t) = A_+ \cos \Phi(t), \qquad h_\times(t) = A_\times \sin \Phi(t) \tag{2.8}$$

where t is the time in the frame of the moving, accelerating detector, $\Phi(t)$ is the phase of the gravitational wave and $A_{+,\times}$ are the amplitudes; $A_{+,\times}$ are constant in time and depend on the other pulsar parameters such as its rotational frequency, moments of inertia, the orientation of its rotation axis, its distance from Earth etc. The phase $\Phi(t)$ takes its simplest form when the time coordinate used is τ, the proper time in the rest frame of the neutron star:

$$\Phi(\tau) = \phi_0 + 2\pi \sum_{n=0}^{s} \frac{f_{(n)}}{(n+1)!} \tau^{n+1} \tag{2.9}$$

where ϕ_0, $f_{(0)}$ and $f_{(n)}$ ($n \geq 1$) are respectively the phase, instantaneous frequency and the spin-down parameters in the rest frame of the star at the fiducial start time $\tau = 0$, and s is the number of spin-down parameters included in our search. If ι is the angle between the line of sight to the star and its axis, then it is useful to write the amplitudes $A_{+,\times}$ in terms of a single number h_0

$$A_+ = \frac{1}{2} h_0 (1 + \cos^2 \iota), \qquad A_\times = h_0 \cos \iota. \tag{2.10}$$

There are a number of mechanisms which may cause the star to be emitting gravitational waves. These include deformations of the neutron star crust, precession, magnetic fields, internal oscillation modes of the neutron star fluid etc. **more**

1. Isolated neutron stars

Krishnan

There are at present hundreds of pulsars known from either radio or X-ray observations. The parameters of many of these systems, i.e. the sky location and frequency evolution, have been accurately measured. We assume the GW phase evolution to be tightly correlated with the rotational phase as inferred from electromagnetic observations. For gravitational wave emission due to a non-negligible ellipticity, the GW emission occurs at twice the rotational frequency of the star. These two assumptions constrain the expected gravitational waveform upto an unknown initial phase ϕ_0, amplitudes $A_{+,times}$ and polarization angle ψ. It is then easy to search over these unknown parameters [66] and to either measure the amplitude h_0, or in the case that no signals are detected, to set upper limits on it.

The benchmark for these searches is the indirect upper bound on h_0 set by assuming that all of the kinetic energy of the star lost in the spindown is channeled into gravitational radiation. A straightforward calculation leads to the so-called spindown limit h_0^{sd}:

$$h_0^{sd} = 8.06 \times 10^{-19} \frac{I_{38}}{d_{kpc}} \sqrt{\frac{|\dot{\nu}|}{\nu}} \tag{2.11}$$

where $I_{38} = I/10^{38} \mathrm{kg\text{-}m}^2$, d_{kpc} is the distance to the star in kpc, $\dot{\nu}$ is the spindown rate and ν is the spin frequency. This assumption is not expected to hold for any of the known pulsars where electromagnetic braking explains most of the spindown. Nevertheless, the spindown limit still a very useful benchmark for quantifying the astrophysical relevance potential targets and search results.

This procedure has been carried out for a number of known pulsars using data from the LIGO, GEO and Virgo detectors [67–69]. One highlight from these results is beating
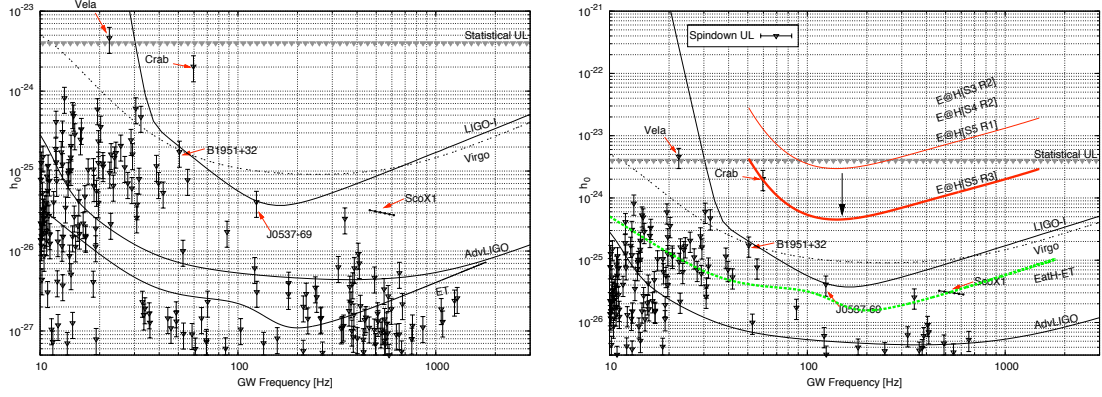
FIG. 5: The left hand plot shows upper limits and the spindown limits for the known pulsars. Adapted from R.Prix, 2006. The right hand plot shows expected sensitivity for blind searches.

the spindown limit for the Crab pulsar [69] where the gravitational wave luminosity os constrained to be less than 6% of the spindown luminosity.

Let us now consider design noise curves for various detectors, including ET, and compare detectable values of h_0 with the spindown limits for a number of known pulsars. A useful benchmark for the detectability is given by

$$h_0 = 11.4\sqrt{\frac{S_n(f)}{DT_{obs}}} \tag{2.12}$$

where $S_n(f)$ is the detector noise power-spectral density at a frequency f, T_{obs} is the observation time, and D is the number of detectors. The factor of 11.4 corresponds to a false alarm rate of 1% and a false dismissal rate of 10%. Figure 5 shows (left panel) the detectable amplitude for Initial and Advanced LIGO, Virgo and ET, and spindown limits for various known pulsars.

Let us turn now to the wide parameter space searches. Here we don't target a known pulsar but rather, as an example, one whose radio pulse is not beamed towards; such a neutron star might still be visible in the GW sky. These searches are computationally limited because the number of templates increases much faster than linearly with the observation time T_{obs}. The large number of templates affects the search sensitivity in three basic ways. The first and most obvious one is simply the discreteness of the template grid. Secondly, it also leads to a large number of statistical trials which increases the false alarm rate and thus leads to a larger effective threshold. Finally, and most importantly, it limits the largest observation time that we can consider; even given the increases in computer power following Moore's law, this will most likely still be true in the ET era.

The problem of computational cost is addressed by the so-called *semi-coherent* methods. These rely on breaking up the full data set into shorter segments, analyzing the segments coherently and combining the power from the different segments incoherently; there are a number of different techniques available for performing the incoherent combination **cites**. For these searches, the sensitivity, incorporating all the effects mentioned above is typically given by

$$h_0 \approx \frac{25}{N^{1/4}}\sqrt{\frac{S_n(f)}{DT_{coh}}}. \tag{2.13}$$

This has been found to be a fairly good estimate (within $\sim 20\%$) of previous semi-coherent searches (see e.g. [70]).

C. Sensitivity trade-off

Two sensitivity curves of ET have been proposed by S. Hild (the "pink" and "green" curves in his presentation at the Cardiff WP4 Meeting:
https://workarea.et-gw.eu/et/WG4-Astrophysics/meetings/cardiff-090325/
ET Sensitivity News, slide 10). One is the *ET-B* curve and the other, that we call it ET-B2, has a much worse sensitivity below $\sim 3~Hz$ but better around 10 Hz. Let us see what changes in the two cases for the search of GW from both known and unknown neutron stars. In Fig.(6) the top plot shows the minimum detectable amplitude, assuming *ET-B* sensitivity, an observation time $T_{obs} = 5~yr$, a false alarm probability of 1% and a false dismissal probability of 10%, see Eq.(2.12), versus the spin-down limit of the known pulsars (taken from the ATNF Catalogue:
http://www.atnf.csiro.au/research/pulsar/psrcat/). The bottom plot is done using (an approximate fit of) the *ET-B2* sensitivity curve. The important point is that no known pulsar (up to now) could emit a detectable signal with frequency below $\sim 2.5Hz$. This means that there is no gain in having a good sensitivity at extremely low frequencies. On the other hand, having a better sensitivity around 10 Hz impacts positively on the possibility of detection. This can be clearly seen also in Fig.(7) where the ellipticity corresponding to the minimum detectable amplitude is plotted, only for the sources for which the spin-down limit can be beaten in the given observation time T_{obs}. Not only the number of pulsars for which the spin-down limit can be beaten is larger for the *ET-B2* curve (774 vs. 444) but, more important, the minimum ellipticy needed to produce a detectable signal is ~ 1 order of magnitude lower in the 10 Hz range. For instance, with *ET-B* we tipically need ϵ in the range $0.1 - 5 \cdot 10^{-4}$ range for pulsars emitting around 10 Hz, while $\epsilon \sim 0.1 - 1 \cdot 10^{-5}$ is enough with *ET-B2*. The very few pulsars at frequencies below $\sim 3~Hz$ for which the spin-down limit could be beaten with *ET-B*, but not with *ET-B2*, correspond to ellipticity in the 10^{-2} range, then not very likely also assuming exotic equation of state for neutron star matter.

The same kind of conclusion is reached when considering the *blind* search for unknown neutron stars. For this case we plot in Fig.(8) the maximum distance of a source to be selected among the candidates of an all-sky incoherent or semi-coherent search. An observation time $T_{obs} = 5~yr$ and an FFT duration $T_{FFT} \simeq \frac{1.1 \cdot 10^5}{\sqrt{f}}~s$, such that the Doppler effect does not spread the signal power outside a frequency bin, are assumed. Moreover, the threshold for the selection of candidates is chosen in order to have 10^9 candidates. In practice, we do not expect detections for signal frequencies below $\sim 10~Hz$ (the corresponding r_{max} becomes unrealistically small). Then, having a better sensitivity at very low frequencies gives basically no gain. On the other hand, having a better sensitivity around 10 Hz somewhat increases the possibility of detection: for instance, assuming $\epsilon = 10^{-5}$, the maximum distance that a search can reach goes from $\sim 10~pc$ with *ET-B* to $\sim 100~pc$ with *ET-B2* at 10 Hz, while it goes from $\sim 150~pc$ to $\sim 500~pc$ at 20 Hz. This conclusion does not change even assuming a long coherent step (compatible with the computing power we can think will be available in the ET era), because the sensitivity increases only as $T_{coh}^{1/4}$, see Eq.(2.13).
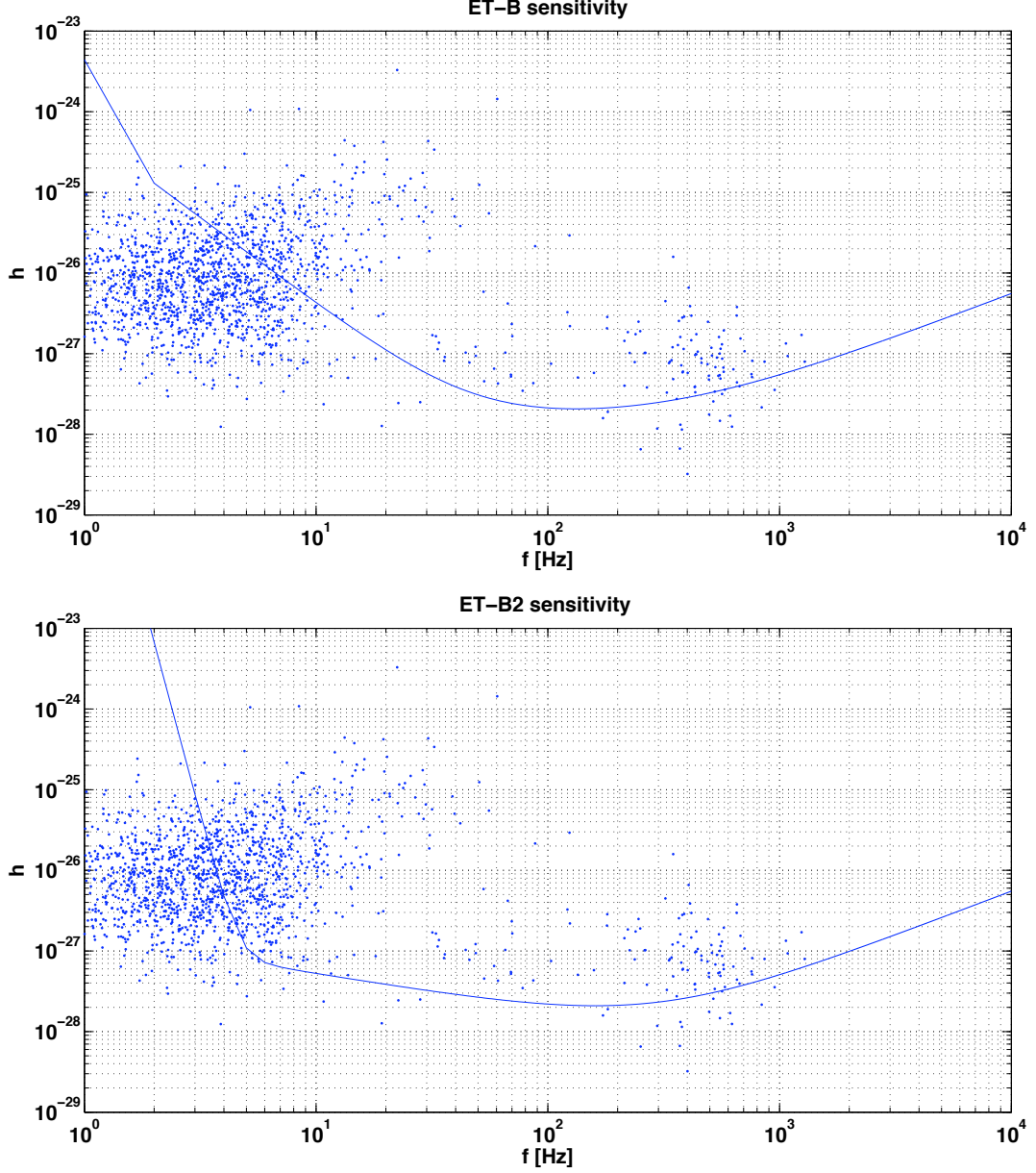
FIG. 6: Minimum detectable amplitude with *ET-B* sensitivity (top) and *ET-B2* (bottom). An observation time $T_{obs} = 5\ yr$, a false alarm probability of 1% and a false dismissal probability of 10% are assumed.

1. Low-mass X-ray binaries

Watts, Krishnan

Observations of accreting neutron stars lead to perhaps the most important reason why, irrespective of the mechanism at work, at least some neutron stars might be actally emitting detectable gravitational waves. This is the observation that even the fastest accreting neutron stars spin at rates much lower than the expected break-up frequency. The current record is 716 Hz **cite**, while the theoretically expected upper limit is more than 1 kHz **cites**. Following a suggestion by Bildsten [71], it is possible that this limit occurs because
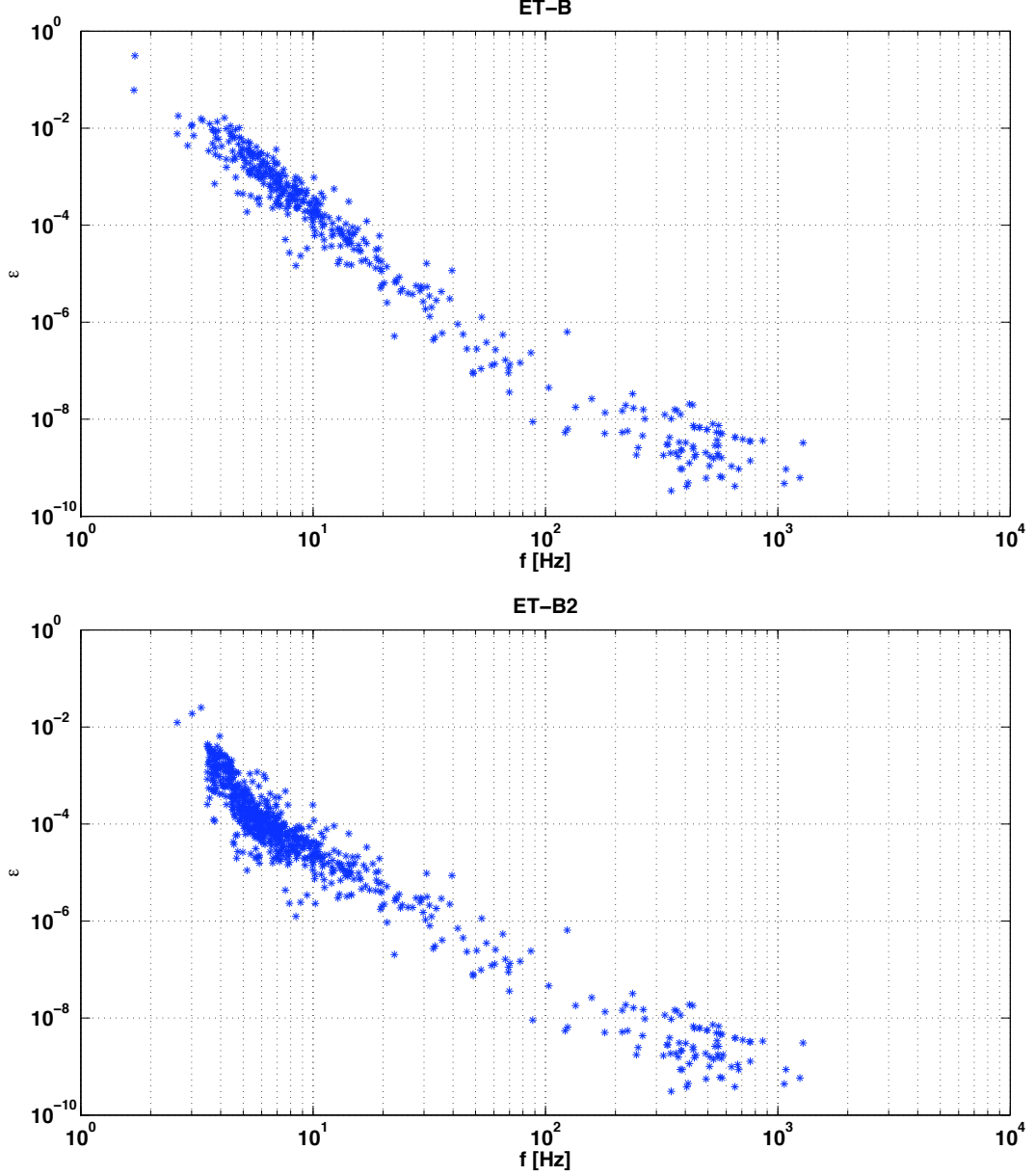
FIG. 7: Minimum detectable ellipticity for known pulsars assuming *ET-B* sensitivity (top) and *ET-B2* sensitivity (bottom). The search parameters are the same as for Fig.(6).

of the balance between the spin-up torque due to the accreting matter, and the spindown torque due to gravitational wave emission. A short calculation assuming a link between the observed X-ray luminosity with the accretion rate, and taking the mountain scenario for the emission mechanism leads to the following estimate of the GW amplitude:

$$h_0 = 3 \times 10^{-27} F_{-8}^{1/2} \left(\frac{R}{10\text{km}} \right)^{3/4} \left(\frac{1.4 M_\odot}{M} \right)^{1/4} \left(\frac{1 \text{ kHz}}{\nu_s} \right)^{1/2}. \tag{2.14}$$

This is seen to be depend on frequency: $h_0 \propto \nu_s^{-1/2}$.

Spin frequency measurement plays an important role in what follows and, as we shall see,
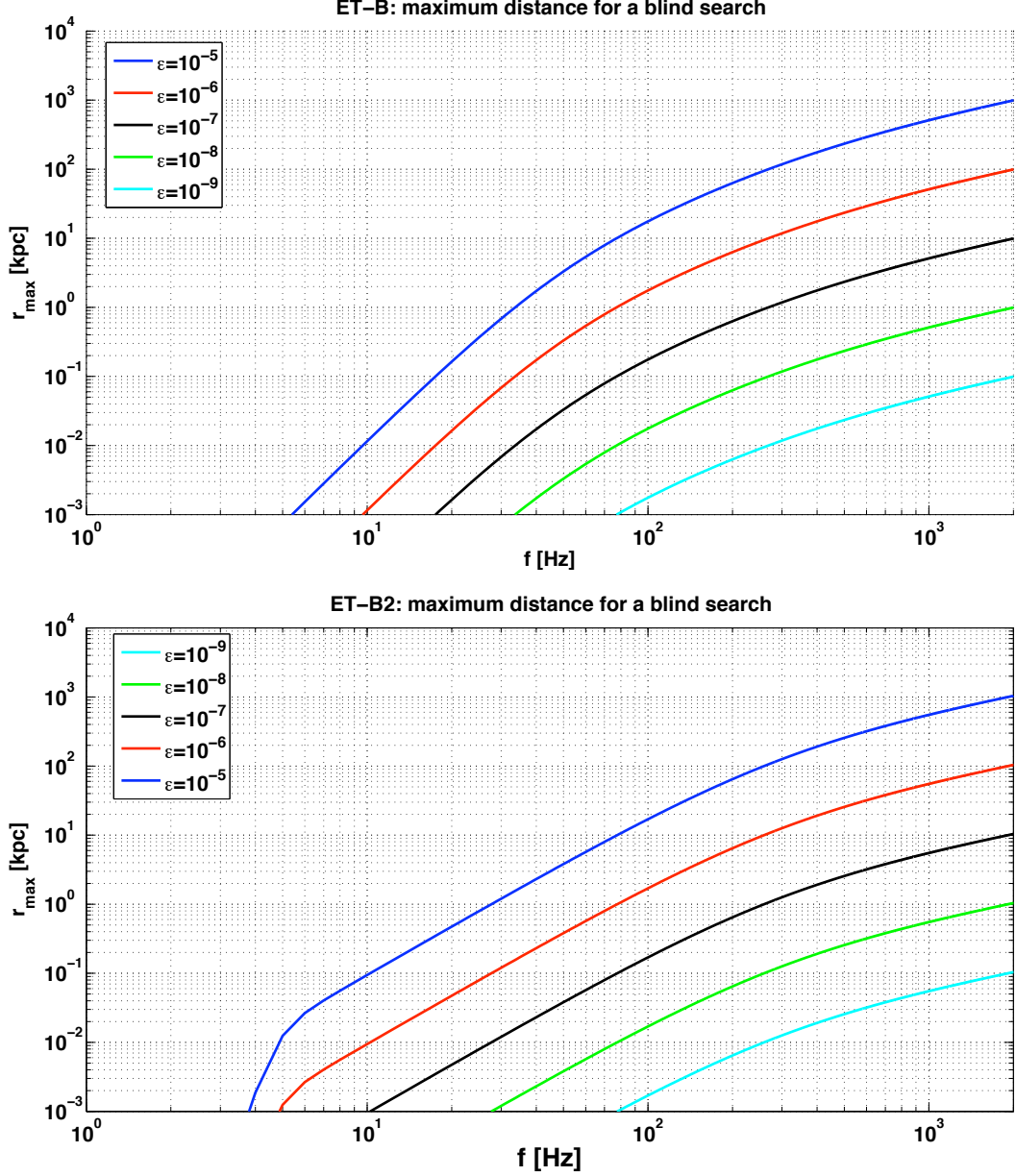
FIG. 8: Maximum distance of an unknown source in order to be selected among the candidates of an all-sky search with *ET-B* sensitivity (top) and *ET-B2* sensitivity (bottom). Search parameters are given in the text.

can [72]

D. Stochastic background

Regimbau

The superposition of all the sources of gravitational waves since the Big Bang produces a stochastic background, which could be detected by cross-correlating two (or more) detectors. We can distinguish between two contributions: a background from cosmological origin,
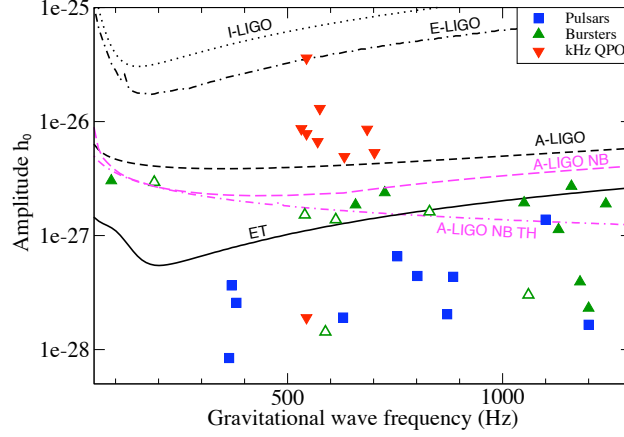
FIG. 9: Sensitivity and the spin-balance limit for the accreting neutron stars.

memory of the early stages of the Universe and often seen as the Graal of GW astronomy, and a background of astrophysical origin, memory of the evolution of the galaxies and star formation. The lastest LIGO upper limit beat the Bing Bang Nucleosynthesis bound in the range $40 - 170$ Hz and put interesting constraints on models of cosmic strings and pre Bing Bang scenarios. The astrophysical background is also promising since its detection would put strong constraints on the physical properties of compact objects and their evolution with redshift, such as the mass of neutron stars or black holes, the ellipticity and the magnetic field of neutron stars, the angular momentum of black holes, the rate of compact binaries. The optimal strategy to search for a Gaussian (or continuous) stochastic background, which can be confounded with the intrinsic noise background of the instrument, is to cross correlate measurements of multiple detectors. The spectrum of the gravitational stochastic background is usually characterized by the dimensionless parameter (Allen and Roman 1999) [73]:

$$\Omega_{gw}(\nu_o) = \frac{1}{\rho_c} \frac{d\rho_{gw}}{d\ln\nu_o} \qquad (2.15)$$

where ρ_{gw} is the gravitational energy density, ν_o the frequency in the observer frame and $\rho_c = \frac{3H_0^2}{8\pi G}$ the critical energy density parameterneeded to close the Universe today. This quantity is related to the spectral energy density parameter through the relation:

$$S_h(\nu_o) = \frac{3H_0^2}{4\pi^2} \frac{1}{\nu_o^3} \Omega_{gw}(\nu_o) \qquad (2.16)$$

When the background is assumed to be isotropic, unpolarized and stationary, the cross correlation product is given by [73]:

$$Y = \int_{-\infty}^{\infty} \tilde{s_1}^*(f)\tilde{Q}(f)\tilde{s_2}(f)df \qquad (2.17)$$

and the expected variance which is dominated by the noise by:

$$\sigma_Y \simeq \int_{-\infty}^{\infty} P_1(f)P_2(f)\tilde{Q}(f)df \qquad (2.18)$$

where

$$\tilde{Q}(f) \propto \frac{\gamma(f)\Omega_{\mathrm{gw}}(f)}{f^3 P_1(f) P_2(f)} \tag{2.19}$$

is a filter that maximizes the signal to noise ratio (S/R). In the above equation, $P_1(f)$ and $P_2(f)$ are the power spectral noise densities of the two detectors and γ is the normalized overlap reduction function, characterizing the loss of sensitivity due to the separation and the relative orientation of the detectors. The three arms of ET form three independent detectors with opening angles $\alpha = 60$ degree and rotated by $\beta = 120$ deg. The overlap reduction function between two detectors is almost constant up to 10^3 Hz and equal to $\gamma = \sin^2(\alpha)\cos(2\beta) = -3/8$ (see Figure). The optimized S/N ratio for an integration time T, a false alarm rate α and a detection rate γ is given by:

$$\frac{S}{N} = \frac{3H_0^2}{10\pi^2}\sqrt{T}((\mathrm{erf}^{-1}(2\alpha) - \mathrm{erf}^{-1}(2\gamma)) \int_{f_l}^{f_h} df \frac{\gamma^2(f)\Omega_{\mathrm{gw}}^2(f)}{f^6 P_1(f) P_2(f)})^{1/2}. \tag{2.20}$$

The sensitivity is usually given in term of the minimal detectable amplitude corresponding to a stochastic background with constant spectrum $\Omega_{gw}(f) = \Omega_0$:

$$\Omega_{\mathrm{min}} = \frac{10\pi^2}{3H_0^2\sqrt{T}}((\mathrm{erf}^{-1}(2\alpha) - \mathrm{erf}^{-1}(2\gamma)) \int_{f_l}^{f_h} df \frac{\gamma^2(f)}{f^6 P_1(f) P_2(f)})^{-1/2} \tag{2.21}$$

and the 90 % confidence level upper limit can be calculated as $1.28\Omega_{\mathrm{min}}$. Using the possible ET design sensitivity defined in this document, we find $\Omega_{\mathrm{min}} \sim 5 \times 10^{-12}$ and an upper limit of $\Omega_{\mathrm{min}} \sim 6.5 \times 10^{-12}$, for one year of integration, a false alarm rate of 10% and a detection rate of 90%, that is to say two orders of magnitude better than two coincident and co-located advanced LIGO. It is worth mentioning that it is not sure yet we can ever get rid of the correlated noise, but we can certainly be able to reduce it by correlating interferometers formed by specific combinations of the three arms. If so we should be able to put very strong constraints on both the cosmological (see section VI) and the astrophysical contributions, and maybe detect some of them. For instance, unless we overestimate the rate by orders of magnitude, we should be able to see the background from coalescing double neutron star binaries (Regimbau and Mandic 2008) [74].

E. Burst sources

Christian Ott,Chassand-Mottin

F. Probing Core-Collapse Supernova Physics

Stellar collapse is the most energetic event in the Universe, releasing $\sim 10^{53}$ erg of gravitational energy in the compression of a massive star's iron core to a neutron star. Most of this energy ($\sim 99\%$) is emitted in neutrinos and only about 10^{51} erg go into energy of the core-collapse supernova (CC-SN) explosion. CC-SNe (SN types II, Ib, Ic) are ~ 10 times more frequent than thermonuclear type-Ia SNe. A SN explosion pollutes the interstellar medium with the nucleosynthetic products of stellar evolution (CC-SNe are the Universe's primary source of oxygen) and enriches via the r-process the universe with rare heavy isotopes. The
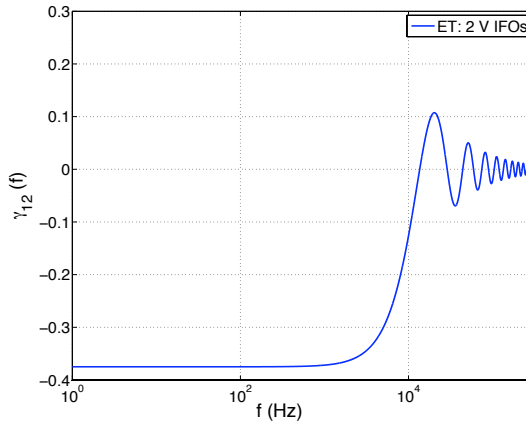
FIG. 10: Overlap reduction function for two ET detectors with opening angles $\alpha = 60$ degree and rotated by $\beta = 120$ deg

perturbation caused by an SN in its vicinity can trigger the formation of stellar systems and stellar collapse and CC-SNe are the birth sites of neutron stars (NSs) and stellar-mass black holes (BHs).

The Supernova Problem and GW observations The precise mechanism of explosion operating in CC-SNe is unknown [75–77]. When the inner part of the collapsing iron core reaches densities close to those in atomic nuclei, the strong force leads to a stiffening of the nuclear equation of state (EOS), resulting in *core bounce* of the inner core into the still infalling outer core. A shock wave is formed that propagates outward in mass and radius, but quickly loses energy due to the breakup of heavy nuclei and neutrinos that carry away energy from the postshock layer. The shock stalls, turns into an accretion shock and must be *revived* to drive a CC-SN explosion. If this does not happen, a BH will form on an accretion timescale of ~ 2 s. *What is the mechanism of shock revival?* This is the fundamental question and primary unsolved problem of CC-SN theory. Indications are strong that the CC-SN mechanism involves a multitude of multi-dimensional processes, including rotation, convection/turbulence, and various hydrodynamic instabilities of the stalled shock and in the proto-NS. This opens up the possibility of probing the supernova mechanism with gravitational waves (GWs). GWs, even more so then neutrinos, carry direct direct dynamical information from the supernova engine deep inside a dying massive star, a region generally inaccessible by the traditional means of observational astronomy. GWs form a core-collapse event have the potential of putting very strong constraints on the CC-SN mechanism [77, 78]. With initial and certainly second-generation interferometric GW detectors, this should be possible for an event in the Milky Way ($D \sim 10 - 15$ kpc) and the Magellanic Clouds [77] ($D \sim 50 - 70$ kpc), but even optimistic estimates of the CC-SN rate in this region do not predict more than $\sim 1 - 2$ events per century. This number roughly doubles if one includes the entire local group ($D \sim 1$ Mpc). In the region from $3 - 5$ Mpc a number of starburst galaxies increase the predicted and observed integrate SN rate to $\sim 0.5 \, \text{yr}^{-1}$. At $D \sim 10$ Mpc it is $\gtrsim 1 \, \text{yr}^{-1}$.

Supernova Science with ET The GW emission processes in a CC event emit GW strains h in the range $10^{-24} - 10^{-22} \, (D/1 \, \text{Mpc})$ and most of the emission takes place at frequencies of $\sim 200 - 1000$ Hz, but the various explosion scenarios exhibit unique spectral

distributions and vary in total emitted energies [77, 78]. In addition, there is likely to be a low-frequency GW-memory-type component with large h up to $10^{-22}\,(D/1\,\mathrm{Mpc})$ at $0-20\,\mathrm{Hz}$. ET as currently envisioned [79] is sufficiently sensitive to detect GWs from various CC-SN scenarios out to $2-4\,\mathrm{Mpc}$. If the high-f sensitivity was increased by a factor of $\sim 2-3$, detection out to $\sim 10\,\mathrm{Mpc}$ may be possible. Even without this improvement, ET may see multiple CC-SNe during its lifetime and would have the power to provide strong hints for a particular SN mechanism and/or smoking-gun evidence against another – crucial astrophysics information that is unlikely to be attainable in other ways. At ET's implementation, megaton-class neutrino detectors will be operative and, having range similar to ET, will be able to provide coincidencent observations, narrowing down the time of the GW emission to $\sim 1\,\mathrm{ms}$. In addition, deep high-cadence optical transient surveys will be operative and targeting near-universe transients, providing additional coincident data as well as additional astrophysics output (progenitor type/mass, explosion morphology/energy etc.).

Impact Constraining the CC-SN mechanism will mean a breakthrough in our understanding of the large range of phenomena associated with stellar collapse, CC-SNe, BH and NS formation, and gamma-ray bursts (GRBs). However, the astrophysics and physics information provided by GWs observed from a CC event with ET goes beyond this: These GWs carry also information on the high-density nuclear EOS, explosion asymmetries and pulsar kicks, the formation of a BH in a failing CC-SN, and can help uncover rare events such as the accretion-induced collapse of a white dwarf to a NS or weak or failing CC-SNe that have very weak or absent EM signatures.

III. FUNDAMENTAL PHYSICS

Sathya The rich variety of sources and phenomena observed by gravitational wave detectors can be potentially used to address outstanding questions in fundamental physics. The sources in question will be in dense environs of ultra strong gravity and thereby provide a cosmic laboratory for understanding phenomena and matter in extreme conditions of density, temperature, magnetic field, etc. Moreover, black hole binaries are fundamentally geometric objects whose interaction close to merger will provide insights into nature of black hole space times and of gravity in ultra-strong fields. In this Section we will discuss what fundamental physics questions and strong-field tests of gravity could be addressed by 3G detectors.

A. Speed of gravitational waves and mass of the graviton

Sathya In Einstein's theory gravitational waves travel with the speed of light. This means that gravitons, particle analogs of gravitational waves, are massless particles. Although there is currently no strong motivation to consider massive graviton theories from an experimental point of view, they are natural extensions of Einstein's theory. In a massive graviton theory, gravitational waves would not travel at the speed of light and this can be tested by observation of gravitational-wave sources at very great distances. To do so we would need a source which emits at the same time both gravitational waves and electro-magnetic radiation. By measuring the difference in their arrival times we could measure or constrain the speed of gravitational waves.

Supernovae in the local Universe and double neutron star and neutron star-black hole binaries are sources that are expected to exhibit after glows in electro-magnetic radiation soon after they emit a burst of of gravitational waves. If the source is near enough (a few Mpc in the case of supernovae and red-shifts of a few in the case of coalescing binaries) and the event is well-localized on the sky (fraction of a degree depending on the distance to the source), then it could be observed in coincidence as a transient EM and a GW event.

Current theories of supernovae and coalescing binaries cannot accurately predict how promptly after the collapse (in the case of SN) or merger (in the case of binaries) EM radiation will follow. However, the expected delay is no more than one second. If gravitational waves arrive a time Δt after EM waves, then the fractional difference in their speeds is given by

$$\frac{|\Delta v|}{c} = 3.2 \times 10^{-18} \left(\frac{|\Delta t|}{1\,\mathrm{s}}\right) \left(\frac{3\,\mathrm{Gpc}}{D}\right) \tag{3.1}$$

where we have assumed that the source is at a distance of $D = 3\,\mathrm{Gpc}$.

$$\tag{3.2}$$

B. Testing alternative theories of gravity
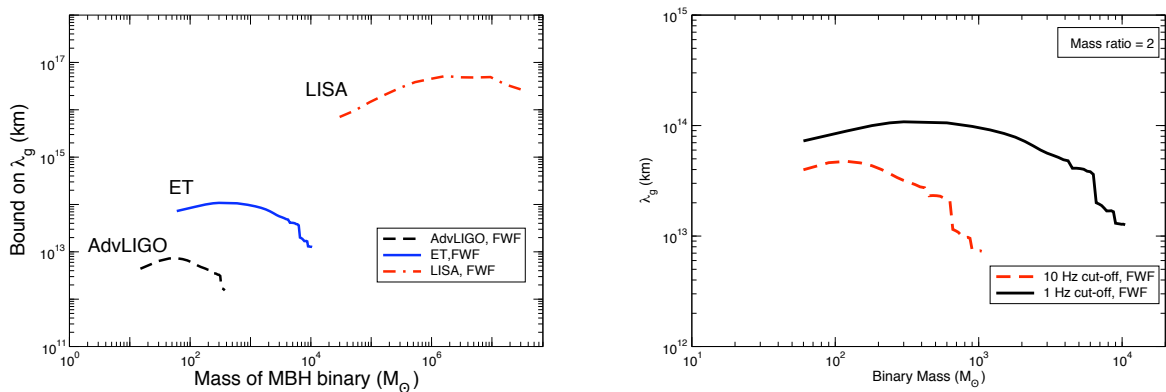
Arun, Veitch, Van Den Broeck

FIG. 11: Left panel: Bounds on the graviton Compton wavelength that can be deduced from AdvLIGO, Einstein Telescope and LISA. The mass ratio is 2. The distance to the source is assumed to be 100 Mpc for AdvLIGO and ET, and 3 Gpc for LISA. Right panel: Possible bounds from ET when 1 Hz and 10 Hz are used as seismic cut-offs.

C. Limiting the mass of the graviton

Arun: June 8th

Observations of inspiralling compact binaries (neutron stars or black holes) can be used to put bounds on the mass of the graviton, or equivalently the compton wavelength of the graviton [80]. These bounds do *not* require the detection of an electromagnetic counterpart associated with the GW signal.

The basic idea is simple: if there is a mass associated with the propagation of gravitational waves ("a massive graviton"), then the speed of propagation will depend on wavelength in the form $v_g \approx 1 - (\lambda/\lambda_g)^2$, where λ_g is the Compton wavelength of the graviton, in the limit where $\lambda \ll \lambda_g$. Irrespective of the nature of the alternative theory that predicts a massive graviton , it is reasonable to expect the differences between such a hypothetical theory and general relativity in the predictions for the evolution of massive compact binaries to be of order $(\lambda/\lambda_g)^2$, and therefore to be very small, given that $\lambda \sim 10^3$ km for stellar mass inspirals and $\sim 10^8$ km for massive black hole inspirals.

As a result, the gravitational waveform seen by an observer close to the source will be very close to that predicted by general relativity. However, as seen by a detector at a distance D, hundreds to thousands of Mpc away, the phasing of the signal will be distorted because of the shifted times of arrival, $\Delta t \sim D(\lambda/\lambda_g)^2$ of waves emitted with different wavelengths during the inspiral. In addition to measuring the astrophysical parameters of the system, such as masses and spins, the matched filtering technique permits one to estimate or bound such effects.

Here we examine the bounds possible from the observations of binary black holes by ET [81]. As our waveform model we begin with amplitude-corrected, general relativistic waveforms which are 3PN accurate in amplitude [4, 5, 82, 83] and 3.5PN accurate in phasing [6, 84–88]. We ignore the spins of the bodies in the binary system. Previous calculations

used waveforms which are of Newtonian order in amplitude and 2PN order in phase. As opposed to the Newtonian waveforms, the 3PN amplitude-corrected waveforms contain all harmonics from Ψ up to 8Ψ, where Ψ is the orbital phase (the leading quadrupole component is at 2Ψ).

The effect of a massive graviton is included in the expression for the orbital phase following Ref. [80]. The wavelength-dependent propagation speed changes the arrival time t_a of a wave of a given emitted frequency f_e relative to that for a signal that propagates at the speed of light; that time is given, modulo constants, by

$$t_a = (1 + Z)\left[t_e + \frac{D}{2\lambda_g^2 f_e^2}\right],\tag{3.3}$$

where f_e and t_e are the wave frequency and time of emission as measured at the emitter, respectively, Z is the cosmological redshift, and

$$D \equiv \frac{(1 + Z)}{a_0} \int_{t_e}^{t_a} a(t)dt,\tag{3.4}$$

where $a_0 = a(t_a)$ is the present value of the scale factor (note that D is not exactly the luminosity distance [1]). This affects the phase of the wave accordingly. In the frequency domain, this adds a term to the phase $\psi(f)$ of the Fourier transform of the waveform given by $\Delta\psi(f) = -\pi D/f_e\lambda_g^2$. Then, for each harmonic of the waveform with index k, one adds the term

$$\Delta\psi_k(f) = \frac{k}{2}\Delta\psi(2f/k) = -\frac{k^2}{4}\pi D/f_e\lambda_g^2.\tag{3.5}$$

Here $k = 2$ denotes the dominant quadrupole term, with phase 2Ψ, $k = 1$ denotes the term with phase Ψ, $k = 3$ denotes the term with phase 3Ψ, and so on.

This is an adhoc procedure because a massive graviton theory will undoubtedly deviate from GR not just in the propagation effect, but also in the way gravitational wave damping affects the phase, as well as in in the amplitudes of the gravitational waveform. If, for example, such a theory introduces a leading correction to the quadrupole phasing $\psi_{\text{quad}} \sim (\pi\mathcal{M}f_e)^{-5/3}$ of order $(\lambda/\lambda_g)^2 \times (\pi\mathcal{M}f_e)^{-5/3}$, where $\mathcal{M}$ is the chirp mass, then the propagation induced phasing term (3.5) will be larger than this correction term by a factor of order $k^2(D/\mathcal{M})(\pi\mathcal{M}f_e)^{8/3} \sim (D/\mathcal{M})v^8$. Since $v \sim 0.1$ for the important part of the binary inspiral, and $D \sim$ hundreds to thousands of Mpc, it is clear that the propagation term will dominate. In any case, given the fact that there is no generic theory of a massive graviton, we have no choice but to omit these unknown contributions.

Our estimate of the bounds on the massive graviton parameter is based on the Fisher matrix formalism. We construct the Fisher matrix for the different detector noise PSDs using the amplitude corrected PN waveform model described earlier, converted to the Fourier domain using the stationary phase approximation. We use a six-dimensional parameter space consisting of the time and phase (t_c, ϕ_c) of coalescence, the chirp mass $\mathcal{M}$, the mass asymmetry parameter $\delta = |m_1 - m_2|/(m_1 + m_2)$, the massive graviton parameter $\beta_g =$

---

[1] For $Z \ll 1$, D is roughly equal to luminosity distance D_L. Hence we have assumed $D \simeq D_L$ in the case of ground based detectors for which we consider sources at 100 Mpc. For LISA, we have carefully accounted for this difference.

$\pi^2 D\mathcal{M}/\lambda_g^2(1 + Z)$, and the luminosity distance D_L. We fix the three angles, θ, ϕ and ψ which appear in the antenna pattern functions to be $\pi/3$, $\pi/6$ and $\pi/4$ respectively and the inclination angle of the binary to be $\iota = \pi/3$. Details of the Fisher matrix approach as applied to the compact binary coalescence signals can be found in Refs. [89–91], and more recently in Ref. [92] ,which critically reexamines the caveats involved in using the Fisher matrix formalism to deduce error bounds for various gravitational wave detector configurations.

The square root of each of the diagonal entries in the inverse of the Fisher matrix gives a lower bound on the error covariance of any unbiased estimator. Our focus here is solely on the diagonal element corresponding to the massive graviton parameter. The $1 - \sigma$ error bar on β_g can be translated into a bound on the Compton wavelength using $\Delta\beta_g = \beta_g$, and this is the quantity that we use in the plots as well as in the discussions.

The results are shown in Figure 11. On the left panel, the bounds on the compton wavelength of the graviton achievable with the second generation detector AdvLIGO and the space based LISA are compared against those possible from ET. The typical bounds from ET could be an order of magnitude better than from AdvLIGO, but worse than LISA. The observable mass range is also much larger for ET in comparison with AdvLIGO and extends up to about $10^4 M_\odot$. In the right panel, we compare the effect of the seismic cut-off on the massive graviton bounds by considering 1 Hz and 10 Hz cut-offs. As one might expect, there is improvement in the accessible mass range by almost an order of magnitude when 1 Hz cut-off is used as cut-off as opposed to 10 Hz.

Note that though we have considered the sources for ET to be at 100 Mpc, the bounds in principle are more or less independent of the distance because in the definition of λ_g, there is a distance scale present. However, for very large distances the SNR may not be high enough and Fisher matrix estimate may not be reliable.

D.   Bounds on Brans-Dicke parameter using ET

Arun: June 11th

Brans-Dicke (BD) theory of gravity[93] is an alternative theory of gravity which has an additional scalar field, which couples to matter, apart from the tensor field of general relativity. The coupling of the scalar field can be described in terms of a coupling constant ω_{BD}. Since scalar-tensor field theories predict dipolar gravitational radation, this parameter is also a measure of the dipolar GW content.

The best bound on this parameter, so far, has come from the solar system experiment *Cassini*, by measuring the frequency shift of the radio photons to and from the space craft as it orbited near sun [94]. This turns out to be about 4×10^4 (note that in the limit of GR, $\omega_{BD} \to \infty$).

Gravitational wave observations can also put interesting bounds on ω_{BD} as first pointed out by [95, 96]. This is possible because the GW phasing formula for the BD case is same as that of GR except for an additional dipolar term proportional to ω_{BD}. Hence it is possible to measure this quantity from the GW observations and to bound it (see Refs [95, 96] for details).

The dipolar GW content also depends on the internal structure of the compact body via

a quantity called "sensitivity" s_A (see Sec. 3.3 of [97]).

$$\left(\frac{dE}{dt}\right)_{\text{dipole}} \propto \frac{\mathcal{S}^2}{\omega_{BD}}, \qquad (3.6)$$

where $\mathcal{S} = s_1 - s_2$ where s_1 and s_2 are the sensitivities of the binary constituents. For binary neutron stars $\mathcal{S} \sim 0.05 - 0.1$ and for NS-BH binaries $\mathcal{S} \sim 0.3$ and for a binary BH $\mathcal{S} = 0$. Therefore, for bounding BD theories one of the components of the binary should be a NS. The bound is also very sensitive to the asymmetry of the binary: the more asymmetric the binary, the worse is the bound. Due to these factors, GW bounds on the ω_{BD} are very weak (~ 5000 at best [95]). However, we point out that if ET has very good low frequency
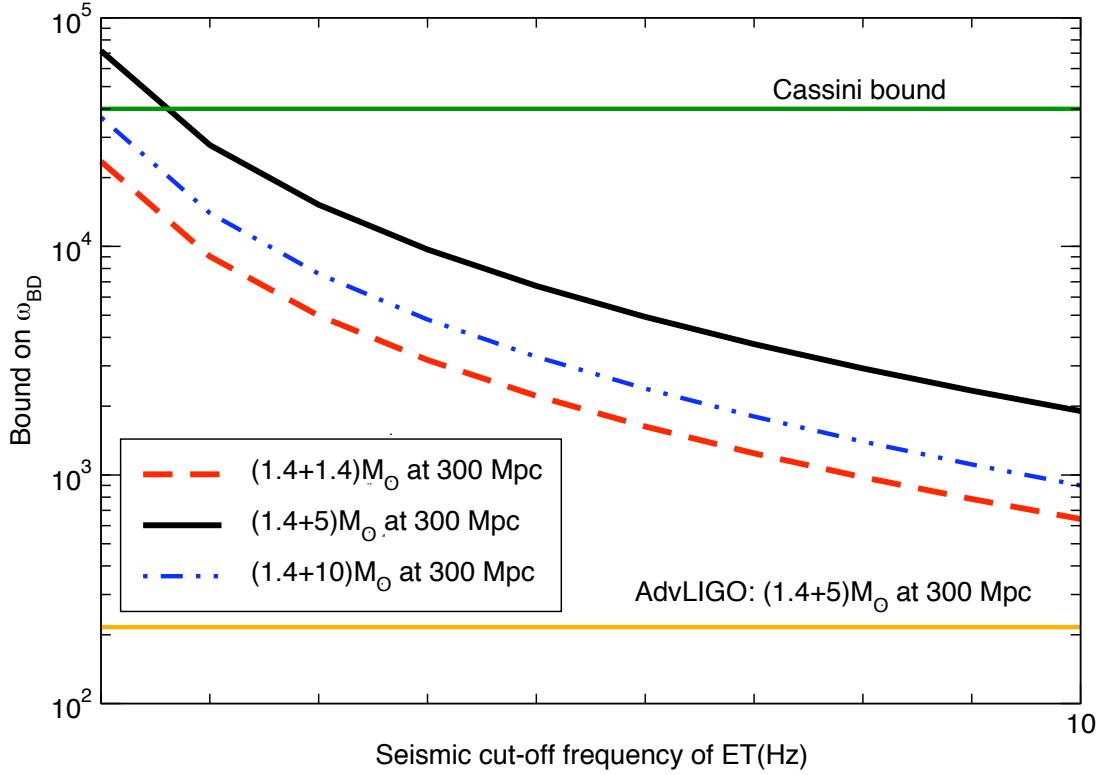

FIG. 12: Bounds on Brans-Dicke parameter (ω_{BD}) from ET as a function of seismic cut-off frequency of ET. The existing bound from the Cassini experiment and the possible bounds from AdvLIGO are also shown.

sensitivity (seismic cut-off frequency between $1 - 10$ Hz), the bounds from ET can beat the solar system bounds. Figure 12 shows the bound on ω_{BD} for different types of sources as a function of the seismic cut-off frequency of ET. The NS mass is assumed to be $1.4M_\odot$ and that of the BH to be either $5M_\odot$ or $10M_\odot$. $\mathcal{S}$ of NS is assumed to be 0.1 and that of the BH is assumed to be 0.3. The best bounds would come from the observations of NS-BH binaries

with the BH mass between $4 - 10 M_\odot$ at 300 Mpc. If ET has a low frequency cut-off of 1Hz, then the bounds on ω_{BD} could be as high as $\sim 10^5$.

These bounds are likely to be the best possible by GW observations because estimates for LISA (a proposed space mission sensitive to low frequency GWs) for NS-BH binaries of total mass $\sim 10^3$ can beat the solar system bounds only if it observes a binary within 20-50 Mpc during it mission life time (see [98–100] for the corresponding LISA estimates).

E. Measuring the dark energy equation of state and its variation with z

Van Den Broeck

Over the past decade, evidence has emerged suggesting that the expansion of the Universe is accelerating. Possible explanations include a failure of general relativity at large length scales, a cosmological constant in the Einstein equations, or a new contributor to the mass/energy content of the Universe called dark energy (see [101] for a review). Assuming a homogeneous and isotropic Universe, dark energy can be characterized by an equation of state of the form $p_{\mathrm{DE}} = w(z)\rho_{\mathrm{DE}}$, where $p_{\mathrm{DE}} < 0$ and $\rho_{\mathrm{DE}} > 0$ are the pressure and density, respectively. If the equation of state parameter $w(z)$ is constant and equal to -1 then this corresponds to having a positive cosmological constant in the gravitational field equations. Current constraints allow for this possibility, but other possibilities are not ruled out. The five year WMAP data combined with supernovae measurements and baryon acoustic oscillations in the galaxy distribution lead to the constraint $-1.11 < w < -0.86$ at the 95% confidence level [102].

The gravitational wave signal from inspiraling compact binaries (neutron stars and black holes) is particularly "clean" and well-understood. Consequently, as suggested by Schutz, one can think of using inspiral events as "standard sirens", much in the way Type Ia supernovae have been used as standard candles [1]. From the gravitational wave signal itself the luminosity distance D_{L} can be inferred, but not the redshift. However, if a particular compact binary coalescence event is accompanied by a sufficiently distinct electromagnetic counterpart, then it will be possible to find its position in the sky, identify the host galaxy, and obtain the redshift z. The relationship $D_{\mathrm{L}}(z)$ depends sensitively on cosmological parameters such as the Hubble constant at the current epoch H_0, the normalized matter and dark energy densities Ω_{M} and Ω_{DE}, and the dark energy equation of state parameter w. For example, in a spatially flat FLRW Universe and assuming a constant w,

$$D_{\mathrm{L}}(H_0, \Omega_{\mathrm{M}}, \Omega_{\mathrm{DE}}, w; z) = (1+z) \int_0^z \frac{dz'}{H_0 \left[\Omega_{\mathrm{M}}(1+z')^3 + \Omega_{\mathrm{DE}}(1+z')^{3(1+w)} \right]^{1/2}}. \tag{3.7}$$

The intrinsic luminosity, and hence the luminosity distance, of an inspiral gravitational wave event can be inferred directly from their amplitude and from the component masses, which govern the structure of the signal. Thus, unlike Type Ia supernovae, their calibration does not depend on the brightness of other sources. This way gravitational wave astronomy opens up the possibility of cosmography *without having to rely on the lower rungs of the cosmic distance ladder.*

Compact binary coalescences that involve a neutron star are assumed to have strong electromagnetic counterparts, mostly in the form of strongly beamed gamma radiation directed perpendicularly to the plane of the inspiral. Such events are believed to be the progenitors of short, hard Gamma Ray Bursts (GRBs): if the beam roughly points towards Earth then

a flash of gamma radiation is seen, followed by an afterglow in the lower-frequency electromagnetic spectrum. This would then allow us to identify the host galaxy and obtain a redshift.

The gravitational wave signal from a NS-BH coalescence will be visible out to $z = 3.5$. Within the corresponding volume, it is reasonable to expect $\sim 10^4$ or more such coalescences per year, but depending on the opening angle of the gamma ray beam only a few percent of these will be visible as a GRB. Hence we should have a few hundred sources at our disposal for which the redshift can be measured. The uncertainty on z will be negligibly small, while D_{L} will be measurable with $\sim 3\%$ inaccuracy at $z = 1$, rising to $\sim 10\%$ at $z = 3.5$. Fitting the measured values of D_{L} against redshift by varying H_0, Ω_{M}, Ω_{DE}, and w in the relationship (3.7) should then allow for the determination of these cosmological parameters with uncertainties of 5% or better.

F.   Testing the uniqueness theorem of black hole spacetimes

Gair It is generally accepted that the massive compact objects observed in the centres of most galaxies are massive, rotating black holes described by the Kerr metric of General Relativity. This belief comes in part from the uniqueness theorem, which is the result that the Kerr metric is the unique endstate of gravitational collapse [103]. However, this theorem is based on several assumptions — the spacetime is vacuum, axisymmetric and stationary; there is a horizon in the spacetime; and there are no closed timelike curves. If one of these assumptions were violated, then objects that deviate from the Kerr metric could exist.

In black hole binary systems where the mass of one object is much bigger than the other, many gravitational wave cycles are emitted while the smaller object is in the strong field region close to the larger object. These gravitational waves encode a map of the spacetime structure in the vicinity of the large black hole, which can be used to measure properties of the central object [104]. Using such observations to measure spacetime structure has been explored extensively in the context of extreme-mass-ratio inspirals (binaries of $\sim 10 M_\odot$ objects with $\sim 10^6 M_\odot$ objects) for LISA (see [105] and references therein). There is an analogous source for ground based detectors, namely the inspiral of a $\sim 1 M_\odot$ object into a $\sim 100 M_\odot$ black hole. We refer to these as intermediate-mass-ratio inspirals (IMRIs) [106].

Explicit calculations have not yet been done for ET, but they do exist for Advanced LIGO [106, 107]. Extrapolating from those results, ET could see IMRI events out to a redshift $z \sim 3$ and could detect as many as several hundred events per year, although a few to a few tens is more likely. ET will observe these events for more cycles than Advanced LIGO, due to its better low-frequency performance, which is very important for the precision of spacetime mapping measurements.

1.   Testing the black hole no-hair theorem

Gair The uniqueness of Kerr black holes as the endstate of collapse is sometimes referred to as the "no-hair theorem". A Kerr black hole has "no-hair" since the entire spacetime structure, characterised by "multipole moments", is determined by just two parameters, the black hole mass, M, and spin, S. It has been demonstrated that gravitational wave observations can measure the multipole moments independently of one another [104]. We

can therefore directly verify that they satisfy the Kerr relationship

$$M_l + \mathrm{i}S_l = M(\mathrm{i}S/M)^l \tag{3.8}$$

We need only to measure three multipole moments to rule out an object as a Kerr black hole.

It has been shown that IMRI observations with Advanced LIGO could detect an $O(1)$ deviation in the quadrupole moment of an object [106]. The precision achievable with ET should be at least a factor of 10 better than this due to the improved low-frequency performance. To put this in perspective, one alternative to black holes, boson stars, have quadrupole moments two orders of magnitude bigger than black holes of the same mass and spin [108].

Any deviations from the no-hair theorem that are detected will have profound implications for our understanding of relativity and of black holes. Persistent deviations from the theory may lead to important insights in the search for a Fundamental Theory that unifies all four forces of nature.

2. Are there naked singularities?

Gair One of the assumptions of the uniqueness theorem is that a horizon exists in the spacetime. This arises from a belief embodied by the "Cosmic Censorship Hypothesis" [109] (CCH), which states that any singularity will be enclosed by a horizon. The CCH arises from a desire for predictability in the Universe — when Physics breaks down at a singularity, we do not want information from that to propagate into the rest of the Universe. However, the CCH is unproven and therefore "naked" singularities not enclosed within a horizon may still exist. Gravitational wave observations provide a unique way to look for these exotic objects. Observations may be indirect, via detection of a violation to the "no-hair" theorem. However, they may also be direct — if a horizon is not present in the spacetime, the gravitational waves will not cut-off when the object crosses the horizon [110], which will be a clear smoking gun signature for the absence of a clothing horizon in the system.

The Einstein Telescope will provide much more stringent constraints on potential violations of the CCH than are possible with Advanced LIGO. ET observations will therefore play an important role in answering the question as to whether naked singularities exist, which could have profound implications for our understanding of various aspects of the theory of relativity.
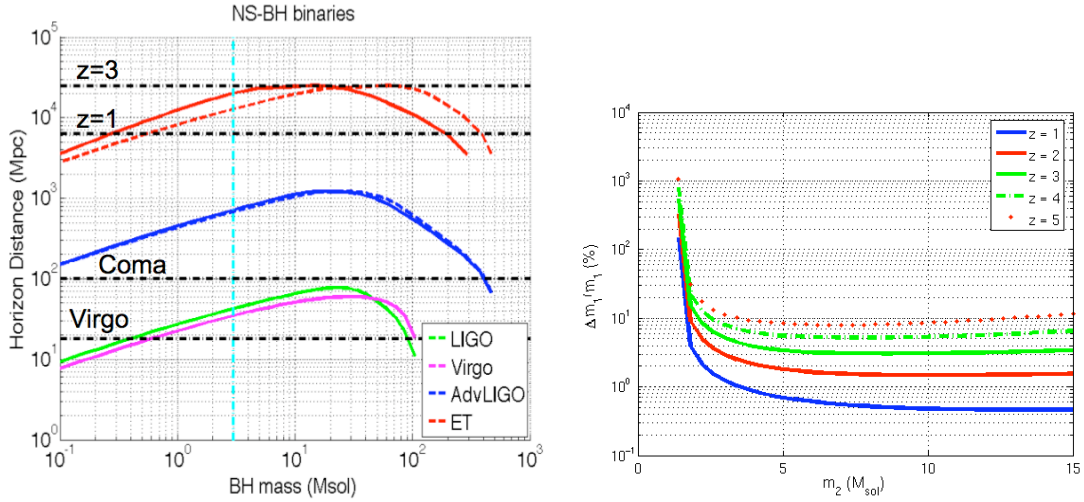
FIG. 13: The plot on the left shows the horizon distance for neutron star-black hole binaries against black hole mass for initial and advanced LIGO, Virgo and ET. The solid coloured curves show the horizon distance against the *instrinsic* (non-redshifted) mass of the source. The dashed coloured curves show the horizon distance against the *observed* (redshifted by a factor of $1 + z$) mass of the source. The plot on the right shows the accuracy with which the mass of a neutron star can be determined from the inspiral signal, as a function of the mass of the companion object.

IV. ASTROPHYSICS

A. What is the mass function of neutron stars, and are there stable stars denser than a neutron star?

Van Den Broeck

It is generally believed that neutron stars have masses between $\sim 1.3\,M_\odot$ and $\sim 2\,M_\odot$ [CITATION], but such statements rely on guesses regarding the equation of state of dense nuclear matter. Above $2\,M_\odot$ a quark star might be created, or some other exotic object. Apart from the existence of such objects and their properties, an interesting question is how massive a star can be while still being stable. The left panel of Fig. 13 shows the maximum distance to which NS-BH binary inspirals can be seen in initial and advanced LIGO and Virgo, and in ET. The latter would have access to sources out to genuinely cosmological distances, up to redshifts of several, with an expected detection rate in the order of $10^6\,\mathrm{yr}^{-1}$. The right panel shows how accurately one would be able to measure the mass of a neutron star in an NS-BH inspiral process, as a function of the mass of the black hole as well as redshift. For a black hole mass $\gtrsim 5\,M_\odot$, the neutron star's mass can be inferred to a fraction of a percent out to $z = 1$, and up to a few percent out to a redshift of 2 or 3. This would enable us not only to establish the mass distribution of neutron stars and dense exotic objects, but also the evolution of this distribution over cosmological timescales.

B. Equation-of-state of neutron stars from binary coalescences

Rezzolla, Read Probing the ground-state of nuclear state over a range of nuclear density, measuring the effects of neutron star equation of state using binary neutron star mergers, and measuring magnetic fields, post-merger oscillations

Binary neutron stars are known to exist and for some of the systems in the Galaxy general-relativistic effects in the binary orbit have been measured to high precision. The inspiral and merger of two neutron stars in binary orbit is the inevitable fate of close-binary evolution, whose main dissipation mechanism is the emission of gravitational waves. The detection of gravitational waves from neutron stars binaries will provide a wide variety of physical information on the component stars, including their mass, spin, radius and equation of state (EOS). The central densities of isolated neutron stars, in fact, can range up to ten times nuclear saturation density, and during the merger and coalescence of two neutron stars the maximum density will rise even further before the remnant object collapses to a black hole. The behaviour of bulk matter at these densities is not well understood, and measurements of gravitational wave signals from neutron star sources can usefully constrain the EOS at the these densities.

Quantum chromodynamics is expected to be a complete description of matter at these energies; the uncertainty in theoretical understanding comes from the many-body problem with strong interactions. The description of bulk neutral matter in terms of hadrons such as protons and neutrons may need to be expanded to accomodate new particles that are formed at these energies, such as hyperons, pions, and kaons. In fact the appropriate degrees of freedom describing cold matter at very high density may no longer be hadrons but the quarks and gluons themselves, in some form of quark matter.

While isolated or inspiralling neutron stars are well described by the ground state of matter, i.e. with a "cold" EOS, the temperatures reached in the coalescence as a result of the strong shocks, will be significant and of the order of $\sim 10^{10} - 10^{12}$ K. Yet, just as measurements of the hot out-of-equilibrium ion collisons in RHIC constrain the ground state of dense nuclear matter, characteristics of the collisions neutron stars may be able to constrain the ground state of dense neutral matter.

Reviews of the current range of candidate equations of state and their constraint using astrophysical and heavy ion collision experiments can be found in [111–113].

The signature of the neutron star EOS can be found in almost any neutron-star sourced gravitational wave; in the peak frequencies of supernova waveforms [114, 115], in the possibility of accretion-induced crust mountains [72, 116], and in the astroseismology of glitches and other oscillation mode excitations [[]]. Studies which have specifically explored the effect of varying EOS (or varying compactness for a given mass, which implies EOS variation) on gravitational wave spectra include [117–121] for binary neutron star inspiral, [122–129] for binary neutron star coalescence, and [111, 130–132] for mixed binaries. The gravitational waves from binary inspiral and merger are expected to be frequantly measured, and the predicted signals have several interesting EOS-dependent features.

This is illustrated as a representative example in Figure 14 and which reports the simulations of [128]. In particular, the left panel on the top row shows the comparison in retarded-time evolution of the real part of the $\ell = m = 2$ component of the gravitational-wave signal $r\Psi_4$ for a high-mass binary (i.e. with a total mass of $3.2\,M_\odot$) when evolved with the a "cold" EOS (i.e. a polytropic one) or with a "hot" EOS (i.e. the ideal-fluid one). Similarly, the right panel on the top row shows the same comparison but for a low-mass
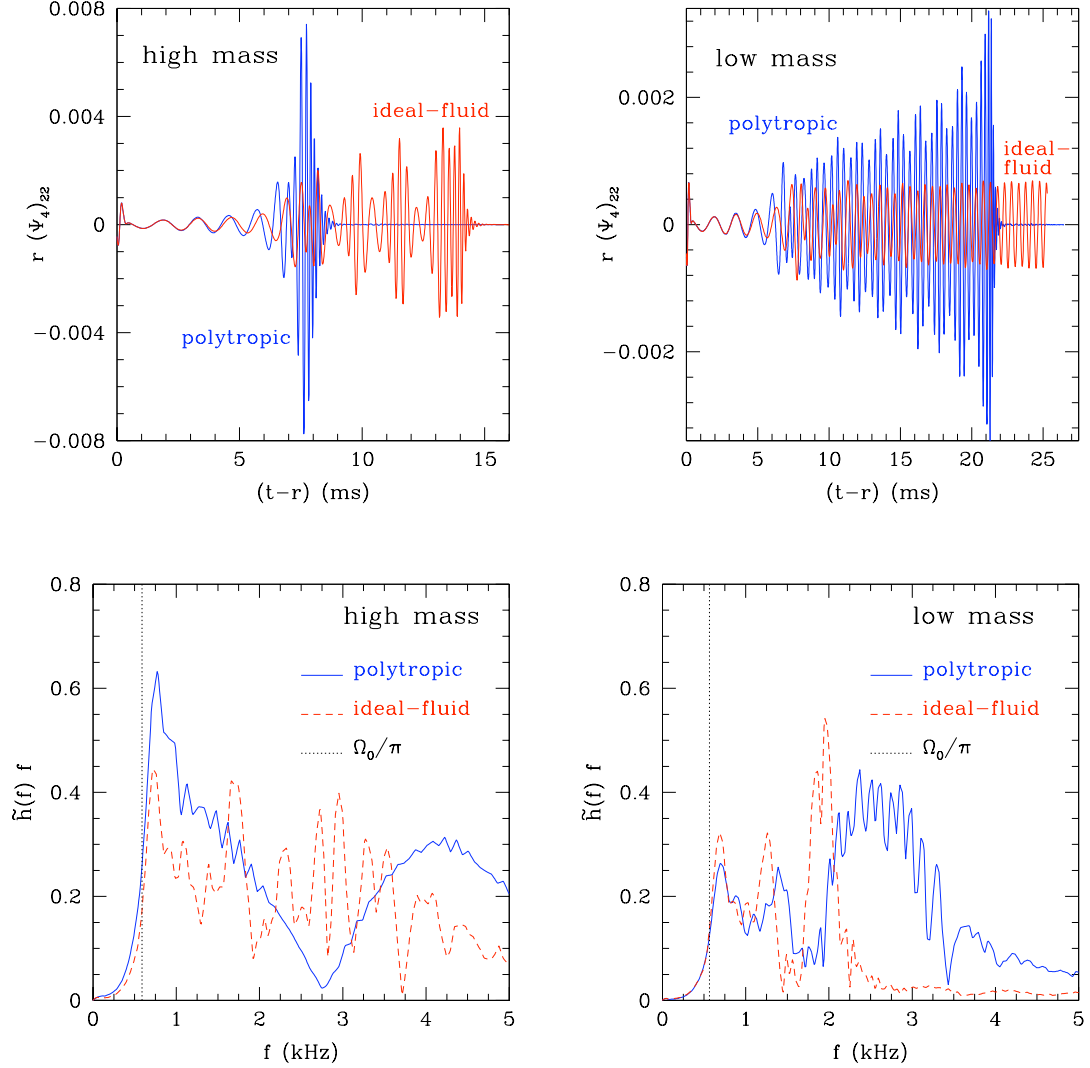
FIG. 14: *Top row, left panel:* Comparison in retarded-time evolution of the real part of the $\ell = m = 2$ component of $r\Psi_4$ for a high-mass binary (i.e. with a total mass of $3.2\,M_\odot$) when evolved with the a "cold" EOS (i.e. a polytropic one) or with a "hot" EOS (i.e. the ideal-fluid one). *Top row, right panel:* The same as in the left panel but for a low-mass binary (i.e. with a total mass of $2.9\,M_\odot$). *Bottom row:* The same as in the top row but with the comparison being made in frequency space. Indicated with a vertical long-dashed line is twice the initial orbital frequency.

binary (i.e. with a total mass of $2.9\,M_\odot$). Finally, the bottom row offers a representation of the same data but in frequency space. While none of the two EOSs considered here is realistic, they span in some sense the extrems of the range of possibilities. Most importantly they show that the gravitational-wave signal will be very sensitive on the mass of the stars and on the EOS.

While this is especially true in the post-merger phase, also the inspiral phase will provide

important information on the EOS. Indeed, although for most of the inspiral of a binary neutron star system the stars are well-modeled as point particles, as they approach each other, an EOS dependent tidal deformation modifies their orbits, changing the late inspiral waveform. The measurability of this effect in gravitational wave detectors can be estimated using both post-Newtonian tidal deformation calculations and full numerical simulations of binary neutron stars with varying EOS.

The set of numerical simulations of [121] using an ET proposed noise curve give, for a $1.35M_\odot$–$1.35M_\odot$ double neutron star binary at 100 Mpc in ET, estimates of the measurement uncertainty δR of isolated neutron star are of the order ± 0.5–1.0 km. This compares favorably to the range in predicted radius of roughly 9–16 km. Parameterizing the variation by the pressure at $5 \times 10^{14}\,\mathrm{g\,cm^{-3}}$, as in [120], gives estimates of δp_1, where p_1 is $\log(p/c^2)$, of order ± 0.05–0.10, compared to a range of roughly 13.0–13.8 for realistic EOS.

Estimates of a post-Newtonian tidal deformation following [119] give for a binary at 50 Mpc

- $\Delta\tilde{\lambda} \sim 1.22 \times 10^{36}$ for $1.35 - 1.35M_\odot$

- $\Delta\tilde{\lambda} \sim 1.6 \times 10^{36}$ for $1.45 - 1.45M_\odot$

- $\Delta\tilde{\lambda} \sim 1.85 \times 10^{36}$ for $1.35 - 1.7M_\odot$

for inspiral *below 400 Hz*, where $\tilde{\lambda}(m_1, m_2)$ is a measure of tidal deformability in a given binary which ranges between 0.5×10^{36} g^2 cm^2 and 10×10^{36} g^2 cm^2 for realistic EOS.

The advantage of ET from the perspective of EOS understanding is not necessarily the larger number of detections possible with increased sensitivity, although information about mass distribuition of neutron star populations can also be useful for EOS constraint. Instead, ET will provide very strong signals at reasonable rates; for example two $1.4\,M_\odot$ neutron stars inspiralling towards each other within an effective distance of 100 Mpc, which is expected roughly once a year [[]] , would give a SNR in ET of over 900. This makes possible for the precise measurement of masses in early inspiral, the detection of small departures from point particle behaviour at moderate frequencies, and discrimination between merger and post-merger signals from different models at high frequencies.

An interesting feature that has emerged from studies of binary neutron star coalescences is the post-merger formation, in some cases, of a hyper-massive remnant object which oscillates and emits gravitational waveforms on fairly long timescales. The presence or absence of such post merger oscillations, as well as their characteristic frequency and duration, varies with the cold EOS. However, they are additionally sensitive to many physical effects from thermal properties, magnetic fields, and particle production, and so forth. The precise details of the signal, similarly to those from supernovae, are not easy to predict. However, the signal from such a post-merger oscillation is potentially visible with advanced detectors [124], and analysis of the signal following a measured inspiral may provide useful constraints on the underlying astrophysics.

It has recently become possible to compute the first complete and accurate simulations of the merger of a neutron stars binary through to the delayed formation of a BH and to its ringdown [128, 129]. By computing the complete gravitational wave signal produced in the process it was possible to show that the gravitational waves are strongly correlated to the properties of the sources emitting them. Differences in the EOS or in the initial mass of the system produced different signals with different power spectra and different durations.

Furthermore, magnetic fields (MFs) are commonly present in neutron stars and their possible impact on the dynamics of binary neutron stars has only begun to be examined. The `Whisky` code has been recently used to investigate the effect that MFs have on the gravitational wave emission produced during the inspiral and merger of magnetized neutron stars [133]. In particular it has been shown that MFs do have an impact after the merger (for initial MFs $B_0 \gtrsim 10^{12}$ G), but also during the inspiral (for sufficiently strong initial MFs with $B_0 \gtrsim 10^{16}$ G). These results, are quantified by computing the overlap between the waveforms produced during the inspiral by magnetized and unmagnetized binaries. Moreover, through the inclusion of more realistic equations of state and of a radiation transport scheme, it will be possible to increase considerably our level of understanding of these objects.

C.   What are the progenitors of gamma-ray bursts?

O'Shaughnessy, Jones, Clark
Gamma-ray bursts (GRBs) are the most luminous explosions in the EM spectrum occurring in the universe. Through observations made by satellite-based gamma-ray observatories it was found that the the duration of the GRBs follows a bimodal distribution [134]. We classify GRBs either as *short-hard* or *long-soft* bursts depending on their duration and spectra. Through follow-up observations of the x-ray, optical and radio afterglow emission of GRBs it is possible to determine their sky-location, redshift and host galaxy.

Long GRBs are always associated with late-type star-forming host galaxies [135]. A handful of long GRBs have also been associated with supernovae [136–139]. It is therefore thought that core-collapse supernovae are the progenitor of long GRBs [140, 141].

Short GRBs are observed at lower redshifts than long GRBs are associated with a variety of galaxy types including early-type elliptical and lenticular galaxies without active star forming regions [142]. Currently, it is widely thought that merger of neutron star binaries or neutron star-black hole binaries (NS-BH) are the progenitors of most short-hard GRBs [143]. Some small fraction of short GRBs (less than 15% of known short GRBs) may be caused by soft gamma repeater flares (SGRs) [144, 145]. SGRs are described further in Section IV C. Accurate predictions for the gravitational wave emission of the inspiral, merger and ringdown of compact binaries are possible through post-Newtonian approximations to Einstein's equations or through numerical relativity simulations. Searches for gravitational waves from inspiralling binaries using matched-filtering on data from initial interferometers (LIGO, Virgo, GEO) are underway. A search for the emission of GRB 070201 whose sky-locatiion error box overlaps the spiral arms of M31 was carried out in Ref. [146]. The matched-filter analysis excluded an inspiral progenitor for GRB 070201 if it was indeed located in M31 with a confidences of 99%.

It is typical to characterise the sensitivity of a gravitational wave observatory to inspiral distances by the horizon distance. The horizon distance is the distance at which we would measure a matched-filter signal-to-noise ratio of 8 for an optimally oriented (i.e., face-on) and overhead source. Figure 13, left plot, shows the horizon distance achieved by initial and advanced LIGO, Virgo and ET for NS-BH binaries with $m_{\mathrm{NS}} = 1.4 M_\odot$ and a range of BH masses.

Predicting the gravitational wave emission of core-collapse supernovae associated with long GRBs is more difficult and involves modelling the complicated internal dynamics of the collapsing star, see e.g., [147]. Searches for unmodelled gravitational emission from GRBs on data from initial interferometers (LIGO, Virgo, GEO) are underway [146, 148].
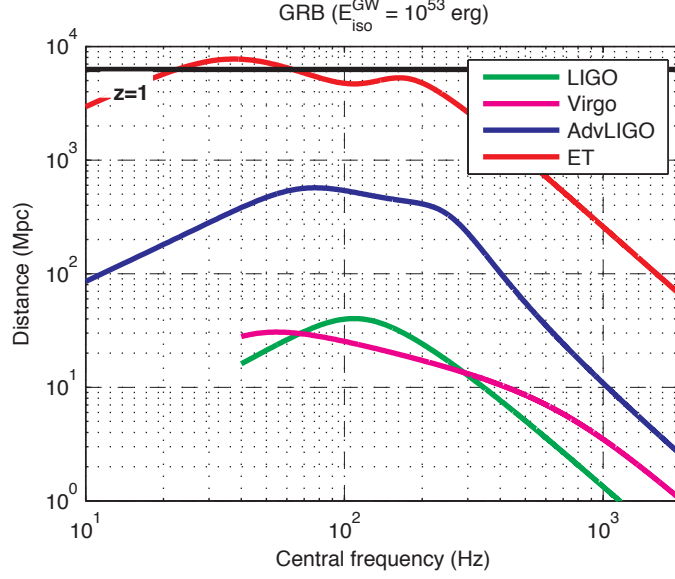
FIG. 15: 90%-confidence lower limit on distance for GRB burst sources assuming a GRB energy emission of $E_{\text{GW}}^{\text{iso}} = 0.05 M_\odot c^2 \sim 9 \times 10^{52}$ergs. The solid horizontal black line near the top of the figure shows a redshift $z = 1$.

From gravitational wave searches using coherent analysis techniques [148] we find that in general the 90%-confidence upper limit on h_{rss} gravitational wave amplitude is around an order of magnitude above the amplitude spectrum of the interferometer, i.e., $\sim 10 \times S_h(f)^{0.5}$. For narrow-band burst signals we can use the following approximation

$$E_{\text{GW}}^{\text{iso}} \simeq \frac{\pi^2 c^3}{G} D^2 f_0^2 h_{rss}^2 \qquad (4.1)$$

where $E_{\text{GW}}^{\text{iso}}$ is the isotropic energy emission in gravitational waves, D is the distance of the source, f_0 is the central frequency, and h_{rss} is the root-sum-square amplitude of the gravitational wave:

$$h_{\text{rss}} = \sqrt{\int \left(|h_+(t)|^2 + |h_\times(t)|^2 \right) \, dt} \; . \qquad (4.2)$$

From Eqn. 4.2 we can calculate a lower limit on source distance from our amplitude upper limit for a given assumption of $E_{\text{GW}}^{\text{iso}}$. For long GRBs the energy of emission in gravitational waves is not well known but has been estimated to be as high as $0.2 M_\odot c^2$ in the LIGO-Virgo frequency band of good sensitivity [149]. In Fig. 15 we estimate the distance to which various detectors are sensitive to a narrow-band burst of gravitational waves assuming $E_{\text{GW}}^{\text{iso}} = 0.05 M_\odot c^2$.

Soft Gamma Repeater Flares

Clark

As described in section IV C, a significant fraction, up to 15%, of short, hard γ-ray bursts may be associated with flaring activity in soft γ-repeaters (SGRs). These sources often
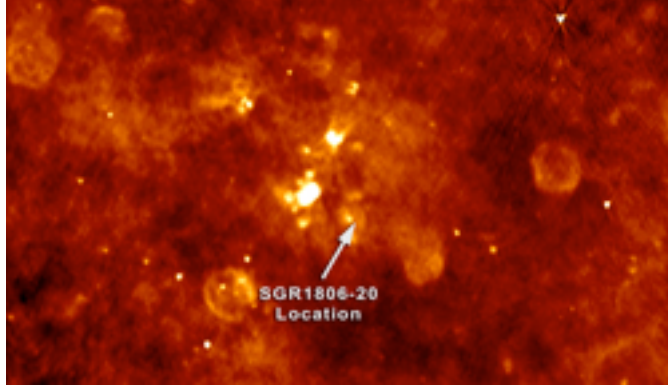
FIG. 16: A high resolution, wide-field image of the area around SGR1806-20 as seen in radio wavelength. SGR1806-20 can not be seen in this image generated from earlier radio data taken when SGR1806-20 was radio quiet. The arrow locates the position of SGR1806-20 within the image. Credit: University of Hawaii.
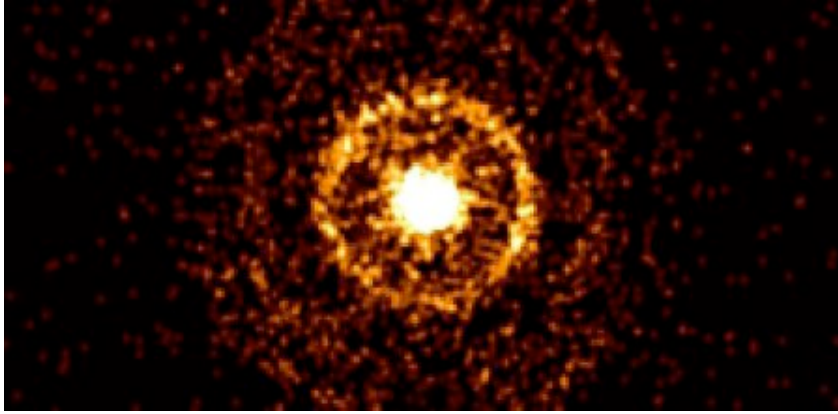

FIG. 17: Swift's X-Ray Telescope (XRT) captured an apparent expanding halo around the flaring neutron star SGR J1550-5418. The halo formed as X-rays from the brightest flares scattered off of intervening dust clouds. Credit: NASA/Swift/Jules Halpern, Columbia University

undergo sporadic periods of activity which last from days to months where they emit short bursts of hard X-rays and soft γ-rays with luminosities $L \sim 10^{41} \, \mathrm{erg \, s^{-1}}$ and photon energies in the range 10-30 keV. Much more occassionally, they exhibit enormous, giant flares with luminosities as large as $10^{47} \, \mathrm{erg \, s^{-1}}$. There exist 4 known soft γ-repeaters, 3 in the milky way and 1 in the Large Magellanic cloud. It is generally believed that SGRs belong to a class of neutron star, magnetars, with extraordinarily large magnetic fields in the the range 10^{14}-$10^{15} \, \mathrm{G}$ where the flaring activity is due to sudden, violent reconfigurations of complex magnetic field topologies.

The hardness of their spectra and the enormous luminosities involved mean that giant flares from nearby SGRs, such as that of SGR 1806-20 [152], represent an intriguing candidate progenitor scenario for some short duration γ-ray bursts. Indeed, in [153], the authors report a correlation between the positions of some short GRBs with those of low redshift galaxies, suggesting that $10-25\%$ of short GRBs occur in the local universe and, therefore,

are likely to be associated with giant SGR flares. Furthermore, evidence for the existence of two classes of progenitors for short GRBs is provided in [145]. Here, it is found that a bimodal luminosity function, representing a dual-population of short GRB progenitors with low and high luminosities, is required to reproduce the observed distributions of short GRB luminosities. As well as statistical evidence, there have been observations of at least three individual short GRBs which present candidates for extragalactic SGR flares. Optical and infrared observations [154] of GRB 050906 suggest a tentative association with the local, fairly massive ($M \sim 10^{11} M_\odot$) starburst galaxy IC328 which lies at a redshift of $z = 0.031$. If GRB 050906 had indeed originated in IC328, the isotropic equivalent energy would be $E_{\rm ISO} \sim 1.5 \times 10^{46}$ erg in the 15-150 keV range. The giant flare from SGR 1806-20, by comparision, emitted $E_{\rm ISO} \sim 4 \times 10^{46}$ erg with photon energies > 30 keV. As well as the potential similarity in the energetics of this burst, the association with a starburst galaxy, where young, shortly lived magnetars are believed to be most prevalent, corroborates the SGR progenitor scenario. Two other short GRB-SGR flare candidates, GRB 051103 and GRB 070201, were detected by the Konus-Wind GRB spectrometer [155, 156]. The localisation area of GRB 051103 was found to lie near M81 (D=3.6 Mpc), suggesting an isotropic equivalent energy $E_{\rm ISO} = 7 \times 10^{46}$ erg. As remarked in [155], if GRB 051103 was *not* related to an SGR flare, we would expect an optical and/or transient in the localisation area, which has not been observed. Finally, the localisation area of GRB 070201 was found to overlap with the spiral arms of M31 (D=0.78 Mpc), leading to an estimate of $E_{\rm ISO} \sim 1.5 \times 10^{45}$ erg under the SGR flare scenario and, again, comparable to the giant flare from SGR 1806-20.

In addition to these types of arguments related to the energetics of the electromagnetic emission, gravitational wave observations can provide an extremely powerful tool to identify SGRs as sGRB progenitors. First, we note that the failure to detect the signature of a compact binary coalescence from sGRBs at distances where such a signal is expected can provide compelling evidence for the SGR progenitor scenario alone. Indeed, observations by the initial LIGO instruments recently excluded the coalescence of a binary neutron star system within M31 at more than 99% confidence as the progenitor for GRB 070201 [146]. Furthermore, a binary neutron star merger is excluded at distances less than 3.5 Mpc with 90% confidence. If, however, the progenitor had been an SGR flare, the LIGO observations imply an upper bound on the isotropic energy released as an unmodeled gravitational wave burst of $E_{\rm ISO}^{\rm GW} < 7.5 \times 10^{50}$ erg, within the bounds permitted by existing models.

The non-detection of an expected inspiral gravitational wave signature, however, is not the only way that an instrument like the Einstein telescope can provide evidence for the SGR progenitor scenario. In section IV E, we discuss giant SGR flares as a source of quasi-periodic oscillations, with quadrupolar components in the $\sim 10 - 40$ Hz range. Observations of these shear mode oscillations in gravitational waves, with no accompanying inspiral signal, would only be explicable under the SGR scenario. It is also possible that non-radial oscillatory modes would become excited by tectonic activity associated with a giant SGR flare [150]. These modes will then be damped by gravitational wave emission, resulting in a characteristic ring-down signal [?]. Various families of oscillatory modes, such as fluid (f), pressure (p) and purely space-time (w) modes may be excited and simultaneous gravitational wave observations of all three of these families can be used to place tight constraints on the neutron star equation of state [?]. The p and w modes, however, tend to have frequencies well above 4 kHz making the f-mode, with frequencies expected in the range $1 - 3$ kHz [?], the most accessible to currently planned gravitational wave observations. Again, gravitational wave observations of f-mode ring-downs associated with sGRBs, where
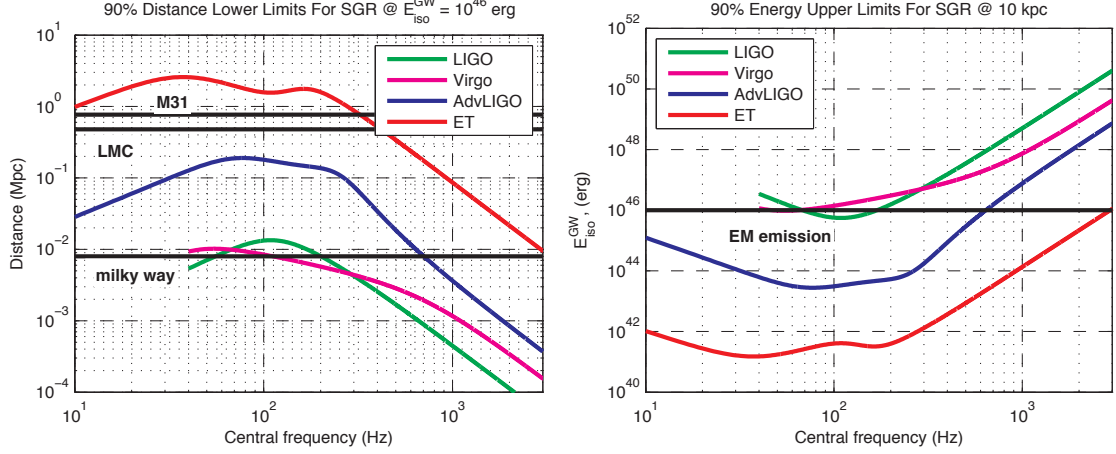
FIG. 18: *Left panel*: 90%-confidence lower limit on distance for burst sources assuming $E_{\mathrm{GW}}^{\mathrm{iso}} = 10^{46}$ergs for an SGR progenitor scenario. Starting from the lower edge of the figure, the solid horizontal black lines show the distances to center of our galaxy, the distance to the large Magellanic cloud and the distance to M31 in Andromeda. *Right panel*: predicted 90% upper limits on isotropically emitted gravitational wave energy from a galactic SGR flare (i.e., distance of 10 kpc). The solid black horizontal line shows the expected upper limit of 10^{46} erg from energetic arguments alone.

.

there is no accompanying inspiral signal, would point directly to an SGR giant flare as the progenitor.

Current models for SGRs [116, 150, 151] indicate that they will emit less than 10^{46}ergs in gravitational waves. In the left panel of Fig. 18 we show 90%-confidence lower limits on the distances to which various gravitational wave detectors will be sensitive to gravitational wave bursts with this energy and we see that, in their most sensitive frequencies, the current generation of interferometers are just able to probe our own galaxy. While advanced LIGO improves this reach substantially, it is really only with the Einstein telescope that observations of gravitational waves associated with extra-galactic SGR flares become possible. Figure 18 shows the complementary plot of 90% energy upper limits obtainable by the various instruments for a galactic SGR. We typically take this to mean a distance of ~ 10 kpc. Again, it is only with an instrument like the Einstein telescope that we are able to probe interesting energy regimes across the entire frequency spectrum one might reasonably expect for gravitational wave emission associated with SGR flares.

D. Why are the spin frequencies of QPOs locked in a small range?
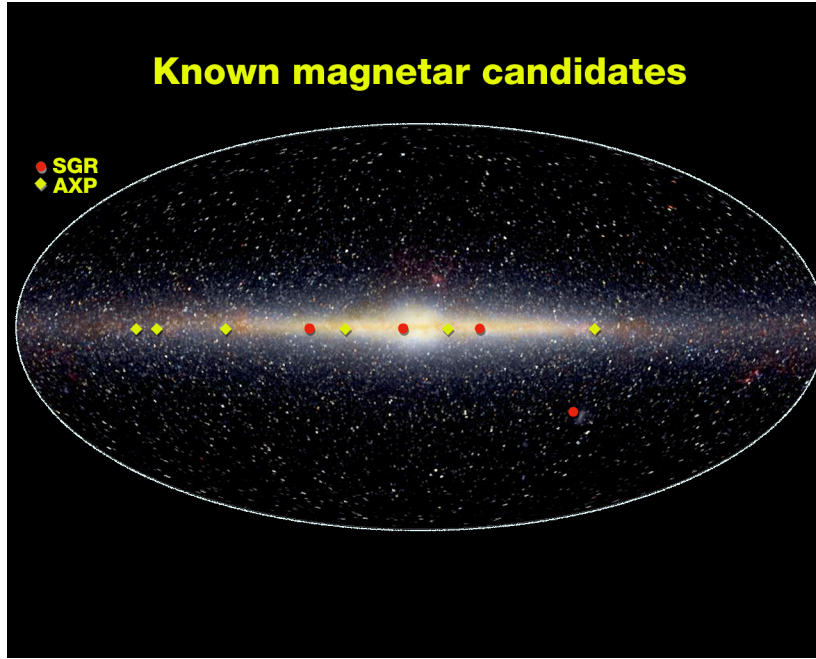
Watts

FIG. 19: The locations of known magnetar candidates (Soft Gamma-ray Repeaters and Anomalous X-ray Pulsars) in the Milky Way. Credit: NASA/Marshall Space Flight Center

E.   What is the origin of magnetar flares?

Glampedakis Neutron stars host the strongest magnetic fields known in nature. The magnetic field of a typical radio pulsar has an already enormous intensity of $\sim 10^{12}$ G. But this is nothing compared to magnetars which can reach or exceed the extraordinary intensity of $\sim 10^{15}$ G. It is now commonly believed that magnetars masquerade as both Anomalous X-ray pulsars (AXPs) and Soft Gamma-ray Repeaters (SGRs). The main energy reservoir in these objects is provided by the magnetic field itself, rather than the rotational energy. Their quiescent electromagnetic emission is punctuated by occasional high-energy bursts which could be the manifestation of magnetic field-driven tectonic activity in the neutron star's crust. By far the most energetic events are the so-called giant flares which have been observed in some SGRs. Most remarkably, the 'tails' of these magnetar flares contain clear signatures of several quasi-periodic oscillations (QPOs) in the $\sim 20 - 2000$ Hz band. The observed frequencies (at least the ones below 200 Hz) appear to match well the seismic mode frequencies of the crust, an interpretation also consistent with the large scale crust fracturing expected to occur during a giant flare. This is an exciting discovery since existing and future observations of SGR giant flares could be used as a tool for performing magnetar seismology through the direct observation of pulsation modes.

Magnetar flares could become a prime target for a gravitational wave detector like ET. It is likely that any vibration in the crust will quickly develop to a global magneto-elastic crust-core oscillation, since these two regions of the star are efficiently coupled by the strong magnetic field. The quadrupolar component of this type of oscillations is expected to have a frequency somewhere in the $\sim 10 - 40$ Hz range (this is the characteristic range for both the Alfvén crossing frequency and the fundamental quadrupole crust shear mode), a bandwidth

where ET is expected to be significantly more sensitive compared to the existing detectors. A gravitational wave signal associated with a global magnetar mode could last about a minute (i.e. the typical lifetime of a QPO observed in X-rays) which translates to about a thousand wavecycles, or a factor ~ 30 boost in the signal-to-noise ratio. This kind of gravitational wave signal would carry precious information about the (largely unknown) interior properties of magnetars, such as the strength and topology of the magnetic field and the elastic properties of the crust. With an instrument like ET operational, magnetar seismology might turn to a strong synergy between the electromagnetic and gravitational wave neutron star communities.

Gravitational wave observations may also provide valuable clues about the precise nature of the magnetar flare-trigger, which is presently a subject of speculation. The current magnetar model envisages that giant flares may be caused by large scale starquakes in the magnetar's crust which is subject to a growing strain due to the secularly evolving magnetic field in the core and the crust. Another possibility could be the triggering of a dynamical hydromagnetic instability somewhere in the core. In both scenarios, the magnetic field (and any matter coupled to it) is likely to undergo a global change which could potentially have an observable gravitational wave burst-like signature, most likely in the same low-frequency band relevant for the QPOs.

F. What causes a glitch in pulsar spin frequency?

Glampedakis

Many radio pulsars exhibit glitches, sudden spin-up events followed by a relaxation period towards stable secular spin-down. Pulsar glitches have a long observational history (beginning shortly after the discovery of the first pulsar) and so far over a hundred pulsars are known to have glitched at least once. Glitches have also been observed in magnetars. The archetypal glitching pulsar is Vela, which exhibits regular large glitches with an amplitude corresponding to a fractional spin frequency jump of the order of 10^{-6}.

Despite the wealth of observational data, the phenomenon of glitches remains an enigma from the theoretical point of view. It is widely believed that glitches are related with the existence of superfluids in the interior of mature neutron stars and that they involve a transfer of angular momentum from a superfluid component to the rest of the star, which includes the crust (to which the pulsar mechanism is presumed to be rigidly attached) and the charged matter in the core. A superfluid rotates by forming an array of quantised vortices and it can spin down provided the vortices can move outwards. If the vortex migration is impeded by 'pinning' to the other component then the superfluid cannot keep up with the spin-down due to electromagnetic braking. As a result a rotational lag develops between the two components until some critical level is reached at which the vortices unpin and transfer angular momentum to the rest of the star, and the two components are driven to corotation.

The nature of the instability causing vortex unpinning and the subsequent stage of relaxation of the system is poorly understood. One might hope that gravitational radiation detected by a glitch event could help unveil the key physics associated with this enigmatic phenomenon. It is likely that a glitch event involves the excitation of some of the inertial modes of the two-component system and the post-glitch relaxation is governed by the coupling of the two components through the vortex-mediated mutual friction force and the magnetic field. In fact, as recent work suggests, the glitch trigger-mechanism may be the result of a superfluid 'two-stream' instability setting in through the inertial modes of the

system.

An instrument like ET would be the ideal tool for detecting a gravitational wave signal in the 10-100 Hz band which is the relevant one for the inertial modes of a Vela-like pulsar. The detection of gravitational wave signals from glitching pulsars would provide a tool for probing the interior matter of neutron stars and supplement the existing and future electromagnetic observations. The realisation of this exciting prospect will require (as in the case of other potential sources of gravitational radiation) the input of theoretical waveform templates. These waveforms should be computed using detailed multifluid hydrodynamical models for superfluid neutron stars, accounting for effects like vortex mutual friction and pinning.

G. r-modes in ET: a neutron star deep probe

Leone B. Bosi

Just after the supernovae core collapse, gravitational waves could be emitted by the new born, hot, rapidly rotating neutron star. In particular gravitational radiation are emitted by neutron star due to r-modes[157], which are non-radial pulsation modes of rotating stars that have the Coriolis force as their restoring force. The characteristic frequency of the GW is comparable to the rotation speed of the star. r-modes modes induce differential rotation at second order in the modes amplitude, driven unstable by gravitational radiation [158]. These second order perturbation plays an important role in the nonlinear evolution of the r-mode instability, which makes gravitational waves detection more difficult.

GW detection and measurement depends strongly on the r-mode saturation amplitude, that recent simulation and theoretical evaluation give much lower than unity. This means that detection of such gravitational waves is more difficult than initially supposed. In this section we considered r-mode, but taking into account another nonlinear effect, the differential rotation induced by r-modes[159]. The ammount of differential rotation associated to the R-mode, the parameter K, depends on the model and initial conditions, varying in the range $[-5/4 - 10^{13}]$.

Such kind of signals could open important opportunity for the ET science goals, representing a deep probe about aspects of the neutron star formation process and nuclear physics.

H. r-modes gravitational waves strength

Detectability of the gravitational waves from r-modes depends on the ammount of angular momentum carried away by gravitational waves. As described in [160], for $K = 0$, the total angular momentum of the star decreases to 65% of its initial value and part of the initial angular momentum of the star, about 58% is transferred to the r-mode, as a consequence of the rapid increase of the average differential rotation . Therefore the initial angular momentum is carried away by gravitational waves is about 35% . This result is really dependent on K value, in fact for higher K the amount of angular momentum carried away by gravitational waves decreases even less then 1%.

From the model in [160] the frequency f of the gravitational wave depends on the star angular velocity ω by $f = \frac{2\Omega}{3\pi}$. An estimation of the frequency range is provided:

- f_{min} is close to $[77 - 80]$Hz and it depends on the final value of the angular velocity $\Omega(t_f)$ and K
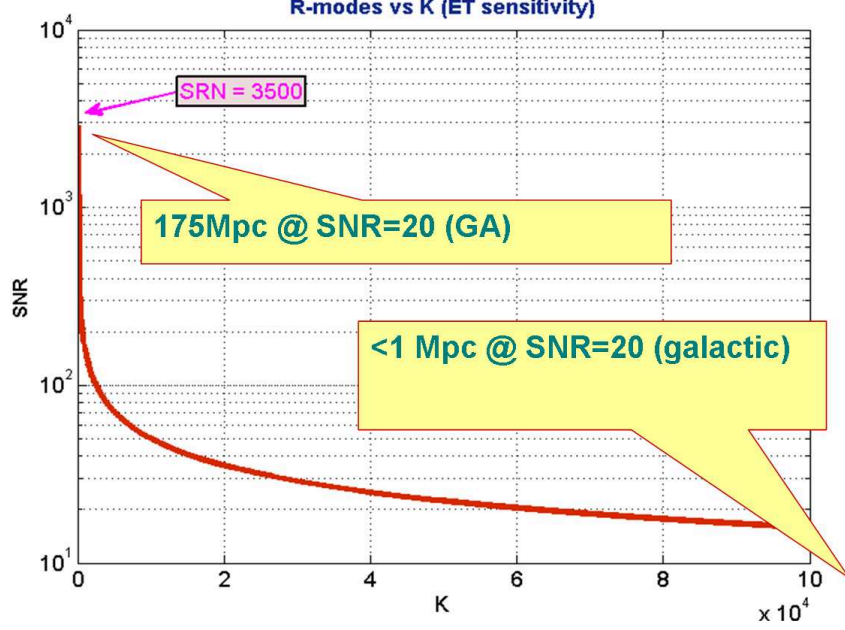
FIG. 20: In figure the Virgo sensitivity at the beginning of VSR1 and just after the science run are shown. Sensitivity improvements during VSR1 are clearly visible.

- f_{max} is close to 1200 Hz and it depends on the initial value of the angular velocity Ω_0

The amplitude in the frequency domain is given by:

$$H(f) = \frac{4.6 * 10^{-25}}{\sqrt{2+K}} \sqrt{\frac{f_{max}}{f}} \frac{20Mpc}{D} Hz^{-1}$$

where D is the source distance in Megaparsec, f the GW signal frequency and f_{max} is its maximum frequency, where $f_{max} = 1191$.

In [160] an estimation of the signal to noise ratio (SNR) for Advanced LIGO is provided. We have remade the estimation but using the ET sensitivity[2]. In this case the optimal signal to noise ratio is given by the formula:

$$\frac{S}{N} = \frac{250}{\sqrt{(2+K)}} \frac{20Mpc}{D}$$

It is clear the strong dependence on the unknown parameter K, as reported in figure 20. On that we consider an SNR of 20, chosen arbitrary just by the fact that we want to observe pretty well the signal. It is possible to conclude that the range of distances on which gravitational signal could be visible is really large. Considering the optimistic case when $K = 0$, we obtain a sight distance for an optimally oriented source of 175Mpc; while considering the pessimistic case when $K = [10^5 - 10^6]$, the sight distance falls down to less than $1Mpc$ (galactic sources).

---

[2] The ET sensitivity used for this estimation it the ET-B

I. r-modes and ET science goals

One of the main reason why gravitational waves from r-mode instability are important as ET science goal is related to the opportunity of producing unique correlation with nuclear physics of the neutron star and formation processes. Such kind of signal could be seen as inner probe of neutron star dynamics.

We want provide just some example on possible implication:

- In principle from gravitational wave signals and signals models it is possible to trace and quantify the initial conditions of the new born star such as initial frequency, initial temperature and others. This could lead to confirm or exclude a set of supernova models, star formation processes and NS models that agree with these experimental data.

- Another implication is about Neutron Star nuclear physics models and the EOS definition, permitting to open a window on the core and crust physics, especially about superfluid aspects.

- Neutron star temperature decreases due to neutrons emission, and also this phenomena interacts with r-modes instability. In this case gravitational waves could provide information about cooling rate and cooling model, that at the moment is assumed to be due to the modified URCA process.

Hence, a possible observation of this signals by Einstein Telescope can put constrains on a set of theories, concerning Neutron Star formation processes, neutron star nuclear physics models and Equation of State.

At the moment a lot of interest exists around the possibility of observing gravitational waves generated by r-modes instability. In the present document we use the results presented in [160], where they consider r-mode with $l = 2$, but more in general there are efforts that leads to understand better the full dynamics of the newborn star considering higher number and type of modes, like the work presented in [161]. On that it is important to investigate more such models and simulations in order to look for science opportunity for ET.

V. COSMOLOGY

Sathya

The goal of modern cosmology is to measure the geometrical and dynamical properties of the Universe by projecting the observed parameters onto a cosmological model. The Universe has a lot of structure on small scales, but on a scale of about 100 Mpc the distribution of both baryonic (inferred from the electromagnetic radiation they emit) and dark matter (inferred from large scale streaming motion of galaxies) components is quite smooth. It is, therefore, quite natural to assume that the Universe is homogeneous and isotropic while describing its large-scale properties. In such a model, the scale factor $a(t)$, which essentially gives the proper distance between comoving coordinates, and curvature of spatial sections k, are the only quantities that are needed to fully characterize the properties of the Universe. The metric of a smooth homogeneous and isotropic spacetime is

$$ds^2 = -dt^2 + a^2(t)\frac{d\sigma^2}{1 - k\sigma^2} + \sigma^2 \left(d\theta^2 + \sin^2\theta\, d\varphi^2\right),$$

where t is the cosmic time-coordinate, $(\sigma,\, \theta,\, \varphi)$ are the comoving spatial coordinates, and k is a parameter describing the curvature of the $t = $ const. spatial slices. $k = 0, \pm 1$, for flat, positively and negatively curved slices, respectively. The evolution of $a(t)$, of course, depends on the parameter k, as well as the "matter" content of the Universe. The latter could consist of radiation, baryons, dark matter (DM), dark energy (DE), and everything else that contributes to the energy-momentum tensor.

The Friedman equation, which is one of two Einstein equations describing the dynamics of an isotropic and homogeneous Universe, relates the cosmic scale factor $a(t)$ to the energy content of the Universe through

$$H(t) = H_0 \left[\hat{\Omega}_{\mathrm{M}}(t) - \frac{k}{H_0^2 a^2} + \hat{\Omega}_{\Lambda}(t)\right]^{1/2}, \tag{5.1}$$

where $H(t) \equiv \dot{a}(t)/a(t)$ is the Hubble parameter ($H_0 = H(t_P)$ being its value at the present epoch t_P), $\hat{\Omega}_{\mathrm{M}}(t)$ and $\hat{\Omega}_{\Lambda}(t)$ are the (dimensionless) energy densities of the DM and DE, respectively. The above equation has to be supplemented with the equation-of-state of DM, assumed to be pressure-less fluid $p = 0$ [$\hat{\Omega}_{\mathrm{M}}(t) = \Omega_M(1 + z)^3$, $\Omega_{\mathrm{M}} = \hat{\Omega}_{\mathrm{M}}(t_P)$] and of DE, assumed to be of the form $p = w\rho_\Lambda$ [$\hat{\Omega}_{\Lambda}(t) = \Omega_\Lambda(1 + z)^{3(1+w)}$, where $\Omega_\Lambda = \Omega_\Lambda(t_P)$], with $w = -1$ corresponding to a cosmological constant. The goal of cosmography is to measure $(H_0, \Omega_{\mathrm{M}}, \Omega_\Lambda, w, k, \ldots)$, which essentially determine the large-scale geometry and dynamics of the Universe. In the rest of this paper we shall assume that the spatial slices are flat (i.e., $k = 0$).

A. Measuring the cosmological parameters

Sathya

Astronomers use "standard candles" to measure the geometry of the Universe and the various cosmological parameters. A standard candle is a source whose intrinsic luminosity L can be inferred from the observed properties (such as the spectral content, time-variability of the flux of radiation, etc.). Since the observations also measure the apparent luminosity
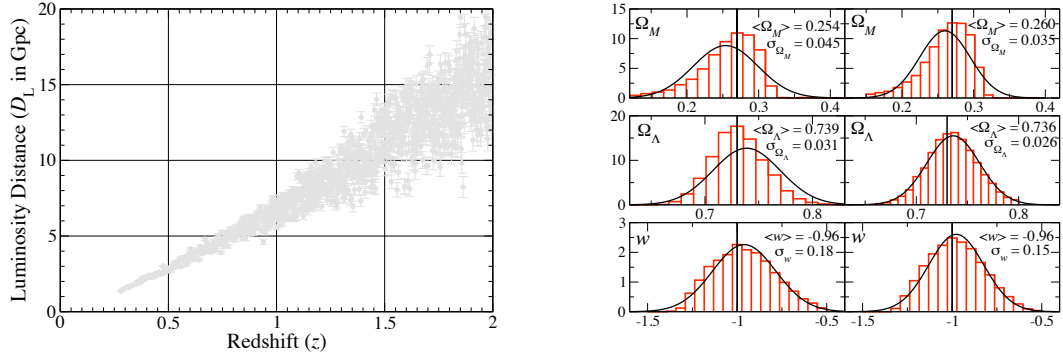
FIG. 21: The plot on the left shows one realization of a catalogue of binary neutron star (BNS) events that might be observed by ET. The plot on the right shows the distribution of errors in Ω_M, Ω_Λ and w obtained by fitting 5,190 realizations of a catalogue of BNS merger events to a cosmological model of the type given in Eq. (5.2), with three free parameters. The fractional 1-σ width of the distributions $\sigma_{\Omega_M}/\Omega_M$, $\sigma_{\Omega_\Lambda}/\Omega_\Lambda$, and $\sigma_w/|w|$, are 18%, 4.2% and 18% (with weak lensing errors in D_L, left panels) and 14%, 3.5% and 15% (if weak lensing errors can be corrected, right panels).

F, one can deduce the luminosity distance D_L to a standard candle from $D_L = \sqrt{L/(4\pi F)}$. In addition, if the red-shift z to the source is known then by observing a population of such sources it will be possible to measure the various cosmological parameters since the luminosity distance is related, when $k = 0$, to the red-shift via

$$D_L = \frac{c(1+z)}{H_0} \int_0^z \frac{dz'}{[\Omega_M(1+z')^3 + \Omega_\Lambda(1+z')^{3(1+w)}]^{1/2}}. \tag{5.2}$$

There is no unique standard candle in astronomy that works on all distance scales. An astronomer, therefore, builds the distance scale by using several steps, each of which works over a limited range of the distance. For instance, the method of parallax can determine distances to a few kpc, Cepheid variables up to 10 Mpc, the Tully-Fisher relation works for several tens of Mpc, the D_n-σ relation up to hundreds of Mpc and Type Ia supernovae up to red-shifts of a few. This way of building the distance scale has been referred to as the *cosmic distance ladder*. For cosmography, a proper calibration of the distance to high red-shift galaxies is based on the mutual agreement between different rungs of this ladder. It is critical that each of the rungs is calibrated with as little an error as possible.

B. Fitting a cosmological model to CBC population

Sathya

The expected rate of coalescences per year within the horizon of ET is $\sim$ several $\times 10^5$ for BNS and NS-BH. Such a large population of events to which luminosity distances are known pretty accurately, would be very useful for measuring cosmological parameters. If, as suspected, BNS and NS-BH are progenitors of short-hard gamma-ray bursts (GRBs) [?], then it might be possible to make a coincident detection of a significant subset of the events
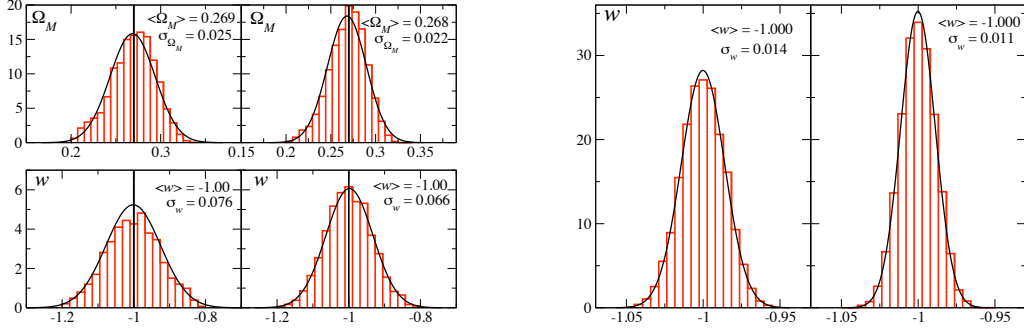
FIG. 22: Same as the right plot of Fig. 21 except that one or more of the cosmological parameters are assumed to be known. The plot on the left assumes that Ω_Λ is known to be $\Omega_\Lambda = 0.73$, and fits the "data" to the model with two free parameters. The fractional 1-σ widths in the distribution $\sigma_{\Omega_\mathrm{M}}/\Omega_\mathrm{M}$ and and $\sigma_w/|w|$, are 9.4% and 7.6% (with weak lensing errors in D_L, left panels) and 8.1% and 6.6% (if weak lensing errors can be corrected, right panels). The plot on the right is the same but assuming that w is the only unknown parameter. The fractional 1-σ width of the distribution $\sigma_w/|w|$ is 1.4% (with weak lensing errors in D_L, left panel) and 1.1% (if lensing errors can be corrected, right panel).

in GW and EM windows and obtain both the luminosity distance to and red-shift of the source.

Since GRBs are believed to be beamed with beaming angles of order $40°$, we assume that only a small fraction ($\sim 10^{-3}$) of binary coalescence events will have GRB or other EM afterglows that will help us to locate the source on the sky and measure its red-shift z. Eventually, we will be limited by the number of short-hard GRBs observed by detectors that might be operating at the time. As a conservative estimate, we assume that about $1,000$ BNS and NS-BH mergers will have EM counterparts over a three-year period. For definiteness we consider only BNS mergers and take these to have component masses of $(1.4, 1.4)M_\odot$.

How well would we measure cosmological parameters with a catalogue of such sources?

To answer this question we simulated 5,190 realizations of the catalogue containing 1,000 BNS coalescences with known red-shift and sky location, but the luminosity distance subject to statistical errors from GW observation and weak lensing. One such realization is shown in Fig. 3 (right panel). We assumed that the sources were all in the red-shift range $0 \leq z \leq 3.5$, distributed uniformly (i.e., with constant comoving number density) throughout this red-shift range. The luminosity distance to the source was computed by assuming an FRW cosmological model with $H_0 = 70\,\mathrm{km\,s^{-1}\,Mpc^{-1}}$, $\Omega_\mathrm{M} = 0.27$, $\Omega_\Lambda = 0.73$, and $w = -1$, but the *measured* distance was drawn from a Gaussian distribution whose width σ_{D_L} was determined by the quadrature sum of the errors due to weak lensing and GW observation. Weak lensing error in D_L was assumed to be 5% at $z = 1$ and linearly extrapolated to other red-shifts. GW observational error was estimated from the covariance matrix C_{km} of the five-dimensional parameter space of the unknown signal parameters $p_k = (M, \nu, t_0, \Phi_0, D_\mathrm{L})$:

$$C_{km} = \Lambda_{km}^{-1}, \quad \Lambda_{km} = \langle h_k, h_m \rangle, \quad h_k = \frac{\partial h}{\partial p_k}. \tag{5.3}$$

Here the angular brackets denote the scalar product, which, for any two functions $a(t)$ and

$b(t)$, is defined as

$$\langle a,\, b \rangle = 4\Re \int_0^\infty \frac{\mathrm{d}f}{S_h(f)} A(f)\, B^*(f) \tag{5.4}$$

where A and B are the Fourier transforms of the functions $a(t)$ and $b(t)$, respectively, and $S_h(f)$ is the ET noise power spectral density. Note that since GRBs are expected to be strongly beamed, we did not take the angles (ι, ψ) associated with the unit normal to the plane of the inspiral as unknown variables. This assumption is justified: even if the opening angle of a GRB beam is as large as $40°$, the unit normal to the plane of the inspiral would still be confined to only 3% of the area of a unit sphere. Averaging errors over (ι, ψ) with the constraint $\iota < 20°$ would then be little different from taking $\iota = 0°$. We did, however, average the errors over the sky position angles (θ, ϕ). We then fitted each realization of the source catalogue to the cosmological model given in Eq. (5.2), using the Levenberg-Marquardt algorithm [162, 163], in order to find a set of best fit parameters. It turns out that a catalogue of 1,000 sources is not quite enough for an accurate determination of all the parameters. However, assuming that H_0 is known accurately, the algorithm gave the best fit parameters in $(\Omega_M, \Omega_\Lambda, w)$ for each of the 5,190 realizations.

The distributions $\mathcal{P}$ of the parameters obtained in this way are shown in Fig. 21, where the vertical line is at the true value of the relevant parameter. The relative 1-σ errors in Ω_Λ, Ω_M and w, are 4.2%, 18% and 18% (with weak lensing, left panels) and 3.5%, 14% and 15% (with weak lensing errors corrected, right panels). Although $\mathcal{P}(w)$ is quite symmetric, $\mathcal{P}(\Omega_M)$ and $\mathcal{P}(\Omega_\Lambda)$ are both skewed and their mean values are slightly off the true values. However, the medians are mostly coincident with the true values.

In addition to H_0 if Ω_Λ is also known (or, equivalently, if $\Omega_M + \Omega_\Lambda = 1$), then one can estimate the pair (Ω_M, w) more accurately, with the distributions as shown in Fig. 21 with greatly reduced skewness and 1-σ errors in Ω_M and w, of 9.4% and 7.6% (with weak lensing) and 8.1% and 6.6% (with lensing errors corrected). Finally, if w is the only parameter unknown, it can be measured to an even greater accuracy as shown in Fig. 21 with 1-σ errors of 1.4% (with weak lensing) and 1.0% (with lensing errors corrected).

The results of our simple simulation are quite encouraging but further work is needed to confirm the usefulness of GW standard sirens in precision cosmology. Let us mention some that are currently being purused. Spins of component stars can be legitimately neglected in the case of neutron stars (and hence in BNS) but not for black holes and the modulation in the signal caused by the spin of the black hole can improve parameter accuracies. We assumed, for simplicity, that all our systems are BNS systems with masses $(1.4, 1.4)M_\odot$. In reality, the catalogue will contain a population consisting of a range of NS and BH masses. A more realistic Monte Carlo simulation would draw binaries from the expected population rather than the same system, some of which (more massive and/or equal-mass systems) would lead to better, but others to worsened, parameter accuracies. The signal contains additional features, such as other harmonics of the orbital frequency than the second harmonic considered in this work and the merger and ringdown signals. Both of these are important for heavier systems and could potentially reduce the errors. These factors are currently being taken into account to get a more reliable estimation of the usefulness of ET in precision cosmography.

C. Stochastic background from inflation or alternatives

Thomas Dent
Inflation

There are very many models of inflation that do the following jobs: exponentially expanding the scale factor in a short time; sourcing primordial scalar density perturbations with amplitude $\mathcal{O}(10^{-5})$ and an approximately Harrison-Zeldovich ($n_s \simeq 1$) spectrum; and finally reheating the Universe to at least the temperature required for primordial nucleosynthesis, ten MeV or so. (A considerably higher temperature $T \geq \mathcal{O}(100)\,\text{GeV}$ is required for generation of most types of dark matter and for baryogenesis.) In standard scenarios of inflation, the scale factor is an approximately exponential function of time over several tens of e-folds. The time translation symmetry during inflation maps to a scaling symmetry of the spectrum: perturbations generated earlier (later) are inflated to larger (smaller) scales but are otherwise (nearly) identical.

In this section we consider the tensor perturbations sourced during inflation. They can generally be described by an amplitude and spectral index, but since they are generated similarly to the scalar perturbations the relevant parameter is usually taken as the *tensor-to-scalar ratio r*. For a "flat" spectrum $\Omega_{gw}(f) = $ const. the conversion is $\Omega_{gw}(f) =$(some function of r). Current observational bound on r from CMB (+BAO, SN) is 0.22, though at frequencies enormously smaller than any GW detector could probe. Planned experiments should take this down to few times 0.01. The bound from BBN on the *integrated* Ω_{gw} over all f is 10^{-5} from BBN.

- Pulsar timing bound
- Energy scale of inflation - Lyth '84
- 'Lyth bound' on r - Lyth '97
- Lyth/Riotto review

Allowing for an independent tensor spectral index n_t (a scale-invariant spectrum would have $n_t =$CHECK), the GW energy density at the nominal frequency of 10 Hz is

$$\Omega_{gw}(10\,\text{Hz}) = something \times 10^{-4} n \times 10^{19(n_t - const)}. \tag{5.5}$$

Thus for significantly blue spectral indices one might see something...

- Curvaton?
- brane inflation (strings) - eg Lidsey / Seery, also Krause
- 'braneworld inflation' - Frolov/Kofman, Langlois th/0006

Alternatives to inflation

Recognized alternatives to exponential inflation with an (effective) scalar field are essentially two. In the 'pre-big-bang' idea coming out of string cosmology, the scale factors of extra dimensions evolve under various forces and may make a transition from a contracting to an expanding Universe. The tensor/ GW spectrum is potentially interesting, however the (scalar) density perturbations are generically wrong. Are there models with a H-Z spectrum or anything close?

The 'ekpyrotic' and 'cyclic' models do not have a clear derivation from fundamental theory, and add a singular event called 'brane collision' at the transition from contraction to expansion, which is claimed to result in an observationally viable spectrum. There is scepticism whether the models are correct or meaningful without an explicit description of the 'collision'. The gravitational wave amplitude is claimed to be undetectably small in any case.

D. Stochastic background from reheating and phase transitions

Thomas Dent
Reheating and related phenomena
- Hybrid models
- Parametric resonance
- Curvaton?
- Flat directions
Phase transitions and colliding bubbles
- GUT / related phase transitions
- EWPT - bubbles, 'turbulence', magnetic fields - Caprini, Durrer, ..
- Others: In the "RS1 model" of a warped brane world (Randall/Servant)...

E. Stochastic background from topological defects

Thomas Dent
In many models of inflation or subsequent phase transitions, there are
Cosmic strings and superstrings
Other defects

F. Black hole seeds and galaxy formation

Gair It is widely accepted that the massive black holes (MBHs) found in the centres of many galaxies grow from initial seeds through the processes of accretion and mergers following mergers between their host dark matter halos. However, little is known about the seeds from which these black holes grow. Open questions include — how and when did they form? What are their masses? Where are they? Current observations are consistent with both *light seed* scenarios, in which $\sim 100 M_\odot$ black hole seeds form at redshift $z \approx 20$ from the collapse of Population III stars [164, 165], and *heavy seed* scenarios, in which black holes of mass $\sim 10^5 M_\odot$ form from direct collapse of dust clouds [166, 167]. Mergers between MBHs in merging dark matter halos will generate gravitational waves. These are a major source for LISA [168], but LISA will only see mergers with total mass $\gtrsim 10^3 M_\odot$. LISA can therefore probe black hole seeds only in the heavy seed scenario and does not have the power to discriminate between the light and heavy scenarios.

The Einstein Telescope will have sensitivity in the 1–50Hz band in which gravitational waves from mergers involving ~ 10–$100 M_\odot$ black holes will lie. It will therefore provide complementary information to LISA and could directly observe the first epoch of mergers between light seeds. Present estimates, based on Monte Carlo simulations of galaxy merger trees [169, 170], suggest the Einstein Telescope could detect between a few and a few tens of seed black hole merger events over three years of operation [171]. Several of these events will be at high redshift, $z \sim 5$, by which time it is unlikely that $100 M_\odot$ black holes could have formed by other routes. ET and LISA in conjunction probe the whole merger history of dark matter halos containing black holes in the 10–$10^6 M_\odot$ range, which will provide detailed information on the hierarchical assembly of galaxies. ET on its own is not able to measure the distance to a gravitational wave source, but provided one additional, non-colocated, interferometer is in operation concurrently with at least two detectors at the ET site, the

network will be able to determine the luminosity distance of a source to $\sim 40\%$ precision and the redshifted total mass of the system to $\lesssim 1\%$. Using a concordance cosmology, this distance estimate can be used to estimate redshift with comparable accuracy and so it should be possible to say that the $z \approx 5$ events are of *low mass* and at *high redshift*, and therefore are convincing candidates as Pop III seed mergers.

Just one detection by ET will rule out the heavy seed model. With several detections, we will be able to make statements about pop III seed black hole properties, such as their mass distribution, their early accretion history etc. [171]. These observations cannot be made be any other existing or proposed detector — it is science that is unique to ET. Such observations will be vital to our understanding of the assembly of structure in the Universe, and of the close link between black holes residing in the centres of galaxies and their hosts [164].

VI. COMPUTATIONAL CHALLENGES

L. Bosi

The opportunity of using gravitational waves detected by ET as carrier of an inner physics have to deal with the computational requirements needed to analyze and achieve the pre-fixed scientific goals. Hence it is important to focus on that, dividing the problem in two main streams. In the fist we have to keep an eye open on the general developments of computational hardware and infrastructure, in order to take advantage of the advances in computational technologies and trying to projecting the available computational power and programming paradigm at the ET era. In the second we need to understand and assess what sort of computational resources might be required for ET data processing and, more importantly, the kind of algorithms required to search for signals in the ET era. This last topic is the more challenging problem, because the detector contain many sources at the same time and extract known and unknown signals from a noise dataset requires data analysis paradigms on for each sources or investigation.

A. Computational infrastructure developments

The exploration of ET-era technological scenario have to cover hardware and software aspects. In order to have a vision of the complexity size that we will be able to address at 10-15 years from now, it is foundamental start to build an idea of which direction we have to follow, concerning computational power availability and programming paradigms. Next 10-15 years, computer hardware and software develop will be full of challenges. Most of these changes are due to the limit in processors realization at which integration scale is approaching. Up to now, usually vendors have applied two main procedure to increase CPU performances. The first concerns the CPU frequency, made increasingly higher. The second concern the realization of ever more complex superscalar architecture, in which CPU pipelines are fragmented in many tens of stages, with an high number of cache levels, control units, superscalar execution units and more. Both these strategies lead to an increase on the transistors density and than to a reduction of the single transistor size. In Fig. 23, left panel, the number of transistors per CPU evolution is shown, permitting to observer the so called Moore's law: Since the invention of the integrated circuit in 1958, the number of transistors on a given chip double every two years. Several measures of digital technology are improving at exponential rates related to this empirical law, including the size, cost, density and speed of components.

Clearly this evolutionary process cannot be infinite, but using the Mr Moore words: by about 2020, my law would come up against a rather intractable stumbling block: the laws of physics. In fact at the moment CPUs are realized involving a 45nm technology [3] and manufacturers will be able to produce chips on the 16-nanometer manufacturing process, that is expected by conservative estimates to arrive in 2018. After that maybe one or two manufacturing processes will be, but no more; The physical limits is imposed by the fact that such integration scale means CPU elements realized with hundred of atomic radii. Awaiting for something really new like quantum computing, the actual semiconductor architectures will be pushed on 2020 to their teoretical limit, introducing many significative innovations.

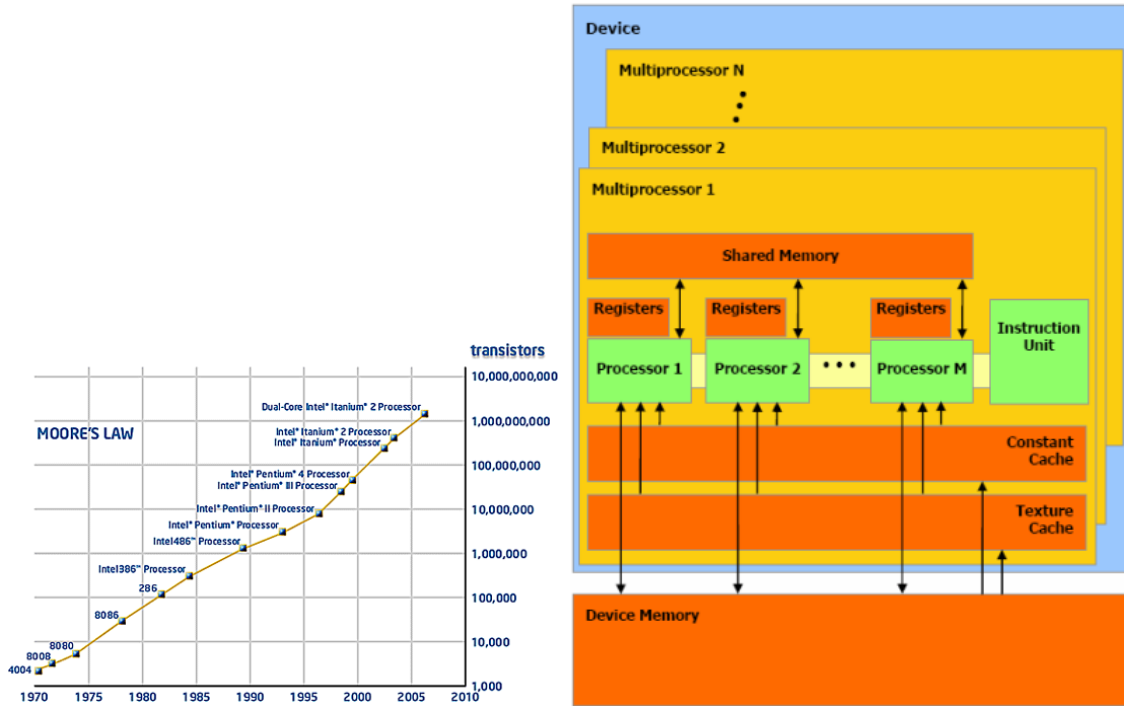[3] The 32nm technology [173] will be released this year (2009)

FIG. 23: The left plot shows the Moore's law. The right plot shows the NVIDIA-CUDA architecture as in [172]. Many processor cores are embedded in the same multiprocessor and many multiprocessor can be mounted in the same graphic board. At the moment NVIDIA boards exist with more than 250 cores.

Obviously a rethinking is necessary and in fact it is already ongoing, involving not only CPUs design but also all the hardware devices(memory, busses, ...), operating systems and programming paradigms. If we follow last 10 years of processors evolution we discover various steps that have introduced several level of parallelism. CPUs had embedded parallel aut-of-order execution units, SIMD instruction set and in the last 6 years Hyperthreading functionalities, permitting to duplicate part of the processing pipeline. Then in the last 3 years we have seen CPUs realized with multi-cores design, where the CPU cores have been duplicate 2,4 or 8 times. The common idea is to improve the number of operations that a single CPU can perform on a single clock beat, moving toward an increasingly parallel architecture. In the next 10-15 years we expect to see a proliferation of the number of cores, defining the so called "Many Cores" architectures. Such evolution means that the number of threads running on each CPU socket will increase significantly, permitting to realize optimized hardware for massive parallel code[4]

Right now we can observe some interesting manufacters efforts on that directions. Such experiences could be important to investigate for ET purpose. For example right know progresses on the side of Graphical Processing Units (GPU) have permitted to propone products not only for graphical purpose, but also for complex computational applications.

---

[4] In this presentation we don't talk about Buses and Memories that are some of the main computer power limitation of the actual architecture. Obviously also a develop on these devices is expected in order to follow the CPU develop.

In fact the architectures of these processors implement a massive parallel approach, where many scalar cores are embedded on a single Processing Units, with a paradigm that can be called "Single Instruction Multiple Thread" (SIMT). About that it is notable the NVIDIA GPUs example, due to level of development of "CUDA"[172] project. This is a general purpose parallel computing architecture that uses the parallel compute engine of NVIDIA (GPUs), as shown in Fig. 23, right panel. A similar project, even if in a smaller scale, is given by AMD-ATI manufacter[174]. Moreover it is important to mention that for the next
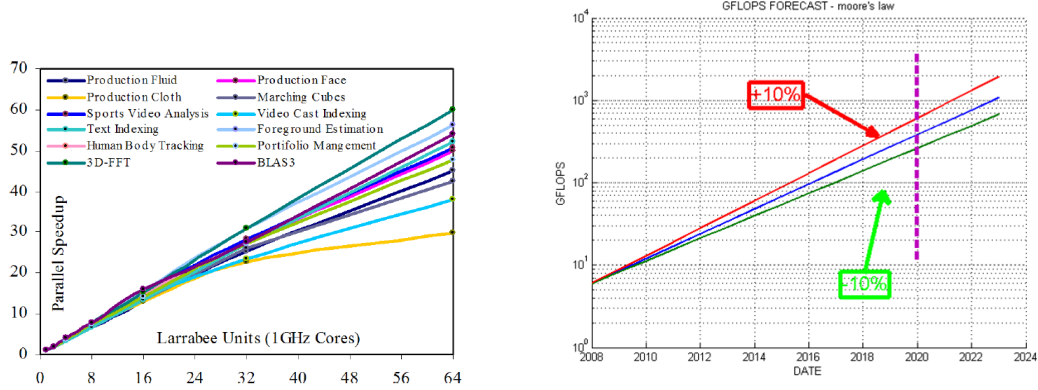

FIG. 24: The left plot shows LARRABEE scalability gain per core of non-graphics applications and kernels, as reported in [175]. The right plot shows the Forecast of Floating operations per second (Floats), based on FFT algorithm benchmarking and applying the Moore's law.

year Intel will release the first GPU based on LARRABBE[175] project. If the promises will be respected, that will be the first example of many-core system based on x86 architecture.

After this very short presentation, it is clear that a change in hardware paradigms affects deep changes in programming paradigms. That is usually the real difficulty because involve conceptual step on the "way of thinking". One of the inner implication on the common "way of thinking" is that, given a specific many-cores hardware, the ammount of floating operations per seconds (Flops) that a CPU can express is not the algebraic sum of the single cores power[5], but it is limited by the used programming models and on how the specific computational problem fits the hardware architecture (e.g Fig. 24, left plot).

If we make the hypothesis that the Moore's law will be valid for the next 15 years, we can try to forecast maximum GFlops available on a single "CPU", as shown in Fig. 24, right plot. That gives a CPU power gain respect to an actual CPU of 300. This means for example that a coalescing binary analysis made with 4000 template of 250s length based on matched filtering will need theoretically a total processing time of only 3 seconds on one CPU, respect a full cluster of nowaday.

Thus, an important step in the evaluation of ET computational requirements is the beginning of the learning process on how to use and make massive-parallel programming in the context of gravitational wave, inquiering, exploring and using the first attempts of new hardware generation. That is necessary first of all if we want to evaluate how many GFlops we will need and how many GFlops we will be able to extract in a many-core distributed

---

[5] This definition instead can be considered as the peak theoretical performance.

memory scenario. Moreover we need to evaluate if and how ET physics will be limited by computation infrastructure constrains.

B. Gravitational wave software developments

As mentioned in the previous section, the software evolution is the other side of the coin, without which any hardware evolution is underused.

For that in ET we need to put an effort in this direction, starting first of all on the definition and exploration of data analysis paradigms, one for each sources or investigation. Jointly we need a process of cataloging the set of detection, reconstruction,.. algorithms for each science case. After that we need to try to map the most significative or representative of them on the computational power that we expect in 10-15 years from now, looking which (if any) science limitations are imposed to ET Physics.

Thus, this investigation consists on dividing the analysis of the computational aspects for each ET DA goals groups. This is the hardest but also most innovative part, because remembering that the observation is the main ET purpose, we can figure out and develop new procedures and methodologies.

To achieve such goal it is really important to coordinate the "data analysis requirements group" together and singlulary with the people of the others groups, in order to create the future ET data analysis scenarios. For that we plan to have also some kind of "private" discussion with each single DA group, in order to understand and explore the specific contexts, implications and computational aspects.

VII.   FURTHER READING AND RESOURCES

1. The ET web pages and resources are at: `http://www.et-gw.eu/`

2. The e-mail address for the group is `WG4-et AT ego-gw.it`. WG4 mailing is at: `https://mail.virgo.infn.it/mailman/listinfo/wg4-et`.

3. WG4 working area at
`https://workarea.et-gw.eu/et/WG4-Astrophysics`
contains sensitivity goals, codes and presentations made by the members at the group's face-to-face meetings as well as invited reviews.

4. The ET Science Team mailing list is at:
`https://mail.virgo.infn.it/mailman/listinfo/science-team-et`.   The e-mail address for the Science Team is: `science-team-et AT ego-gw.it`

APPENDIX A: WG4 ASSUMPTIONS REGARDING ET AND ASTROPHYSICS

To arrive at preliminary estimates as to what ET might be capable of in terms of astrophysics and cosmology, some assumptions have to be made about the design of ET. This document provides one possible set of assumptions for the noise curve and particularly the topology which new members of WG4 can use as a starting point. However, it is important to note that (a) the noise curve is very provisional and will presumably get more sophisticated through the course of the design study; and (b) the final topology of ET is yet to be decided on.

APPENDIX B: NOISE CURVE

ET will probably consist of several different interferometers, with opening angles of either 60° or 90°, and as yet unspecified arm lengths. The power spectral density (PSD) we are about to specify is for a single interferometer with 90° opening angle and 10 km arm length. To compute signal-to-noise ratios or Fisher matrices for a combination of interferometers from this PSD, the opening angles and arm lengths of the various interferometers will need to be folded in appropriately; this will be discussed in the next section.

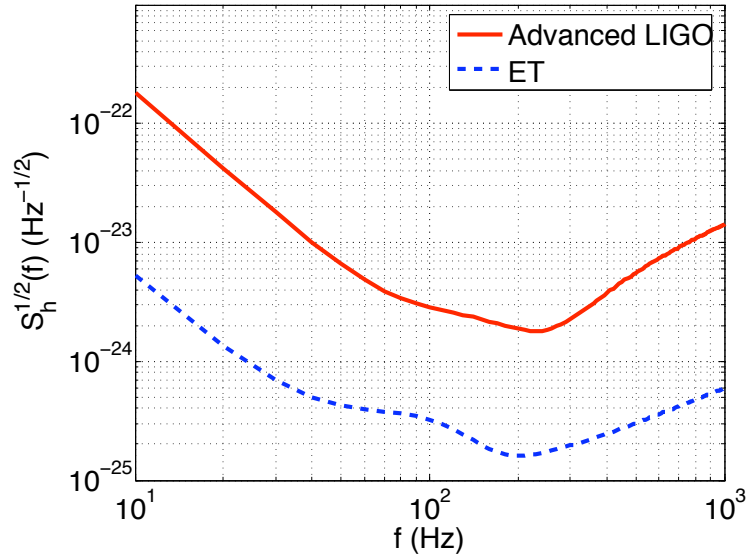Fig. 25 compares the sensitivity of ET with that of Advanced LIGO.

FIG. 25: The strain sensitivities of Advanced LIGO and ET as functions of frequency.

For a single L-shaped interferometer with $90°$ opening angle and 10 km arms, we take the PSD to be[6]

$$S_h(f) = S_0 \left[x^{p_1} + a_1 x^{p_2} + a_2 \frac{1 + b_1 x + b_2 x^2 + b_3 x^3 + b_4 x^4 + b_5 x^5 + b_6 x^6}{1 + c_1 x + c_2 x^2 + c_3 x^3 + c_4 x^4} \right] \quad \text{(B1)}$$

---

[6] We note that this PSD differs from what one finds in some of the earlier literature by a factor of $(3/10)^2$; in some papers an arm length of only 3 km was assumed.

where $x = f/f_0$ with $f_0 = 200$ Hz, and $S_0 = 1.449 \times 10^{-52}$ Hz^{-1}. One has

$$p_1 = -4.05, \qquad p_2 = -0.69,$$
$$a_1 = 185.62, \qquad a_2 = 232.56,$$
$$b_1 = 31.18, \quad b_2 = -64.72, \quad b_3 = 52.24, \qquad b_4 = -42.16, \quad b_5 = 10.17, \quad b_6 = 11.53,$$
$$c_1 = 13.58, \quad c_2 = -36.46, \qquad c_3 = 18.56, \quad c_4 = 27.43.$$

$$\text{(B2)}$$

We also need to specify a lower cut-off frequency, f_{lower}. A value of $f_{lower} = 1$ Hz is commonly used, but for this particular noise curve and, say, inspiral signals, there will be little difference in signal-to-noise ratios whether one takes that value or $f_{lower} = 10$ Hz.

APPENDIX C: SENSITIVITY LOBES OF VARIOUS DETECTOR DESIGNS

One possible set-up for ET would be a triangular tube with 10 km edges containing three interferometers (ifos) with 60 degree opening angles. We first consider the combined signal-to-noise ratio (SNR) for the three ifos together. We then show that the triangular, three ifo design produces the same combined SNR as a combination of two appropriately scaled ifos with 90 degree opening angles.

1. Triangle with three interferometers

Consider three ifos with 60 degree opening angles, arranged in an equilateral triangle. Let $\hat{l}_i$, $i = 1, 2, 3$ be unit vectors tangent to the edges of the triangle as in Fig. 26, left panel. These can be expressed in terms of unit vectors $(\hat{x}, \hat{y}, \hat{z})$ defining a Cartesian coordinate system, where $(\hat{x}, \hat{y})$ are in the detector plane:

$$\hat{l}_i = \cos(\alpha_i)\,\hat{x} + \sin(\alpha_i)\,\hat{y}, \tag{C1}$$

with

$$\alpha_i = \frac{\pi}{12} + (i-1)\frac{\pi}{3}. \tag{C2}$$

The three ifos inside the triangular tube have detector tensors

$$d_1^{ab} = \frac{1}{2}(\hat{l}_1^a \hat{l}_1^b - \hat{l}_2^a \hat{l}_2^b),$$
$$d_2^{ab} = \frac{1}{2}(\hat{l}_2^a \hat{l}_2^b - \hat{l}_3^a \hat{l}_3^b),$$
$$d_3^{ab} = \frac{1}{2}(\hat{l}_3^a \hat{l}_3^b - \hat{l}_1^a \hat{l}_1^b), \tag{C3}$$

where $a = 1, 2, 3$ are spatial indices. Using (C3) we can compute the responses of the three interferometers. Let $h_{ab}(t)$ be the metric perturbation in transverse-traceless gauge; then the strain h_K in the K-th interferometer is

$$h_K(t) = h_{ab}(t)\,d_K^{ab}, \tag{C4}$$

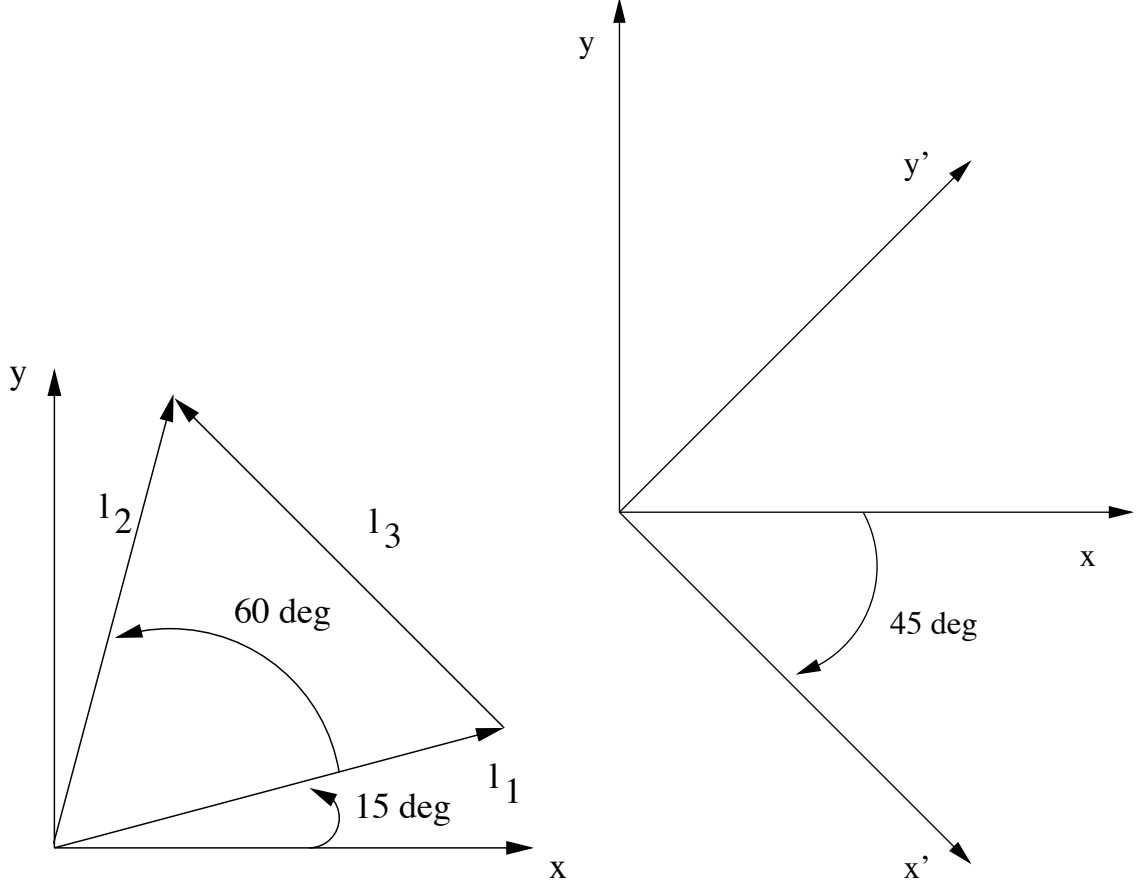where summation over repeated indices is assumed.

FIG. 26: Unit vectors defining the detector tensors for a triangular ET (left) and unit vectors defining the detector tensors for two ifos with 90 degree opening angles at 45 degrees from each other (right).

Now suppose we are looking for the signal in the outputs of the interferometers by means of matched filtering. Assuming that the noise in the three ifos is completely uncorrelated, their outputs can be coherently combined. If ρ_K, $K = 1, 2, 3$ are the signal-to-noise ratios (SNRs) in the individual ifos, the combined SNR ρ is given by

$$\rho = (\rho_1^2 + \rho_2^2 + \rho_3^2)^{1/2} \tag{C5}$$

If the templates and the signals are from the same waveform families then

$$\rho_K^2 = 4 \int_{f_{lower}}^{f_{upper}} \frac{|\tilde{h}_K(f)|^2}{S_h(f)} df, \tag{C6}$$

for some lower and upper cut-off frequencies f_{lower}, f_{upper}, and $\tilde{h}_K(f)$ are the Fourier transforms of the ifo responses $h_K(t)$. Hence

$$\rho = \left(4 \int_{f_{lower}}^{f_{upper}} \frac{\sum_{K=1}^{3} |\tilde{h}_K(f)|^2}{S_h(f)} df \right)^{1/2}. \tag{C7}$$

With some algebra, one can show that

$$\sum_{K=1}^{3} |\tilde{h}_K|^2 = \frac{9}{32}\left(4\tilde{h}_{xy}^2 + (\tilde{h}_{xx} - \tilde{h}_{yy})^2\right), \tag{C8}$$

where $\tilde{h}_{xx}(f) = \tilde{h}_{ab}(f)\hat{x}^a\hat{x}^b$, $\tilde{h}_{yy}(f) = \tilde{h}_{ab}(f)\hat{y}^a\hat{y}^b$, and $\tilde{h}_{xy}(f) = \tilde{h}_{ab}(f)\hat{x}^a\hat{y}^b$.

2. 'Double L' configuration

The triangular set-up we just described is equivalent to having two co-located interferometers with 90 degree opening angles, but rotated 45 degrees with respect to each other (Fig. 26, right panel), and with appropriately scaled arm lengths. Define

$$\hat{x}'^a = \frac{\sqrt{2}}{2}(\hat{x}^a - \hat{y}^a) \qquad \hat{y}'^a = \frac{\sqrt{2}}{2}(\hat{x}^a + \hat{y}^a). \tag{C9}$$

Then the detector tensors associated with the two 'L-shaped' ifos are

$$\begin{aligned} D_1^{ab} &= \frac{1}{2}(\hat{x}^a\hat{x}^b - \hat{y}^a\hat{y}^b), \\ D_2^{ab} &= \frac{1}{2}(\hat{x}'^a\hat{x}'^b - \hat{y}'^a\hat{y}'^b). \end{aligned} \tag{C10}$$

The responses of the individual ifos are

$$H_A(t) = H_{ab}(t)\, D_A^{ab} \tag{C11}$$

for $A = 1, 2$, and the combined SNR is given by

$$\rho = \left(4\int_{f_{lower}}^{f_{upper}} \frac{\sum_{A=1}^{2}|\tilde{H}_A(f)|^2}{S_h(f)}df\right)^{1/2}. \tag{C12}$$

It is not difficult to show that

$$\sum_{A=1}^{2}|\tilde{H}_A(f)|^2 = \frac{1}{4}\left(4\tilde{h}_{xy}^2 + (\tilde{h}_{xx} - \tilde{h}_{yy})^2\right). \tag{C13}$$

Comparing this with (C8), we see that the three 10 km V-shaped ifos in a triangle are equivalent to two L-shaped ifos at 45 degrees to each other and with arm lengths of $3/(2\sqrt{2}) \times 10$ km.

Note that this is *also* equivalent to having two L-shaped tubes at 45 degrees to each other and with $(3/4) \times 10$ km arm length, but with *two ifos in each of the two tubes* ($\sqrt{2} \times 3/4 = 3/(2\sqrt{2})$). In this configuration the total tube length is again 30 km, as with the triangle configuration, but now we would have a total of four L-shaped ifos with 7.5 km arm length.

Instead of multiplying $S_h(f)$ by a factor of $(2\sqrt{2}/3)^2$, it is convenient to multiply the responses (C11) by $3/(2\sqrt{2})$:

$$H_A'(t) = \frac{3}{2\sqrt{2}}H_A(t). \tag{C14}$$

The explicit expressions for these in terms of the gravitational wave polarizations h_+, $h_\times$ and as functions of sky position (θ, ϕ) and polarization angle ψ are simply

$$H_1'(\theta, \phi, \psi; t) = \frac{3}{2\sqrt{2}} \left(F_+(\theta, \phi, \psi) h_+(t) + F_\times(\theta, \phi, \psi) h_\times(t) \right),$$

$$H_2'(\theta, \phi, \psi; t) = \frac{3}{2\sqrt{2}} \left(F_+(\theta, \phi + \pi/4, \psi) h_+(t) + F_\times(\theta, \phi + \pi/4, \psi) h_\times(t) \right), \quad \text{(C15)}$$

where

$$F_+(\theta, \phi, \psi) = \frac{1}{2} \left(1 + \cos^2(\theta) \right) \cos(2\phi) \cos(2\psi) - \cos(\theta) \sin(2\phi) \sin(2\psi),$$

$$F_\times(\theta, \phi, \psi) = \frac{1}{2} \left(1 + \cos^2(\theta) \right) \cos(2\phi) \sin(2\psi) + \cos(\theta) \sin(2\phi) \cos(2\psi). \quad \text{(C16)}$$

The combined SNR for the rescaled detectors is just

$$\rho' = \left(4 \int_{f_{lower}}^{f_{upper}} \frac{\sum_{A=1}^{2} |\tilde{H}_A'(f)|^2}{S_h(f)} df \right)^{1/2}. \quad \text{(C17)}$$

[1] B. F. Schutz, Nature (London) **323**, 310 (1986).

[2] L. Blanchet, Living Rev. Relativity **9** (2006), URL `http://www.livingreviews.org/lrr-2006-4`.

[3] B. Schutz, Nature **323**, 310 (1986).

[4] L. Blanchet, B. R. Iyer, C. M. Will, and A. G. Wiseman, Class. Quantum Grav. **13**, 575 (1996), gr-qc/9602024.

[5] K. G. Arun, L. Blanchet, B. R. Iyer, and M. S. S. Qusailah, Class. Quantum Grav. **21**, 3771 (2004), erratum-ibid. **22**, 3115 (2005), gr-qc/0404185.

[6] L. Blanchet, G. Faye, B. R. Iyer, and B. Joguet, Phys. Rev. D **65**, 061501(R) (2002), Erratum-ibid **71**, 129902(E) (2005), gr-qc/0105099.

[7] L. Blanchet, T. Damour, G. Esposito-Farèse, and B. R. Iyer, Phys. Rev. Lett. **93**, 091101 (2004), gr-qc/0406012.

[8] C. Van Den Broeck, Class. Quantum Grav. **23**, L51 (2006), gr-qc/0604032.

[9] C. Van Den Broeck and A. Sengupta, Class. Quantum Grav. **24**, 155 (2007), gr-qc/0607092.

[10] K. Arun, B. Iyer, B. Sathyaprakash, and S. Sinha, Phys. Rev. D **75** (2007), arXiv:0704.1086.

[11] A. M. Sintes and A. Vecchio, in *Rencontres de Moriond:Gravitational waves and experimental gravity*, edited by J. Dumarchez (Frontières, Paris, 2000), gr-qc/0005058.

[12] A. M. Sintes and A. Vecchio, in *Third Amaldi conference on Gravitational Waves*, edited by S. Meshkov (American Institute of Physics Conference Series, New York, 2000), p. 403, gr-qc/0005059.

[13] T. A. Moore and R. W. Hellings, Phys. Rev. D **65**, 062001 (2002).

[14] R. W. Hellings and T. A. Moore, Class. Quant. Grav. **20**, S181 (2003), gr-qc/0207102.

[15] C. Van Den Broeck and A. S. Sengupta, Class. Quantum Grav. **24**, 1089 (2007), gr-qc/0610126.

[16] F. Pretorius, Phys. Rev. Lett. **95** (2005), gr-qc/0507014.

[17] M. Campanelli, C. Lousto, P. Marronetti, and Y. Zlochower, Phys. Rev. Lett. **96** (2006), gr-qc/0511048.

[18] J. Baker, J. Centrella, D.-I. Choi, M. Koppitz, and J. van Meter, Phys. Rev. Lett. **96** (2006), gr-qc/0511103.

[19] M. Hannam (2009), 0901.2931.

[20] J. G. Baker, J. R. van Meter, S. T. McWilliams, J. Centrella, and B. J. Kelly, Phys. Rev. Lett. **99**, 181101 (2007), gr-qc/0612024.

[21] M. Hannam, S. Husa, U. Sperhake, B. Bruegmann, and J. A. Gonzalez, Phys. Rev. **D77**, 044020 (2008), 0706.1305.

[22] M. Boyle, D. Brown, L. Kidder, A. Mroué, H. Pfeiffer, M. Scheel, G. Cook, and S. Teukolsky, Phys. Rev. D **76** (2007), arXiv:0710.0158.

[23] M. Campanelli, C. O. Lousto, H. Nakano, and Y. Zlochower, Phys. Rev. **D79**, 084010 (2009), 0808.0713.

[24] J. Gonzalez, U. Sperhake, B. Brügmann, M. Hannam, and S. Husa, Phys. Rev. Lett. **98** (2007), gr-qc/0610154.

[25] J. A. Gonzalez, M. D. Hannam, U. Sperhake, B. Bruegmann, and S. Husa, Phys. Rev. Lett. **98**, 231101 (2007), gr-qc/0702052.

[26] M. Campanelli, C. Lousto, Y. Zlochower, and D. Merritt, Astrophys. J. **659**, L5 (2007),

gr-qc/0701164.

[27] L. Boyle, M. Kesden, and S. Nissanke, Phys. Rev. Lett. **100**, 151101 (2008), 0709.0299.

[28] A. Buonanno, L. Kidder, and L. Lehner, Phys. Rev. D **77** (2008), arXiv:0709.3839.

[29] L. Rezzolla, E. Barausse, E. Dorband, D. Pollney, C. Reisswig, J. Seiler, and S. Husa, Phys. Rev. D **78** (2007), arXiv:0712.3541.

[30] S. Komossa, H. Zhou, and H. Lu, Astrophys. J. Lett. **678**, L81 (2008), arXiv:0804.4585.

[31] B. Aylott et al. (2009), 0901.4399.

[32] M. Hannam, S. Husa, B. Bruegmann, and A. Gopakumar, Phys. Rev. **D78**, 104007 (2008), 0712.3787.

[33] I. Hinder, F. Herrmann, P. Laguna, and D. Shoemaker (2008), 0806.1037.

[34] P. e. a. Ajith, Class. Quantum Grav. **24**, S689 (2007), arXiv:0704.3764.

[35] P. Ajith et al., Phys. Rev. **D77**, 104017 (2008), 0710.2335.

[36] P. Ajith, Class. Quant. Grav. **25**, 114033 (2008), 0712.0343.

[37] A. e. a. Buonanno, Phys. Rev. D **76** (2007), arXiv:0706.3732.

[38] T. Damour and A. Nagar, Phys. Rev. D **77** (2008), arXiv:0711.2628.

[39] T. Damour, A. Nagar, E. N. Dorband, D. Pollney, and L. Rezzolla, Phys. Rev. D **77** (2008), arXiv:0712.3003.

[40] T. Damour, A. Nagar, M. Hannam, S. Husa, and B. Brügmann, Phys. Rev. D **78** (2008), arXiv:0803.3162.

[41] T. Damour and A. Nagar (2009), 0902.0136.

[42] A. Buonanno et al. (2009), 0902.0790.

[43] P. Ajith and S. Bose (2009), 0901.4936.

[44] S. Babak, M. Hannam, S. Husa, and B. Schutz (2008), arXiv:0806.1591.

[45] J. I. Thorpe et al., Class. Quant. Grav. **26**, 094026 (2009), 0811.0833.

[46] M. Hannam et al. (2009), 0901.2437.

[47] A. M. Hopkins and J. F. Beacom, Astrophys. J. **651**, 142 (2006), arXiv:astro-ph/0601463.

[48] M. Burgay, N. D'Amico, A. Possenti, R. Manchester, A. Lyne, B. Joshi, M. McLaughlin, M. Kramer, J. Sarkissian, F. Camilo, et al., Nature **426**, 531 (2003), astro-ph/0312071.

[49] C. Kim, V. Kalogera, and D. R. Lorimer, Astrophys. J. **584**, 985 (2003).

[50] C. Kim, V. Kalogera, and D. R. Lorimer, in *A life with stars* (2006), URL `http://xxx.lanl.gov/abs/astro-ph/0608280`.

[51] T. Regimbau and S. Hughes (2009), arXiv:0901.2958.

[52] R. O'Shaughnessy, V. Kalogera, and K. Belcynski, in preparation (2009).

[53] K. Belczynski, V. Kalogera, F. Rasio, R. Taam, A. Zezas, T. Maccarone, and N. Ivanova, ApJ S **174**, 223 (2008), URL `http://xxx.lanl.gov/abs/astro-ph/0511811`.

[54] K. Kulczycki, T. Bulik, K. Belczyński, and B. Rudak, aap **459**, 1001 (2006), astro-ph/0602533.

[55] R. O'Shaughnessy, C. Kim, V. Kalogera, and K. Belczynski, ApJ **672**, 479 (2008), URL `http://arxiv.org/abs/astro-ph/0610076`.

[56] K. Belczynski, R. E. Taam, V. Kalogera, F. A. Rasio, and T. Bulik, ApJ **662**, 504+ (2007), astro-ph/0612032.

[57] K. Belczynski, T. Bulik, C. L. Fryer, A. Ruiter, J. S. Vink, and J. R. Hurley, ArXiv e-prints (2009), 0904.2784.

[58] K. Belczynski, D. H. Hartmann, C. L. Fryer, D. E. Holz, and B. O'Shea, ArXiv e-prints (2008), 0812.2470.

[59] R. O'Shaughnessy, R. Kopparapu, and K. Belczynski, submitted to ApJ; arXiv:0812.0591

(2008), URL http://xxx.lanl.gov/abs/0812.0591.

[60] T. Bulik, K. Belczynski, and A. Prestwich, (arXiv:0803.3516) (2008), URL http://xxx.lanl.gov/abs/arXiv:0803.3516.

[61] R. O'Shaughnessy, R. O'Leary, and F. A. Rasio, Phys. Rev. D **76**, 061504 (2007), URL http://arxiv.org/abs/astro-ph/0701887.

[62] A. Sadowski, K. Belczynski, T. Bulik, N. Ivanova, F. A. Rasio, and R. O'Shaughnessy, Astrophys. J. **676**, 1162 (2008), arXiv:0710.0878.

[63] S. F. Portegies Zwart and S. L. W. McMillan, Astrophysical Journal **528**, L17 (2000), URL http://adsabs.harvard.edu/cgi-bin/nph-bib_query?bibcode=2000ApJ...528L..17P&db_key=AST.

[64] S. B. et al., Class. Quantum Grav. **25**, 184026 (2008).

[65] C. Cutler and J. Harms, Phys. Rev. D **73**, 042001 (2006).

[66] P. Jaranowski, A. Krolak, and B. F. Schutz, Phys. Rev. **D58**, 063001 (1998), gr-qc/9804014.

[67] B. e. a. L. S. C. Abbott, Phys. Rev. Lett. **94** (2005), gr-qc/0410007.

[68] B. e. a. L. S. C. Abbott, Phys. Rev. D **76** (2007), gr-qc/0702039.

[69] B. e. a. L. S. C. Abbott, Astrophys. J. Lett. **683** (2008), arXiv:0805.4758.

[70] B. e. a. L. S. C. Abbott, Phys. Rev. D **72** (2005), gr-qc/0508065.

[71] L. Bildsten, Astrophys. J. Lett. **501**, L89 (1998), astro-ph/9804325.

[72] A. Watts, B. Krishnan, L. Bildsten, and B. Schutz (2008), arXiv:0803.4097, arXiv:0803.4097.

[73] B. Allen and J. Romano, Phys. Rev. D **59** (1999), gr-qc/9710117.

[74] T. . Regimbau and V. Mandic, Class. Quantum Grav. **25**, 184018 (2008).

[75] H. A. Bethe, Rev. Mod. Phys. **62**, 801 (1990).

[76] H.-T. Janka, K. Langanke, A. Marek, G. Martínez-Pinedo, and B. Müller, Phys. Rep. **442**, 38 (2007).

[77] C. D. Ott, Class. Quant. Grav. **26(6)**, 063001 (2009).

[78] C. D. Ott, Submitted to Class. Quant. Grav. (2009), arXiv:0905.2797.

[79] *Einstein telescope home page*, URL http://www.et-gw.eu.

[80] C. Will, Phys. Rev. D **57**, 2061 (1998).

[81] K. G. Arun and C. M. Will (2009), arxiv: 0904.1190[gr-qc].

[82] L. Blanchet, G. Faye, B. R. Iyer, and S. Sinha, Class. Quantum. Grav. **25**, 165003 (2008), arXiv:0802.1249.

[83] C. Van Den Broeck and A. Sengupta, Class. Quantum Grav. **24**, 155 (2007), gr-qc/0607092.

[84] L. Blanchet, T. Damour, B. Iyer, C. Will, and A. Wiseman, Phys. Rev. Lett. **74**, 3515 (1995), gr-qc/9501027.

[85] L. Blanchet, Phys. Rev. D **54**, 1417 (1996), Erratum-ibid.**71**, 129904(E) (2005), gr-qc/9603048.

[86] L. Blanchet, T. Damour, G. Esposito-Farese, and B. Iyer, Phys. Rev. Lett. **93** (2004), gr-qc/0406012.

[87] T. Damour, B. Iyer, and B. Sathyaprakash, Phys. Rev. D **63** (2001), erratum-ibid. D**72** 029902 (2005), gr-qc/0010009.

[88] T. Damour, B. R. Iyer, and B. S. Sathyaprakash, Phys. Rev. D **66**, 027502 (2002), erratum-ibid **66**, 027502 (2002), gr-qc/0207021.

[89] C. Cutler and E. Flanagan, Phys. Rev. **D49**, 2658 (1994), gr-qc/9402014.

[90] E. Poisson and C. Will, Phys. Rev. D **52**, 848 (1995), gr-qc/9502040.

[91] K. Arun, B. Iyer, B. Sathyaprakash, and P. Sundararajan, Phys. Rev. D **71** (2005), gr-qc/0411146.

[92] M. Vallisneri, Phys. Rev. D **77** (2008), gr-qc/0703086.

[93] C. Brans and R. H. Dicke, Phys. Rev. **124**, 925 (1961).

[94] B. Bertotti, L. Iess, and P. Tortora, Nature **425**, 374 (2003).

[95] C. M. Will, Phys. Rev. **D 50**, 6058 (1994), gr-qc/9406022.

[96] A. Królak, K. Kokkotas, and G. Schäfer, Phys. Rev. D **52**, 2089 (1995).

[97] C. M. Will, *Theory and experiments in gravitational physics* (Cambridge University Press, New York, USA, 1981).

[98] P. D. Scharre and C. M. Will, Phys. Rev. **D 65**, 042002 (2002), gr-qc/0109044.

[99] C. M. Will and N. Yunes, Class. Quantum Grav. **21**, 4367 (2004), gr-qc/0403100.

[100] E. Berti, A. Buonanno, and C. Will, Phys. Rev. D **71** (2005), gr-qc/0411129.

[101] P. J. E. Peebles and B. Ratra, Rev. Mod. Phys. **75**, 559 (2005), astro-ph/0207347.

[102] G. Hinshaw et al. (2008), arXiv:0803.0732 [astro-ph].

[103] B. Carter, Physical Review Letters **26**, 331 (1971).

[104] F. D. Ryan, Phys. Rev. D **52**, 5707 (1995).

[105] P. Amaro-Seoane, J. Gair, M. Freitag, M. Coleman, I. Mandel, C. Cutler, and S. Babak, Class. Quantum Grav. **24**, R113 (2007), astro-ph/0703495.

[106] D. A. Brown, J. Brink, H. Fang, J. R. Gair, C. Li, G. Lovelace, I. Mandel, and K. S. Thorne, Physical Review Letters **99**, 201102 (2007), arXiv:gr-qc/0612060.

[107] I. Mandel, D. A. Brown, J. R. Gair, and M. C. Miller, Astrophys. J. **681**, 1431 (2008), 0705.0285.

[108] F. D. Ryan, Phys. Rev. D **55**, 6081 (1997).

[109] R. Penrose, Nuovo Cimento Rivista Serie **1**, 252 (1969).

[110] M. Kesden, J. Gair, and M. Kamionkowski, Phys. Rev. D **71**, 044015 (2005), arXiv:astro-ph/0411478.

[111] J. M. Lattimer and M. Prakash, J. Phys. Rep. **442**, 109 (2007), arXiv:astro-ph/0612440.

[112] T. Klähn, D. Blaschke, S. Typel, E. N. E. van Dalen, A. Faessler, C. Fuchs, T. Gaitanos, H. Grigorian, A. Ho, E. E. Kolomeitsev, et al., Phys. Rev. C **74**, 035802 (2006), arXiv:nucl-th/0602038.

[113] D. Page and S. Reddy, Annual Review of Nuclear and Particle Science **56**, 327 (2006), arXiv:astro-ph/0608360.

[114] H. Dimmelmeier, C. Ott, H.-T. Janka, A. Marek, and E. Müller, Phys. Rev. Lett. **98** (2007), astro-ph/0702305v2.

[115] A. Marek, H.-T. Janka, and E. Müller, AAP **496**, 475 (2009), 0808.4136.

[116] B. J. Owen, Phys. Rev. Lett. **95**, 211101 (2005).

[117] X. Zhuge, J. M. Centrella, and S. L. W. McMillan, Phys. Rev. D **54**, 7261 (1996).

[118] F. A. Rasio and S. L. Shapiro, Class. Quantum Grav. **16**, R1 (1999).

[119] É. É. Flanagan and T. Hinderer, Phys. Rev. D **77**, 021502 (2008), 0709.1915.

[120] J. S. Read, B. D. Lackey, B. J. Owen, and J. L. Friedman (2008), 0812.2163.

[121] J. S. Read et al. (2009), 0901.3258.

[122] M. Bejger, D. Gondek-Rosińska, E. Gourgoulhon, P. Haensel, K. Taniguchi, and J. L. Zdunik, Astron. Astrophys. **431**, 297 (2005).

[123] M. Shibata, K. Taniguchi, and K. Uryū, Phys. Rev. D **71**, 084021 (2005), gr-qc/0503119.

[124] M. Shibata, Phys. Rev. Lett. **94**, 201101 (2005).

[125] R. Oechslin and H. T. Janka, MNRAS **368**, 1489 (2006).

[126] R. Oechslin and H. T. Janka, Phys.Rev.Lett. **99**, 121102 (2007).

[127] T. Yamamoto, M. Shibata, and K. Taniguchi, Phys. Rev. D **78**, 064054 (2008), 0806.4007.

[128] L. Baiotti, B. Giacomazzo, and L. Rezzolla, Phys. Rev. D **78**, 084033 (2008), ArXiv e-prints 0804.0594.

[129] L. Baiotti, B. Giacomazzo, and L. Rezzolla, Class. Quantum Grav., *in press*, arXiv:0901.4955 (2009), 0901.4955.

[130] J. A. Faber, T. W. Baumgarte, S. L. Shapiro, K. Taniguchi, and F. A. Rasio, Phys. Rev. D **73**, 024012 (2006), astro-ph/0511366.

[131] M. Shibata and K. Taniguchi, Phys. Rev. D **77**, 084015 (2008), arXiv:0711.1410.

[132] M. Shibata, K. Kyutoku, T. Yamamoto, and K. Taniguchi, Phys. Rev. **D79**, 044030 (2009), 0902.0416.

[133] B. Giacomazzo, L. Rezzolla, and L. Baiotti, arXiv:0901.2722 (2009), 0901.2722.

[134] C. Kouveliotou, C. A. Meegan, G. J. Fishman, N. P. Bhat, M. S. Briggs, T. M. Koshut, W. S. Paciesas, and G. N. Pendleton, Astrophys. J. Letters **413**, L101 (1993).

[135] C. Conselice et al., Astrophys. J. **633**, 29 (2005).

[136] T. J. Galama et al., Nature **395**, 670 (1998).

[137] S. R. Kulkarni et al., Nature **395**, 663 (1998).

[138] J. Hjorth et al., Nature **423**, 847 (2003).

[139] S. Campana et al., Nature **442** (2006).

[140] S. E. Woosley, Astrophys. J. **405**, 273 (1993).

[141] K. Iwamoto et al., Nature **395**, 672 (1998).

[142] J. S. Bloom and J. X. Prochaska, *Constraints on the diverse progenitors of grbs from the large-scale environments* (2006), URL `http://www.citebase.org/abstract?id=oai:arXiv.org:astro-ph/0602058`.

[143] J. S. Bloom et al., Astrophysical Journal **654** (2007).

[144] E. Nakar, A. Gal-Yam, T. Piran, and D. B. Fox, Astrophys. J. **640**, 849 (2006).

[145] R. Chapman, R. S. Priddey, and N. R. Tanvir, Mon. Not. R. Astron. Soc. pp. 430–+ (2009), 0802.0008.

[146] B. e. a. L. S. C. Abbott and K. Hurley, Astrophys. J. **681**, 1419 (2008), arXiv:0711.1163.

[147] C. D. Ott (2008), 0809.0695.

[148] B. e. a. L. S. C. Abbott (2009).

[149] M. H. van Putten et al., Phys. Rev. D **69**, 044007 (2004).

[150] J. A. de Freitas Pacheco, Astronomy and Astrophysics **336**, 397 (1998).

[151] K. Ioka, MNRAS **327**, 639 (2001).

[152] K. Hurley, S. E. Boggs, D. M. Smith, R. C. Duncan, R. Lin, A. Zoglauer, S. Krucker, G. Hurford, H. Hudson, C. Wigger, et al., nature **434**, 1098 (2005), arXiv:astro-ph/0502329.

[153] N. R. Tanvir, R. Chapman, A. J. Levan, and R. S. Priddey, Nature **438**, 991 (2005), arXiv:astro-ph/0509167.

[154] A. J. Levan, N. R. Tanvir, P. Jakobsson, R. Chapman, J. Hjorth, R. S. Priddey, J. P. U. Fynbo, K. Hurley, B. L. Jensen, R. Johnson, et al., Mon. Not. R. Astron. Soc. **384**, 541 (2008), 0705.1705.

[155] D. Frederiks, R. Aptekar, T. Cline, J. Goldsten, S. Golenetskii, K. Hurley, V. Ilinskii, A. von Kienlin, E. Mazets, and V. Palshin, in *American Institute of Physics Conference Series*, edited by M. Galassi, D. Palmer, and E. Fenimore (2008), vol. 1000 of *American Institute of Physics Conference Series*, pp. 271–275.

[156] E. O. Ofek, M. Muno, R. Quimby, S. R. Kulkarni, H. Stiele, W. Pietsch, E. Nakar, A. Gal-Yam, A. Rau, P. B. Cameron, et al., Astrophys. J. **681**, 1464 (2008), 0712.3585.

[157] B. Owen, L. Lindblom, C. Cutler, B. Schutz, A. Vecchio, and N. Andersson, Phys. Rev. D

58 (1998), gr-qc/9804044.

[158] N. Andersson, Astrophys. J. **502**, 708 (1998), gr-qc/9706075.

[159] P. Sá and B. Tome', Phys. Rev. D **74**, 044011 (2006).

[160] P. Sá, Astrophys Space Sci. **308**, 557 (2007).

[161] L. Baiotti, R. De Pietri, G. Manca, and L. Rezzolla, Phys. Rev. D **75**, 044023 (2007).

[162] K. Levenberg, The Quarterly of Applied Mathematics **2**, 164 (1944).

[163] D. Marquardt, SIAM Journal on Applied Mathematics **11**, 431 (1963).

[164] A. Sesana, M. Volonteri, and F. Haardt, MNRAS **377**, 1711 (2007), arXiv:astro-ph/0701556.

[165] P. Madau and M. J. Rees, APJL **551**, L27 (2001), arXiv:astro-ph/0101223.

[166] S. M. Koushiappas, J. S. Bullock, and A. Dekel, MNRAS **354**, 292 (2004), arXiv:astro-ph/0311487.

[167] M. C. Begelman, M. Volonteri, and M. J. Rees, MNRAS **370**, 289 (2006), arXiv:astro-ph/0602363.

[168] P. Bender, A. Brillet, I. Ciufolini, A. Cruise, C. Cutler, K. Danzmann, F. Fidecaro, W. Folkner, J. Hough, P. McNamara, et al., Tech. Rep., Max-Planck-Institut für Quantenoptik, Garching (1998).

[169] M. Volonteri, F. Haardt, and P. Madau, APJ **582**, 559 (2003), arXiv:astro-ph/0207276.

[170] M. Volonteri, R. Salvaterra, and F. Haardt, MNRAS **373**, 121 (2006), arXiv:astro-ph/0606675.

[171] A. Sesana, J. Gair, I. Mandel, and A. Vecchio, ArXiv e-prints (2009), 0903.4177.

[172] URL `http://www.nvidia.it/object/cuda\_what\_is\_it.html`.

[173] URL `http://www.intel.com/technology/architecture-silicon/32nm/index.htm?id=tech\_mooreslaw+\%20body\_32nm`.

[174] URL `http://developer.amd.com/gpu/ATIStreamSDK/Pages/default.aspx`.

[175] URL `http://download.intel.com/technology/architecture-silicon/Siggraph\_Larrabee\_paper.pdf`.